

INVESTIGATION OF COMPLEXITY DYNAMICS AND THE STUDY OF NONLINEARITY IN THE SELF AND EXTERNALLY EXCITED GLOW DISCHARGE PLASMA

By

DEBAJYOTI SAHA

(Enrolment No.-PHYS05201204017)

Saha Institute of Nuclear Physics, Kolkata

*A thesis submitted to the
Board of Studies in Physical Sciences*

*In partial fulfillment of requirements
for the degree of*

DOCTOR OF PHILOSOPHY

of

HOMI BHABHA NATIONAL INSTITUTE




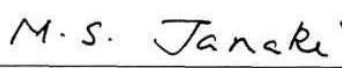
September 2017

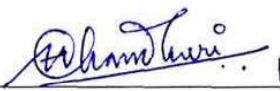
Homi Bhabha National Institute

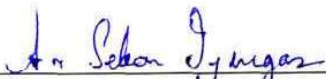
Recommendations of the Viva Voce Committee


As members of the Viva Voce Committee, we certify that we have read the dissertation prepared by **Debajyoti Saha** entitled "**Investigation of complexity dynamics and the comprehensive study of nonlinearity in self and externally excited glow discharge plasma**" and recommend that it may be accepted as fulfilling the thesis requirement for the award of Degree of Doctor of Philosophy.


Chairman - Prof. Dhananjay Bhattacharyya
Date: 13/4/2018


Guide / Convener - Prof. M.S. Janaki
Date: 13/4/18


Examiner - Prof. Hirok Chaudhuri
Date: 13/04/18.


Member 1- Prof. A.N. Sekar Iyengar
Date: 13/04/18


Member 2- Prof. Dulal Senapati
Date: 13.4.18

Final approval and acceptance of this thesis is contingent upon the candidate's submission of the final copies of the thesis to HBNI.

I/We hereby certify that I/we have read this thesis prepared under my/our direction and recommend that it may be accepted as fulfilling the thesis requirement.

Date: 13/04/2018

Place: KOLKATA

M.S. Janaki

Guide

STATEMENT BY AUTHOR

This dissertation has been submitted in partial fulfillment of requirements for an advanced degree at Homi Bhabha National Institute (HBNI) and is deposited in the Library to be made available to borrowers under rules of the HBNI.

Brief quotations from this dissertation are allowable without special permission, provided that accurate acknowledgement of source is made. Requests for permission for extended quotation from or reproduction of this manuscript in whole or in part may be granted by the Competent Authority of HBNI when in his or her judgment the proposed use of the material is in the interests of scholarship. In all other instances, however, permission must be obtained from the author.

Debajyoti Saha

Debajyoti Saha

DECLARATION

I, hereby declare that the investigation presented in the thesis has been carried out by me. The work is original and has not been submitted earlier as a whole or in part for a degree / diploma at this or any other Institution / University.

Debajyoti Saha

Debajyoti Saha

List of Publications arising from the thesis

a. Publications in peer reviewed Journals

1. "*Investigation of complexity dynamics of inverse and normal homoclinic bifurcation in a glow discharge plasma*", **Debajyoti Saha**, P. K. Shaw, M. S. Janaki, A. N. Sekar Iyengar, S. Ghosh, V. Mitra, A. M. Wharton, *Physics of Plasmas* (**2014**), 21, 032301.
2. "*Investigation and quantification of nonlinearity using surrogate data in a glow discharge plasma*", **Debajyoti Saha**, P. K. Shaw, S. Ghosh, M. S. Janaki, A. N. Sekar Iyengar *Physics of Plasmas*, (**2015**), 22, 022307.
3. "*Evidence of nonlinearity in presence of external forcing and magnetic field in a glow discharge plasma*", **Debajyoti Saha**, P. K. Shaw, S. Ghosh, M. S. Janaki, A. N. Sekar Iyengar, *Chaos, Solitons and Fractals*, (**2017**), 98, 46-55.
4. "*Investigation and quantification of phase coherence index for different types of forcing in DC glow discharge plasma*", **Debajyoti Saha**, P. K. Shaw, S. Ghosh, M. S. Janaki, A. N. Sekar Iyengar, *Chaos, Solitons and Fractals*, (**2017**), 104, 173-181.
5. "*Quantification of scaling exponent with crossover type phenomena for different types of forcing in DC glow discharge plasma*", **Debajyoti Saha**, P. K. Shaw, S. Ghosh, M. S. Janaki, A. N. Sekar Iyengar, *Physica A*, (**2018**), 490, 300-310.
6. "*Interplay of transitions between oscillations with emergence of fireballs and*

quantification of phase coherence, scaling index in a magnetized glow discharge plasma in a toroidal assembly", D. Saha, S. Ghosh, P.K Shaw, M. S. Janaki, A. N. Sekar Iyengar, Chaos, Solitons and Fractals, (2018), 106, 295-303.

b. Publications in Conference proceedings

1. **Debajyoti Saha**, P. K. Shaw, S. Ghosh, M. S. Janaki, A. N. Sekar Iyengar, Proceedings of the tenth Asian plasma and fusion association conference (APFA), 47, 2015

2. **Debajyoti Saha**, Ramesh Narayanan, R.D Tarey, M.S Janaki, A.N. Sekar Iyengar, Proceedings International work conference on time series analysis (ITISE) 2016 ISBN: 978-84-16478-93-4

Debajyoti Saha

Debajyoti Saha

Dedicated to my “Baba”, “Maa” and “Vai”

Acknowledgements

The research included in this dissertation could not have been performed without the assistance, patience, and support of many individuals. Specially, I am grateful to my supervisors Prof. M. S. Janaki and Prof. A.N Sekar Iyengar for their teaching, careful guidance, encouragement and moral support in pursuing this doctoral research. Under their guidance, I successfully overcame many difficulties and learned a lot. I am indebted to them for foreseeing the gradual development from the beginning of this work. It has been a great pleasure and honour to work with them at Saha Institute of Nuclear Physics.

I thank my doctoral committee members in making yearly evaluation of my progress report and giving valuable suggestions.

I express my heartiest thanks to my colleagues cum collaborator Pankaj Kumar Shaw, Sabuj Ghosh with whom I shared and learnt a lot in the field of my research. We spent a lot of joyful moments together. I would also like to thank my another collaborator Dr. Arun Kumar Sarma, VIT, Chennai for his invaluable helps and suggestions. This thesis would not have been possible without their cooperation.

I would like to thank the technical and scientific staff of the division, for providing me with various assistances during the course of this thesis work. I thus acknowledge the efforts of Dipankar Das, Santanu Chaudhuri, Asok Ram.

My special words of thankfulness should also acknowledge Prof. S. Saha, Prof. R. Pal and Prof N Chakrabarti for their fruitful comments and discussions.

This research would not have been possible without the assistance and cooperation of my seniors Sourav Da, Sudip Da, Abhijit Da, Anwesha di, Subir Da. I must thank Sourav Da individually for giving me helping hands not only during my thesis work but also in various other activities. I also feel very lucky to spend innumerable joyful moments with Satyajit, Vramori, Mithun, Sayanee, and Subha. I should extend my words of appreciation to Monobir Da, Subhasish Da, Santanu Da, Dipankar Da and many other colleagues in SINP.

I express my heartiest thanks specially to Prof. Satyaranjan Bhattacharjee (HOD of surface physics division in SINP) for motivating and inspiring in my research work.

I am thankful to Prof. Cristina Masoller of Universitat Politècnica de Catalunya, Barcelona, Spain and Md. Nurujjaman for the useful discussions on nonlinear dynamics. I would also like to acknowledge Prof. Norbert Marwan (Potsdam Institute for Climate impact research) for using the recurrence toolbox.

I should convey my deepest gratitude to my beloved parents and my brother. My father Dr. Manik Chandra Saha has always motivated and encouraged me by sharing the view, knowledge and experience of his Ph.D life. My mother as a teacher has given me moral support for the completion of my research work. Without their love, support and understanding I could never have completed this doctoral degree. Lastly, I want to express my sincere apologies for my inability to individually acknowledge many others, who might have helped me in the completion of this Ph.D. work one way or another.

SINP, Kolkata

September, 2017

Debajyoti Saha

Contents

Synopsis	xi
List of figures	xix
List of tables	xxv
1 Introduction	1
1.1 Plasma Physics: An introduction and its importance	3
1.2 Brief historical backdrop of Nonlinearity and relevance with Plasma Physics	4
1.3 Definition of nonlinearity and approach to complexity dynamics . .	7
1.4 Nonlinear Oscillations in Plasma and transitions amongst them . .	10
1.4.1 Motivation to study the nonlinearity, phase coherence index in glow discharge plasma	12
1.4.2 Need for the study of nonlinearity	13
1.4.3 Time series Analysis: Its Motivation	14
1.4.4 Nonstationarity, Detrended fluctuation analysis and its mo- tivation	17
2 Experiment, diagnostics and data analysis procedures	19
2.1 Experimental Setup	19
2.1.1 DC Discharge Plasma	19
2.1.2 Toroidal discharge device	22

2.3.9	Bicoherency analysis based on empirical mode decomposition	33
2.3.10	Surrogate data: Delay vector variance, Rank test, Zscore, Nonlinearity metrics, Structure function, Phase coherence index	36
2.3.11	The Continuous Wavelet Transform (CWT)	43
2.3.12	Detrended fluctuation analysis	44
3	Investigation of complexity dynamics of inverse and normal ho- moclinic bifurcation in a glow discharge plasma	47
3.1	Introduction	48
3.2	Floating potential fluctuations, Amplitude Bifurcation and Time Period	49
3.3	Power Spectral Analysis	54
3.3.1	Correlation dimension, Lyapunov exponent, Renyi Entropy .	56
3.4	Numerical Modelling of homoclinic bifurcations	57
3.5	Conclusion	60
4	Investigation and quantification of nonlinearity using surrogate data in a DC glow discharge plasma	63
4.1	Introduction	64
4.2	Floating potential fluctuation, power spectral analysis	65
4.3	Dimensionality analysis	66
4.4	Analysis with the surrogate data	70
4.5	Delay vector variance analysis	72
4.5.1	Nonlinearity analysis of Floating potential fluctuations for P=0.056mbar	72
4.5.2	Analysis of nonlinearity for P=0.085 mbar with rank test and DVV method	75
4.6	Conclusion	77
5	Evidence of nonlinearity in presence of external forcing and mag- netic field in a glow discharge plasma	79

6	Investigation and quantification of phase coherence index for different types of forcing in DC glow discharge plasma	101
6.1	Introduction	103
6.2	Floating potential fluctuation, Recurrence plot	105
6.3	Method of analysis: structure function, Phase coherence index . . .	109
6.4	Nonlinearity analysis with delay Vector Variance for different types of forcing	115
6.5	Conclusion	118
7	Quantification of scaling exponent with crossover type phenomena for different types of forcing in DC glow discharge plasma	121
7.1	Introduction	123
7.2	Floating potential fluctuation, Recurrence plot, Recurrence quantification analysis	125
7.3	Nonstationary, Detrended fluctuation analysis	127
7.4	Results of DFA analysis with crossover phenomena	130
7.5	Conclusion	135
8	Interplay of transitions between oscillations with emergence of fireballs and quantification of phase coherence, scaling index in a magnetized glow discharge plasma in a toroidal assembly	137
8.1	Introduction	139
8.2	Floating potential fluctuation, power spectral analysis, phase space plot	141
8.2.1	Increasing DV, vertical and toroidal magnetic field (B_V, B_T)	141
8.3	Evolution of Fireballs with DV, B_V, B_T, B_{V+T}	143
8.4	Method of analysis: path length, phase coherence index	149
8.5	Results of detrended fluctuation analysis (DFA)	153
8.6	Conclusion	156
9	Overall Conclusion	159
9.1	A quick recapitulation	160
9.2	Future prospects and conclusive remarks	167

Synopsis

The contents of this thesis are mainly centered around the investigation of nonlinearity, complexity dynamics and the evidence of phase coherence in floating potential fluctuation (FPF) acquired from the self and externally excited glow discharge plasma (GDP). A detailed analysis of the study of nonlinearity has been carried out for increasing discharge voltage (DV), externally applied sinusoidal forcing as well as magnetic field using methods based on surrogate data technique. Most statistical signal nonlinearity analyses adopt the approach namely the surrogate data method [1, 2] which is generated as a realization of the null hypothesis of linearity. A measure (test statistic) is computed for the original time series and it is compared to those computed for an ensemble of surrogates. If the test statistic computed for the original is significantly different from that computed for the surrogates, the null hypothesis is rejected, and the original time series is judged nonlinear.

Nonlinear dynamics started with the work of Henri Poincare in the late 1800s to solve the three body problem. Things like predictability, nonlinearity [3, 4] have gained ample attention from various areas of science like physiology, earth science [5], geoscience [6], biology or especially complex plasma system which is a typical complex medium exhibiting a wide variety of nonlinear phenomena such as self oscillations, chaos and intermittency [7, 8]. The investigation of nonlinearity and the introduction of new methods for nonlinear time-series analysis are of great interest in this context. The effect of nonlinearity is manifested as hysteresis [9], wave breaking [10], chaos and turbulence [11], and different kinds of coherent structures like solitons [12] and shocks. Sudeshna et al. [13] have observed the phenomena of hysteresis in amplitude and frequency bifurcations of floating potential fluctuations in glow discharge plasma. Koenke et al [14] have identified a

verify the existence of the underlying nonlinear processes that convey information concerning the absence or presence of nonlinearity. In the field of biomedical signal processing [17] techniques such as electrocardiogram, electroencephalogram reveal information about nonlinearity that help us to glean about health condition.

Much effort has been endeavoured to study the intricacies involving the topics like finite nonlinear interactions and its associated phase coherence index. The investigation of the nonlinear wave wave interaction is based on the decomposition of a signal into its amplitude and phase part albeit we have to assume implicitly weak nonlinearity. From this point of view the amplitude along with the phase information obtained from the Fourier transform is convenient for our analysis permitting us wave number/frequency decomposition. Koga et al. have evaluated the experimental evidence of phase coherence index [18, 19] of magnetohydrodynamic turbulence in the solar wind. The result demonstrate the existence of finite phase correlation indicating the nonlinear wave wave interaction are in progress. Structure function or path length analysis [19, 20] bears a significant aspect in this regard. Besides the approach nonlinearity, phase coherence index, the aspect of nonstationarity [21] have also gained ample attention in the field of time series analysis encompassing a wide range of interdisciplinary phenomena. Many signals that are output of complex physical and biological system [22] are said to contain the trace of nonstationarity. Almost all methods of time series analysis, traditional linear or nonlinear, must assume some kind of stationarity. A number of statistical tests for stationarity [23] in a time series have been proposed in the literature. Most of the tests we are aware of are based on ideas similar to the following: Estimate a certain parameter using different parts of the sequence. If the observed variations are found to be significant, that is outside the expected statistical fluctuations, the time series is regarded as nonstationarity which allows us carrying out modified root mean square analysis termed as detrended fluctuation

fluctuations self similarity and scaling in physics and socio economic sciences in the last several years has brought in new insights and new ideas for modeling them. For instance one of the important empirical results of the market dynamics is that the probability distribution of price returns r in a typical market displays a power law i.e $P(r) \sim r^{-\alpha}$ with α being the power law exponent and $\alpha = 3$.

In our first study we have investigated the appearance of inverse and normal homoclinic bifurcation and the associated complexity dynamics in the relaxation oscillations of the glow discharge plasma system (GDP) exhibiting an order-chaos-order transitions. In order to comprehend the complex dynamics, we have carried out a detailed analysis using standard nonlinear techniques like Correlation dimension (CD) [26] and largest Lyapunov Exponent (LLE) for the two regimes of observations. The estimation of Renyi number conforms well with the observations of complexity in the fluctuating data. In the second chapter we have described elaborately our experimental setups, diagnostics and acquainted us with various nonlinear techniques required for data analysis and interpreting the system dynamics. The experiments were conducted in a cylindrical hollow cathode glow discharge argon plasma with a typical density and temperature of $\sim 10^7/cm^3$ and 2-4eV respectively. It has a cylindrical cathode of length and diameter ~ 17 cm and ~ 10 cm, respectively, and a central anode rod of diameter ~ 1.6 mm. The whole assembly was mounted inside a vacuum chamber and was pumped down to a pressure of about 0.001 mbar using a rotary pump. To carry out the observations in presence of magnetic field, an external magnetic field (axial) was applied to the plasma by passing a steady current through the coils wound over the cylindrical chamber. GDP operating under steady state conditions is subjected to an oscillatory external voltage that constitutes forcing. For this, a signal generator was coupled with the discharge voltage (DV) through a capacitor. We have also conducted our experiment in the toroidal vessel of SINP tokamak with major radius of

excited due to nonlinear processes. Rejection of null hypothesis has been verified by performing the rank test method that further confirms the presence of nonlinearity quantitatively. In the next chapter we have explored the feature of nonlinearity in an experimental time series data obtained in the FPF's of GDP for various values of external forcing as well as magnetic field (B) by providing some easy to interpret diagrams obtained using the novel DVV analysis. An estimate of the Zscore [28] has been carried out to detect the presence of nonlinearity in a somewhat quantitative sense. The experimental DVV plots have been compared with those obtained from the numerical model depicting ion acoustic fluctuation in presence of ionization and recombination effect. An informal test for bicoherency has been applied to detect the interaction amongst different modes obtained by performing empirical mode decomposition to strengthen the analysis on nonlinearity. The nonlinear effects obtained from DVV plots turn out to be almost similar with the results of bicoherency analysis and quantitative estimation of Zscore confirming the robustness of all the methods.

After exploring the nonlinearity with increasing DV, forcing, magnetic field we approach to find the evidence of finite nonlinear interaction in GDP by estimating phase coherence index for different types external forcing techniques likewise noise, sinusoidal, square etc to characterise the correlation of phases among Fourier modes in a given time series by employing surrogate data technique. The existence of finite phase coherence index (C_ϕ) i.e finite correlation corroborates our nonlinearity analysis using DVV. The positive correlation in the value of C_ϕ are in agreement with the finite nonlinearity. Origin of this type of correlation is illustrated using continuous wavelet transform with Morlet wavelet. Characterization of the difference in the phase distribution by the difference in the waveform in real space instead of dealing in Fourier space has been facilitated by introducing structure function or path length for different orders to study and identify the dynamical

experiments in the glow discharge plasma of toroidal vacuum vessel of the SINP tokamak to observe the interplay of transition of floating potential fluctuations and its associated phase coherence index. Fluctuations display nearly regular \rightarrow relaxation oscillations \rightarrow inverted relaxation oscillations \rightarrow regular sinusoidal oscillations. However for small value of toroidal magnetic field the transitions follow relaxation \rightarrow chaotic oscillations \rightarrow and prevails that chaotic nature with high value of toroidal magnetic field. Evolution of the associated anode fireball dynamics under the action of vertical, toroidal magnetic fields as well as the composition of the both field with different strengths has been presented.

Glow discharge plasma being rich in high energy electrons and ions are capable of exhibiting many such nonlinear phenomenon mentioned above and are widely used in various industrial applications [29]. Nonlinear phenomena including nonlinear structures are observed in laboratory plasmas, fusion devices, radiofrequency plasmas, microwave devices, and in naturally occurring plasmas such as in magnetosphere, inter stellar plasma. Interpretation of any plasma phenomena is dependent on an understanding of nonlinear dynamics. So as an potential application of our work we can suggest characterising the devices using various nonlinear methods and techniques which is extremely beneficial in improving their performance. We also believe that our work will enrich the understanding of the concept of nonlinearity not only in GDP but also in other plasma devices.

The submission of this synopsis is recommended and approved by the Doctoral committee.

Bibliography

- [1] Thomas Schreiber, Andreas Schmitz, *Physica D* **142**, 346382 (2000)
- [2] D. Kugiumtzis, *Physical Review E* **60**, 2808-2816 (1999)
- [3] Thomas Schreiber and Andreas Schmitz, *Physical Review E* **55**, 5443 (1997)
- [4] Holger Kantz and Thomas Schreiber (Cambridge University Press, New York, 2003) 48-58
- [5] Bradley Matthew Battista, Camelia Knapp, Tom McGee and Vaughn Goebel, *Geophysics* **72**, H29 (2007).
- [6] D Koga, A.C.-L Chian, T Hada and E.L Rempel, *Phil. Trans. R. Soc. A*, **366** 447-457, 2008
- [7] S. Ghosh, Pankaj Kumar Shaw, A. N. Sekar Iyengar, M. S. Janaki, Debajyoti Saha, Alpha Michael Wharton, and Vramori Mitra, *Physics of Plasmas* **11**, 032303 (2014)
- [8] Pankaj Kumar Shaw, Debajyoti Saha, Sabuj Ghosh, M.S. Janaki, A.N. Sekar Iyengar, *Chaos Solitons and Fractals*, **78**, 285-296, 2015

[9] A. M. Delgado, G. A. M. de Lencastre, T. J. M. de Lencastre, P. B. P. de Lencastre, and W. G.

- [13] S. Lahiri, D. Roychowdhury, and A. N. S. Iyengar, Phys. Plasmas **19**, 082313 (2012).
- [14] M. E. Koepke, T. Klinger, F. Seddighi, and A. Piel Phys. Plasma **3**, 4421, (1996)
- [15] Md. Nurujjaman, A. N. Sekar Iyengar, Physical Review E, **82**, 056210, (2010)
- [16] T. M. Flanagan and J. Goree, Phys. Plasmas **18**, 013705 (2011)
- [17] T. Schreiber, Phys. Rep. **308**, 2 (1999).
- [18] D. Koga, A. C.-L. Chian, T. Hada and E. L. Rempel, Phil. Trans. R. Soc. A, **366**, 447-457
- [19] T. Hada, D. Koga, E. Yamamoto, Space Science Reviews, **107**:463-466, (2003)
- [20] Budaev V.P, Savin S, Ohno N, Takamura S., Plasma Phys Control fusion2008; **50**:7
- [21] C.K. Peng, Shlomo Havlin, H. Eugene Stanley, Ary L. Goldberger, Chaos, **5**, 1, 1995
- [22] S.L. Gonzalez Andino, R. Grave de Peralta Menendez, G. Thut, L. Spinelli, O. Blanke, C.M. Michel, M. Seeck, and T. Landis, Human Brain Mapping **11**, 46-57 (2000)
- [23] C.K. Peng, J. Mietus, J.M Hausdorff, Shlomo Havlin, H. Eugene Stanley, Ary L. Goldberger, Phys Review Letter, **70**, 1343-1346, 1993
- [24] Md. Nurujjaman, A.N. Sekar Iyengar, Phys Letters A, **360**, 717-721, 2007

- [29] Michael A. Lieberman, Allan J. Lichtenberg, 2005, Principles of Plasma Discharges and Materials Processing, (John Wiley and Sons).

List of Figures

2.1	Schematic diagram of experimental setup for glow discharge plasma with external forcing and magnetic field	21
2.2	Schematic diagram of the measurement circuit	21
2.3	Picture of the dc glow discharge plasma device: 1) Vacuum chamber, 2) Stand, 3) High voltage power supply, 4) Argon gas cylinder, 5) Rotary pump, 6) Digital oscilloscope, 7) Pressure reading meter, 8) Langmuir probe, 9) Power supply connection, 10) Pressure control unit: needle valve, 11) Pirani gauge, and 12) Side cylindrical chambers attached with main vacuum chamber	22
2.4	Schematic diagram of the experimental setup for glow discharge plasma in a toroidal assembly	23
2.5	Picture of the glow discharge plasma in a toroidal assembly: 1) Viewing port 2) Vertical magnetic field coils, 3) Pressure control unit 4) Toroidal magnetic field coils 5) Constant current source 6) Pressure reading meter 7) Place for inserting Langmuir probe . . .	24
2.6	Picture of the Langmuir probe used in the experiments	25
3.1	Experimental setup for glow discharge plasma	49
3.2	Sequential change in the raw signal at 0.490 mbar for different DV(volts): (a) 412V (b) 429 V (c) 436V (d) 440V (e) 446V (f)	

3.6	Noise to signal ratio with variation in DV	53
3.7	Plot of frequency spectrum at DVs a) 412V (b) 429V (c) 436 V (d) 440V (e) 446V (f) 451V (g) 453V (h) 455V (i) 458V (j) 462V (k) 468V (l) 469 V (m) 488V (n) 495V for the left figure and DVs for the right figure (o) 514V (p) 521V (q) 549V (r) 565V (s) 570V (t) 578V (u) 605V (v) 615V (w) 625V (x) 650V (y) 680V (z) 700V . . .	53
3.8	Contour Plot of Fourier spectrum with variation in discharge voltages	54
3.9	Frequency spectrum at different discharge voltages	55
3.10	Plot of correlation dimension (CD) with embedding dimension(m) for a particular DV=549volt	55
3.11	Plot of (a) Correlation dimension (d), (b) Largest Lyapunov exponent (LLE) and (c) Renyi entropy (R) with DV	56
3.12	Amplitudes of the numerical solutions with the variation in A and their corresponding phase space plots	57
4.1	Sequential change in the FPF and frequency spectrum at 0.085 mbar for different DV(in volts) in the left and right panel respectively: (a) 335V (b) 337 V (c) 341V (d) 350V (e) 355V (f) 361V (g) 369V (h)378V	67
4.2	Plot of dominant frequencies with different DVs (volt)	67
4.3	Sequential change in the raw signals at 0.056 mbar for different DV(volts): (a) 320V (b) 328 V (c) 338V (d) 344V (e) 350V (f) 357V (g) 365V (h)372V (i)378V (j)384V (k)390V (l)395V (m)402V (n)410V	68
4.4	Plot of frequency spectrum at DVs are (a) 320V (b) 328 V (c) 338V (d) 344V (e) 350V (f) 357V (g) 365V (h)372V (i)378V (j)384V (k)390V (l)395V (m)402V (n)410V	68

4.9	Sequential change in DVV scatter plots for $P=0.056$ mbar volt with DVs are a) 320V b) 328V c) 344V d) 365V e) 372V f) 384V g) 395V h) 402V i) 410V	73
4.10	Contribution of the sum of power in different DV (in volt) for $P=0.056$ mbar	74
4.11	DVV scatter plots for $P=0.085$ mbar for a) DV=335V b) DV=341V c) DV=350V d) DV=355V e) DV=361V f) DV=378V	76
5.1	Plot of rawsignal as well as Fourier spectrum with amplitude of sinusoidal forcings (A) are 0, 2, 3, 5, 6, 8 volt for $P=0.085$ mbar . .	83
5.2	Contour Plot of Fourier spectrum with amplitude of sinusoidal forcings (A) for $P=0.085$ mbar	83
5.3	Plot of FPFs and amplitude of peaks from FFT with variation of forcing (A) for $P=0.180$ mbar	83
5.4	Plot of rawsignal as well as power spectrum with magnetic field strengths 0, 15, 30, 60, 90, 105 Gauss	84
5.5	Correlation dimensions of floating potential fluctuations shown for increasing magnetic field	85
5.6	Plot of Zscores of Renyi entropy, E_r statistics for different values of B and A	85
5.7	Sequential change in DVV scatter plots for $P=0.085$ mbar with magnetic field strength: B=0, 30G, 60G, 90G, 105G	87
5.8	Sequential change in DVV scatter plots with forcing amplitudes(A) are 0V, 2V, 3V, 5V, 6V, 8V	87
5.9	Contribution of the sum of power with different B (in Gauss)	91
5.10	Bicoherency factor for A a) 0V b) 2V c) 3V d) 5V e) 6V	92
5.11	Bicoherency factor for B a) 0G b) 30G c) 60G d) 90G e) 105G . . .	92

6.2	Noise by signal ratio with increase in amplitude of the a) sinusoidal b) square forcing	107
6.3	Recurrence plots for different types of forcing: a) No forcing b) Noise (A=4V) c) Square (A=1V) d) Square (A=2V) e) Sinusoidal (A=1V) f) Sinusoidal A=5V	107
6.4	Recurrence plot with increase in the amplitudes of sinusoidal forcing (A)	108
6.5	Original raw signal decomposed into its amplitude and phase part .	109
6.6	Distribution of wave phases for original FPF (ORG), phase-randomized surrogate (PRS) and phase-correlated surrogate (PCS) from upper to lower panel	109
6.7	Path length $S(\tau)$ with increasing order no (m) for a) noise forcing b) square forcing and $S(\tau)$ with ORG, PRS, PCS for c) sinusoidal forcing in the lower panel	111
6.8	Path length $S(\tau)$ for increase in amplitude of different types of forc- ing (A) a) Noise forcing b) Sinusoidal forcing c) Square forcing . . .	112
6.9	Profile of phase coherence index with τ for a) no forcing b) noise c) sinusoidal forcing d) square forcings with A=2V	113
6.10	Phase coherence index values with the amplitude and frequency of noise, sinusoidal , square forcing	114
6.11	Continuous wavelet transformation of that fluctuation containing a) maximum C_ϕ with square forcing in the left panel b) small C_ϕ for sinusoidal forcing	114
6.12	DVV scatter plots for increasing noise amplitudes : a) 0V b) 3V c) 5V d) 7V e) 9V	116

7.2	plot of kurtosis, skewness, time reversal t_{rev} , and third autocovariance t_{C3} at different segments of the time series for a) noise b) sinusoidal c) square forcing with $A=2V$	128
7.3	Integrated time series superposed on least square fitted trend	129
7.4	Plot of $\log F(n)$ vs $\log(n)$ for increase in a) sinusoidal forcing b) square forcing c) sinusoidal forcing on FPF for $P=0.04\text{mbar}$	132
7.5	Variation of scaling exponent with increase in amplitudes of the sinusoidal as well as square forcing for $P=0.12\text{mbar}$	132
7.6	Shift in the values of α from low n to high n for sinusoidal forcing applied on fluctuation acquired for $P=0.04\text{mbar}$	133
7.7	Plot of $\log F(n)$ vs $\log(n)$ for no forcing and different types of forcing i.e noise, sinusoidal, square applied with $A=2V$ for $P=0.12\text{mbar}$. .	133
7.8	Plot of $\log F(n)$ vs $\log(n)$ for increase in a) sinusoidal forcing ($A=2V$) and the same plot for increase in b) square forcing with $A=2V$ for $P=0.12\text{mbar}$	133
8.1	Sequential change in the raw signals and frequency spectrum for different DV (in Volts) in the left and right panel respectively: a) 390V b) 400V c) 410V d) 420V e) 430V f) 450V g) 460V h) 480V i) 500V j) 520V k) 550V l) 600V	144
8.2	Plot of FPF and power spectrum with the variation in B_V a)0G b) 3.36G c) 3.65G d) 4.21G e) 6.17G f) 7.29G g) 7.57G h) 8.70G i) 9.54G j) 10.11G k) 11.23G l) 11.79G for $DV=0.44\text{kV}$	144
8.3	Plot of FPF and power spectrum with the variation in B_T in the left and right panel respectively: a)0G b) 1.28G c) 2.30G d) 3.07G e) 5.63G f) 7.098G g) 8.06G h) 8.76G i) 8.98G j) 9.6G k) 10.24G l) 11.2G m) 11.52G n) 11.84G o) 12.8G p) 14.4G for $DV=0.44\text{kV}$. . .	145

8.6	Dominant frequency with the variation in a) Discharge voltage(DV) b) Vertical magnetic field (B_v) c) Toroidal magnetic field (B_T) d) Vertical field at fixed B_T of 8.45G (B_{V+T})	147
8.7	Photograph of the anode glow with variation in DV a) 390V b) 400V c) 420-440V d) 460V e) 520V	149
8.8	Sequential change in the anode glow for increasing vertical magnetic field B_V a) 3.65G b) 4.21G c) 6.18G d) 7.29G e) 8.70G f) 9.54G g) 10.10G h) 11.23G i) 11.79G for DV=0.44kV	149
8.9	Sequential change in the glow for increasing toroidal magnetic field B_T a) 1.28-2.30G b) 3.07-5.63G c) 7.09G d) 8.06-8.98G e) 9.6G f) 10.24G g) 11.2-11.84G h) 11.84-14.4G for DV=0.44kV	150
8.10	Photographs of the anode glow for increasing B_{V+T} a) 0.84G-2.47G b) 4.09-7.02G c) 8.98-10.67G d) 12.63G	150
8.11	Profile of phase coherence index with τ for a) $B_T = 9.6G$ b) $B_{V+T} =$ $12.63G$	152
8.12	Plot of phase coherence index with variation in a) Discharge volt- age(DV) b) Vertical magnetic field (B_V) c) Toroidal magnetic field (B_T) d) Vertical field at fixed B_T (B_{V+T})	153
8.13	Plot of $\log F(n)$ vs $\log(n)$ for increasing toroidal voltage a) 0G b) 1.28G c) 5.63G d) 7.09G e) 8.06G f) 8.98G in the left panel and a) 9.34G b) 10.24G c) 11.52G d) 11.84G e) 12.8G f) 14.4G	155
8.14	Plot of $\log F(n)$ vs $\log(n)$ increasing B_V at fixed B_T (B_{V+T}) a) 0.84G b) 2.47G c) 5.61G d) 7.01G e) 10.66G f) 12.63G	155

List of Tables

4.1	Results of the rank test of nonlinearity with varying DV for P=0.056 mbar	73
4.2	Results of the rank test of nonlinearity for P=0.085 mbar	76
5.1	Results of the rank test of nonlinearity with varying magnetic field (B) for P=0.085 mbar	89
7.1	Results of the quantitative values of the scaling exponent for forcing applied on FPF's obtained at low P=0.04 mbar	134
7.2	Scaling exponent values for increasing frequencies of square and si- nusoidal forcing for P=0.12mbar	134
8.1	Results of the quantitative values of the scaling exponent for in- creasing discharge voltage (DV) and vertical magnetic field (B_V) .	156

Chapter 1

Introduction

The objective of this thesis is to contribute to the investigation of nonlinearity, complexity dynamics in a self and externally excited DC glow discharge plasma. A detailed analysis for the detection of nonlinearity has been carried out in floating potential fluctuations (FPF) measured in the glow discharge plasma for various values of discharge voltage, externally applied sinusoidal perturbations as well as magnetic field. We introduce delay vector variance analysis (DVV) for the first time in our analysis of experimental floating potential fluctuations acquired from glow discharge plasma, which allows reliable detection of nonlinearity and provides some easy-to-interpret diagram conveying information about the nature of the FPF. The emergence of nonlinearity has been ensured by taking into consideration the

observe the critical regime dynamical transitions. The existence of finite nonlinear interaction has been demonstrated by estimating phase coherence index using a method based on the surrogate data technique. A comprehensive study of the dynamics of the fireball in the glow discharge plasma in a toroidal vacuum vessel has been corroborated with the values of phase coherence and scaling index estimated using detrended fluctuation analysis (DFA). An attempt to model the experimental observations by a second order nonlinear ordinary differential equation derived from the fluid equations of plasma has validated our experimental results. The origin of the self and externally excited oscillations has also been explained from the perspective of plasma physics. Before going deep into the investigation, we present a brief historical overview on the past works as well as the motivation of studying nonlinearity and nonstationarity, phase coherence index in self, externally excited glow discharge plasma.

1.1 Plasma Physics: An introduction and its importance

Neutral gas transforms into a cloud of electrons and ions when its molecules/atoms are ionized by some means of energy absorption mechanisms (electron impact, photo-detachment, photo-ionization, electrical discharge etc.). In this process, a partially or fully ionized gas of negative electrons and positive ions and/or neutrals may be formed. The cloud is generally known as plasma and the state is known to be the fourth state of matter. Examples of plasma are ubiquitous i.e in the sun, in the solar wind, in the magnetosphere and the ionosphere, in fluorescence tube, in flames, etc. In fact, most of the matter (~ 99 percent) in the known universe exists as plasma. The word plasma comes from the Greek and means something molded. It was applied for the first time by Tonks and Langmuir [1] in 1929 to describe the inner region remote from the boundaries, of a glowing ionized gas produced by electric discharge in a tube, the ionized gas as a whole remaining electrically neutral. The most important application of the man made plasmas is in the control of thermonuclear fusion reactions which hold a vast potential for the generation of power. The nuclear fusion reaction is the source of energy in the stars including the sun. So for studying various phenomena occurring in the magnetosphere and

dynamics of a system involving such a huge number of particles interacting over a large scale. It is obvious that charge particles (ions and electrons) would respond collectively to any applied electromagnetic fields or internal perturbation through long range electromagnetic interactions and would try to shield, i.e., minimize their effects on plasma. This collective behavior then suggests that the motion of charge particles not only depend on local conditions, but also on the state of the plasma in remote regions as well. Thus, the wealth of important physical phenomena arises in plasma because of the collective effect, where a charged particle interacts simultaneously with a large number of other charged particles. Due to these features of plasma, it can be considered as a complex system.

1.2 Brief historical backdrop of Nonlinearity and relevance with Plasma Physics

The origin of nonlinear dynamics dates back to mid 1600's in the guise of planetary motion, when Newton discovered his laws of motion and universal gravitation and invented the theory of differential equations to solve the two body problem: the motion of earth around the sun, given the inverse square law of gravitational attraction between them. The force being nonlinear in nature gave rise to nonlinear differential equation of motion, embarking the development of nonlinear dynam-

qualitative nature of the solutions rather than quantitative questions. The advent of high speed computers in 1950's served as the stepping stone for nonlinear dynamics. It accelerated the study of nonlinear systems by allowing the exploration of equations via numerical simulations which were impossible before. Following Lorenz's discovery of chaos [2] the subject of nonlinear dynamics has gained ample attention and found its application in various areas of science like fluid mechanics [7], earth science [3], geoscience [4], biology [5]. In any physical system it is of utmost significance to detect the presence of nonlinearity and identify the underlying nonlinear process. Due to the interdisciplinary nature of nonlinear dynamics, it has found numerous applications throughout the realms of physics, biology, engineering, chemistry [6], especially complex plasma system [8, 9]. Dissipative physical system like plasma being highly nonlinear dynamical medium with a large number of degrees of freedom is capable of sustaining a wide spectrum of waves, instabilities and the nonlinear coupling between the waves results in several interesting phenomena such as self-oscillation, period doubling, bifurcation, period subtracting, period adding, chaos, intermittency and various complex structures [10, 11, 12]. DC glow discharge plasma, which is widely used in various applications like laser production, plasma processing [13], exhibits different types of nonlinear oscillations [24] depending on the control parameters like neutral pressure

[7] proposed a new theory for the onset of turbulence in the fluids. Those attempting to evaluate the practical relevance of this subject confront a confusing array of terms and concepts, such as non-linearity, fractals, periodic oscillations, bifurcations, and complexity, as well as chaos [16]. Feigenbaum in the late 70s discovered the universal constant called the Feigenbaum constant to characterize the universal features of the period doubling bifurcation [17], one important class of abrupt, non-linear transitions. Later bifurcation diagrams, Lyapunov exponent, correlation dimension, etc., derived on the basis of chaos theory, have been used to characterize chaos and its different routes. Study of the nonlinear processes in plasmas started in the sixties. Many nonlinear phenomenon had been observed and nonlinear dynamics experiments had been performed in different types of laboratory plasmas. Since the development of nonlinear dynamics, most applications have been in the field of fluid dynamics, particularly fluid turbulence and as fluid and plasma turbulence are closely related, the concepts of nonlinear dynamics have been successfully utilized in plasmas. Koepke et al. [18] have identified a periodic nonlinear interaction between pairs of self-excited, propagating, ionization waves simultaneously present in the positive column of a neon glow discharge with no external oscillatory driving force. In one of the theoretical works by Chung and Yoon [19], they have shown that in an RF plasma system, period

synchronization of paced chaotic plasma discharge have been reported by Ticos et al.[25]. Current and plasma potential in a magnetized thermionic plasma discharge have been investigated by Klinger et al.[26]. Investigation of nonlinearity using harmonic detection method [27, 28] has been performed in RF discharge and glow discharge plasma respectively. M. Ciszak et al. [29] studied the response of excitable systems driven by random forcing. Talking about the phase coherence, Koga et al. [30] introduced a method to examine the experimental evidence of phase coherence index [32, 31] of magnetohydrodynamic turbulence in the solar wind. The result demonstrate the existence of finite phase correlation indicating that nonlinear wave wave interaction are in progress. Their discovery serves as an excellent subject for the research of nonlinear phenomena in the solar wind of magnetohydrodynamic turbulence (MHD) which is ubiquitous in space. In their study the phase correlation in MHD turbulence observed by the geotail satellite near the upstream region of earth bow shock was evaluated.

1.3 Definition of nonlinearity and approach to complexity dynamics

Nonlinearity of a system is defined as a property which indicates a system response that is not directly proportional to the input. From our everyday perception we

of surrogates. If the test statistic computed for the original is significantly different from that computed for the surrogates, the null hypothesis is rejected, and the original time series is judged nonlinear which is taken to be the definition of nonlinearity in this thesis work. A novel delay vector variance (DVV) method for detecting the presence of nonlinearity in a time series is introduced. This provides consistent and easy-to-interpret diagrams, which convey information about the nature of a time series using the optimal embedding dimension of the original time series. One of the key issues in signal nonlinearity analysis is the definition of a linear signal. Linear systems are well behaved. Further, linear systems can be fully understood and predicted by dissecting out their components. The sub-units of a linear system add up so there are no surprises or anomalous behaviours. The standard definition is that such a signal is generated by a Gaussian linear stochastic process. A linear signal x , is generally defined as the output of a linear shift-invariant system that is driven by Gaussian, white noise. By contrast, for non-linear systems proportionality does not hold: small changes can have striking and unanticipated effects. Another complication is that non-linear systems cannot be understood by analysing their components individually. In terms of mathematics linear phenomenon are describable by equations in which dependent variable occurs to no higher than the first power. This is generally called the

amplitude exponentially. A wave can undergo a number of changes such as changing its shape when its amplitude gets large. This is same as saying that Fourier components at other frequencies are generated. Nonlinear effects also occur when a large amplitude plasma wave is excited by an external means. For example, the dispersion in the ion acoustic wave can be counter-balanced by nonlinearity and an ion acoustic soliton can propagate without appreciable deformation. Nonlinear effects tend to limit the growth of instabilities through nonlinear saturation. Also, through mode coupling, energy transfer occurs toward modes which are linearly stable. From the perspective of the concept of plasma physics, modes with growing amplitudes resulting from the various instabilities would attribute to the study of nonlinearity. So the conventional plasma physics would generally give emphasis on oscillation from the spectral point of view such as the identification of frequencies, measuring the amplitude of the frequency carrying maximum power, detecting the interaction amongst the dominant modes. In a rf dusty plasma experiment, Flanagan and Goree [27] have studied nonlinearity in a naturally occurring dust density wave using neutral gas pressure as the control parameter, with the nonlinearity indicated by the presence of harmonics and quantified by total harmonic distortion. Now from the perspective of nonlinear dynamics the analysis of the nonlinearity resting on the surrogate data strategy can often provide insights

combination with the surrogate data method, the measures yield a reliable two tailed test for nonlinearity. The concept of complexity dynamics encompassing the broader area of nonlinearity (including phase coherence), chaoticity is also well explored in our thesis work. So far the following approaches have been undertaken to illustrate the idea of complexity dynamics of the fluctuations associated with noise both qualitatively and quantitatively. a) Entropy measures (Renyi Entropy) derived in the framework of information and calculated on the basis of probabilistic models. b) Estimate of correlation dimension on the basis of Gaussian kernel algorithm, Grassberger Proccacia techniques c) Recurrence plot in conjunction with recurrence quantification measure to identify the transitions between the different complex states d) Detrended fluctuation analysis technique for characterizing the persistent behaviour of the plasma time series to explore the complexity in terms of long range correlation. Our work presented in this thesis work enrich the complexity study of the plasma instability and its associated nonlinear dynamical phenomenon.

1.4 Nonlinear Oscillations in Plasma and transitions amongst them

A plasma is inherently a nonlinear medium and the waves and oscillations that

Under various operating conditions the glow discharge plasma device has given way to numerous experimental observations. Periodic, different kind of intermittent oscillations [35, 36], relaxation oscillations [11], various types of chaos etc. are a few among many nonlinear oscillations observed in the plasma systems. If any oscillatory motion repeats itself about after equal intervals of time then such oscillation is called periodic oscillation. The plasma system that can exhibit nice relaxation oscillations is capable of manifesting chaotic oscillations. Talking about chaos it is a long term aperiodic behaviour in a deterministic system, and shows sensitive dependence on initial conditions. Chaotic dynamics are neither recurring nor settles down to a particular fixed point and are possible only for the system having phase space dimension ≥ 3 . It is often observed in plasma system that one kind of nonlinear oscillation transforms into another kind of nonlinear oscillation when some control parameter is varied. Sometimes very small change in the system parameters can trigger this kind of a transition. This qualitative changes in the dynamics of the system with the change in the control parameter values are generally classified as bifurcation and the parameter values at which they occur are called bifurcation points. Bifurcations are important scientifically as they provide models of transitions and instabilities when some control parameter is varied. Amongst several kind of bifurcations there are scenarios like homoclinic and in-

a particular kind of nonlinear oscillation can be observed in various systems but to find a system that can exhibit various kinds of nonlinear oscillations is not that trivial. For that kind of a system our consideration is that of a plasma system.

1.4.1 Motivation to study the nonlinearity, phase coherence index in glow discharge plasma

Plasmas are intrinsically nonlinear whose effects manifest in the form of various exotic structures such as double layers, solitons, vortices, different types of waves, instabilities and turbulence. Glow discharge plasmas being rich in high energy electrons and ions are capable of exhibiting many such nonlinear phenomena. Non-linear phenomena including nonlinear structures are observed in laboratory plasmas, fusion devices, radio-frequency plasmas [40], microwave devices [41], laser devices[42] and in naturally occurring plasmas such as in magnetosphere, interstellar plasma. Interpretation of any plasma phenomena is dependent on an understanding of nonlinear dynamics. Characterising the devices like GDP and their counterparts such as magnetrons [39] used in the industrial application with the help of various nonlinear methods and techniques is extremely beneficial in improving their performance. So exploring the idea of nonlinearity is important not only for glow discharge plasma but also for many other devices. Hence nonlinearities

geometry with the scope of applying different magnetic fields. The study of matters pertaining to phase information can be best explored by the study of phase coherence index. A wealth of nonlinear phenomena can be found in the solar wind especially in the vicinity of planetary bow shock interplanetary shocks wherein the magnetic, electric field and velocity fields show turbulent fluctuations. MHD turbulence is considered to play crucial role in heating of plasma and acceleration of energetic particles. In space plasma research in the context of geomagnetic pulsation and the power law type spectrum of magnetic field turbulence [43] amplitude spectrum has always been in discussion in the literature for many years. The investigation of the nonlinear wave wave interaction is based on the decomposition of a signal into its amplitude and phase part albeit we have to assume implicitly weak nonlinearity. From this point of view the amplitude along with the phase information obtained from the Fourier transform is convenient for our analysis permitting us wave number/frequency decomposition. The phase distribution on the other hand has not achieved much attention in space plasma application. A possible reason may be that the phase distribution in Fourier space appears to be completely random. In fact the purpose of their work was to discuss the experimental evidence of nonlinear wave-wave interaction in MHD turbulence detected in the solar wind. Their results prove that the finite phase coherence is the origin

biomedical signals, such as heart rate variability (HRV), electrocardiogram (ECG), hand tremor and electro-encephalogram (EEG) [48], there is a need to assess the presence or absence of nonlinear behaviour within the signal, as opposed to that of the system, because the linear/nonlinear nature of the signal conveys information concerning the health condition of a subject. Although there exist several established methods for performing signal nonlinearity analysis, the outcome of a test, e.g., the rejection of a null hypothesis of linearity ensured from surrogate data analysis [33, 45], needs to be interpreted with due caution. For real-life time series, estimation of invariant quantities are not problem free. Further, both correlated stochastic noise and noise-free deterministic signals produce convergent invariant measures, a sign of low-dimensional nonlinearity. Thus, any absolute quantity does not provide concrete information about the underlying dynamics. Now, a chaotic system is a low-dimensional nonlinear system. So, the detection of nonlinearity is a necessary condition for observation of chaos. The variety of approaches with the difficulty of interpretation of the results, clearly indicate the need for a unifying approach with straightforwardly interpretable results which is consummated especially using surrogate data analysis and backed by physical interpretation.

1.4.3 Time series Analysis: Its Motivation

study. A time series is nothing but a sequence of data points of an observed variable at equally spaced time intervals. Many quantities in nature fluctuate in time. Examples are the stock market, the weather, seismic waves, sunspots, heartbeats, and plant, animal populations. Until recently it was assumed that such fluctuations are a consequence of random and unpredictable events. With the discovery of chaos, it has come to be understood that some of these cases may be a result of deterministic chaos and hence predictable in the short term and amenable to simple modeling. The fluctuations that we have studied in this thesis were recorded in the form of time dependent floating potential fluctuations. With probability law governing the time series formulated by the statisticians , we can understand the underlying dynamics, forecast future events, and control them via suitable intervention. The analysis of a time series should be able to detect the stochastic [60]or deterministic nature of the underlying process, the presence of nonlinearity or non-stationarity[61] and finally the predicability of the future states. Time series analysis can be categorized in two classes: linear and nonlinear time series analysis. Examples of time series include

- Weather [62], ECG and EEG data [63]
- Financial markets [64]

analysis while the latter consists of estimating the auto-correlation and cross-correlation in the time series. Linear analysis tools treat all the irregular or chaotic behavior as a stochastic processes though these instabilities may be generated by deterministic dynamics. Based on chaos theory, nonlinear tools have been developed to characterize such complicated data. Nonlinear methods (for chaotic underlying dynamical system) consist of estimating or analysing the following

- State space reconstruction [69]
- Correlation dimension and Entropy [71]
- Lyapunov exponent [73]
- Surrogate data [68]
- Recurrence plot [74]
- Multifractal spectrum [75]
- Principle component analysis [76]

So many tests have been developed to determine whether a time series is random or chaotic, and if the latter, to quantify the chaos. Chaos refers to a seemingly random type of variability that can arise from the operation of even the most simple

1.4.4 Nonstationarity, Detrended fluctuation analysis and its motivation

Almost all methods of time series analysis, traditional linear or nonlinear, must assume some kind of stationarity [61]. Traditional approaches such as power spectrum, correlation analysis are suited to quantify correlations in a stationary signal [77, 78]. However many signals that are output of complex physical [79] and biological system are said to contain nonstationarity. A number of statistical tests for stationarity [80, 82] in a time series have been proposed in literature. Most of the tests we are aware of are based on ideas similar to the following: Estimate a certain parameter using different parts of the sequence. If the observed variations are found to be significant, that is, outside the expected statistical fluctuations, the time series is regarded as nonstationary. In case of traces of nonstationarity being detected, we are allowed to carry out modified root mean square analysis termed as detrended fluctuation analysis (DFA) [83]. The advantages of DFA is that it permits the detection of long range correlation embedded [85] in a seemingly non- stationary time series and allows the detection of scaling exponent in noisy signal with embedded trend that can mask the true correlations. In the last one decade DFA has emerged as an important technique to study scaling and long

cubic higher order polynomial in a piecewise manner. Most real time series exhibit persistence i.e subsequent element of the time series are correlated [86]. Persistence literally means that an increase in the values of the time series will most likely be followed by an increase in short term and decrease in the values will be followed by another decrease. The study of the self similarity and scaling in physics, socio economic sciences in the last several years has brought in new insights and new ideas for modeling them. For instance one of the important empirical results of the market dynamics is that the probability distribution of price returns r in a typical market displays a power law [141] i.e $P(r) \sim r^\alpha$ where $\alpha = 3$. Similar power laws appear for the cumulative frequency distribution of earthquake magnitudes [142]. So the investigation and study of scaling exponents relevant in case of stock market, econophysics, foreign exchange rates, neuron spiking, that is in diverse areas of research field will also be beneficial for our case in exploring, understanding and developing the nonlinear dynamical system theory of plasma oscillation in different plasma systems like glow discharge, double plasma device, dusty plasma device. So all of the aforementioned overview of nonlinearity, non-stationarity, phase coherence nicely orchestrate the aim of exploring the complexity dynamics of the system under control.

Chapter 2

Experiment, diagnostics and data analysis procedures

In this chapter we present a detailed description of the experimental devices on which we carried out our experiments. The floating potential fluctuations (FPF) were acquired with the help of langmuir probe. A comprehensive discussion of the data analysis has been presented in the framework of linear and nonlinear analysis tools. The experiments have been carried out in the following devices.

- DC discharge plasma in a cylindrical vacuum vessel
- DC discharge in the toroidal vacuum vessel of the SINP tokamak

2.1 Experimental Setup

assembly was mounted inside a vacuum chamber and was pumped down to a pressure of about 0.001 mbar using a rotary pump. The chamber was subsequently filled with argon gas up to a predetermined value of neutral pressure by a needle valve. Finally a discharge was struck by a direct current discharge voltage, which could be varied in the range of 0-1000 V shown in the laboratory view of the whole experimental system in Fig. 2.3. To carry out the observations in presence of a magnetic field, an external magnetic field (axial) was applied to the plasma by passing a steady current through the coils wound over the cylindrical chamber as shown in the right panel of Fig 2.1. A glow discharge plasma operating under steady state conditions is subjected to an oscillatory external voltage that constitutes forcing. For this, a signal generator was coupled with the discharge voltage (DV) through a capacitor for observing fluctuations as shown in the left panel of Fig 2.1. The schematic of the measurement circuit for floating potential measurement is also depicted in Fig. 2.2 which shows that the probe is connected to the oscilloscope having input resistance and capacitance of the order of $1M\Omega$ and $13pF$ respectively. So the maximum values of frequencies obtained must lie in the regime much less than the cut off frequency of the low pass filter combined between the sheath resistance ($R_{sh} \sim 0.2M\Omega$) and stray capacitance ($C_s \sim$ in order of tens of pF) in Fig. 2.2.

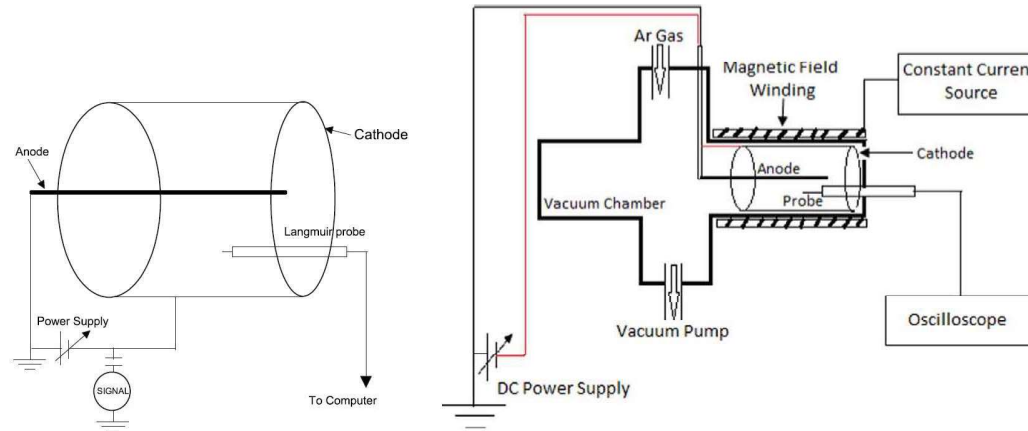


Figure 2.1: Schematic diagram of experimental setup for glow discharge plasma with external forcing and magnetic field

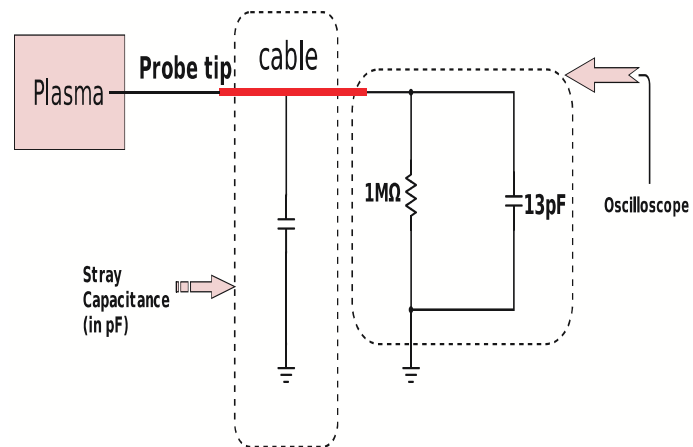


Figure 2.2: Schematic diagram of the measurement circuit



Figure 2.3: Picture of the dc glow discharge plasma device: 1) Vacuum chamber, 2) Stand, 3) High voltage power supply, 4) Argon gas cylinder, 5) Rotary pump, 6) Digital oscilloscope, 7) Pressure reading meter, 8) Langmuir probe, 9) Power supply connection, 10) Pressure control unit: needle valve, 11) Pirani gauge, and 12) Side cylindrical chambers attached with main vacuum chamber

2.1.2 Toroidal discharge device

The toroidal vessel of SINP tokamak with a major radius 30 cm and a minor radius 7.5 cm has been used as the discharge chamber. The grounded vessel was evacuated to a base pressure of 0.01 mbar using a rotary oil pump. The vessel was filled with hydrogen gas upto a pressure of 0.45 mbar and a discharge voltage of 0.54 kV was applied to sustain the discharge plasma. A Langmuir probe was inserted at diametrically opposite position to the electrode along the minor axis of the toroid

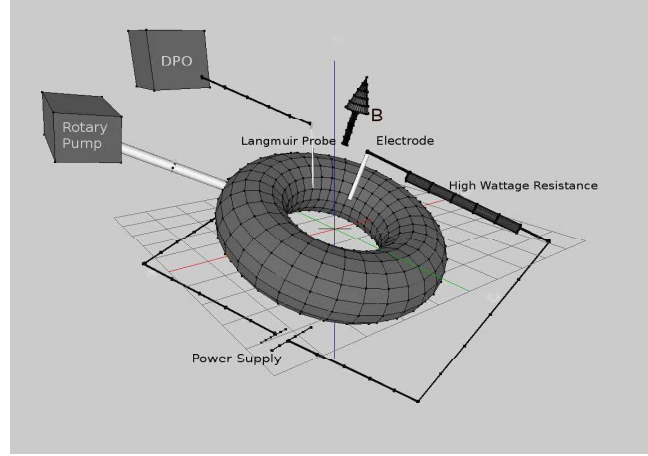


Figure 2.4: Schematic diagram of the experimental setup for glow discharge plasma in a toroidal assembly

(B_T) with 1A current in the coil producing 1.28G B_T . The direction of B in the Fig. 2.4 is same as that of vertical magnetic field (B_V). We have performed only one experiment in this device under the action of increasing discharge voltage (DV), vertical, toroidal magnetic field, and increasing vertical magnetic field at a fixed toroidal magnetic field of 8.5G.

2.2 Diagnostic

- Langmuir probe, Floating Potential Fluctuations

The plasma probe is a device that has been widely used to measure the temperature and density of a plasma both in the laboratory and in space.

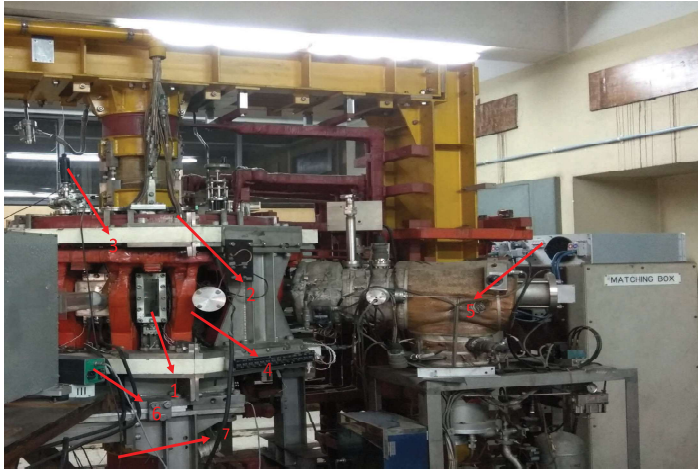


Figure 2.5: Picture of the glow discharge plasma in a toroidal assembly: 1) Viewing port 2) Vertical magnetic field coils, 3) Pressure control unit 4) Toroidal magnetic field coils 5) Constant current source 6) Pressure reading meter 7) Place for inserting Langmuir probe

as shown in Fig. 2.6. The probe when inserted in the plasma is surrounded by the electron and ions falling on the probe. The imbalance between the ion and electron current, due to the higher mobility of the electrons than the ions results in an accumulation of the electrons on the surface of the probe, setting up an electric field. This electric field repels the electrons and attracts ions towards the probe so that the net current is zero and hence the surface acquires a potential, which is called floating potential. Under these equilibrium conditions the number of electrons reaching the probe per

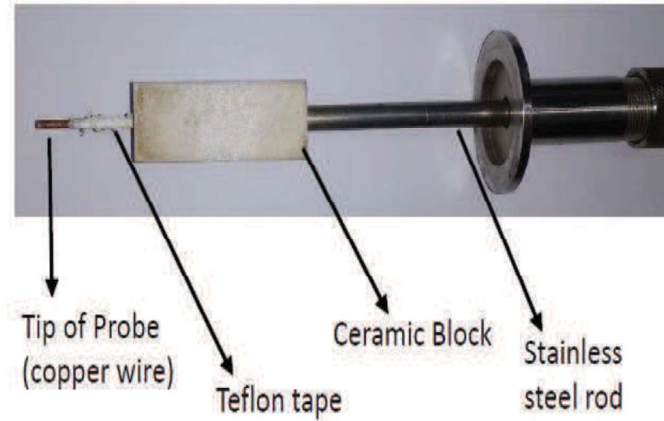


Figure 2.6: Picture of the Langmuir probe used in the experiments

2.3 Data analysis techniques

The analysis of the floating potential fluctuations (FPF) has been carried out using the linear and nonlinear time series analysis. Linear analysis tool deals with the use of power spectrum, autocorrelation, probability density function, etc. whereas in nonlinear analysis Lyapunov exponent, correlation dimension, recurrence plot and recurrence quantification analysis [46, 47], detrended fluctuation [80, 82] analysis, surrogate data involving structure function[38], phase coherence index [30], delay vector variance, Zscore etc., have been used. We will discuss in detail the aforesaid techniques used for the first time in plasma physics (i.e delay vector variance, structure function, phase coherence etc) to have a clear understanding of the

- Look at power spectrum, autocorrelation function [12]
- Estimate the correlation dimension, Lyapunov exponent, entropy [70]
- Compare the original time series with surrogate data sets to verify the existence of nonlinearity [48, 68].
- Test for stationarity, and look for the recurrence plots [74, 80]
- Estimate phase coherence index to find the correlation between Fourier modes [81]
- Construct models for validation [9]

2.3.1 Power spectral method

A time series which has a certain periodicity may be represented as a superposition of periodic components of sine and cosine functions with different frequencies. Power spectrum analysis deals with the determination of their relative strengths. When the time series is periodic, the spectrum may be expressed as a linear combination of oscillations whose frequencies are integer multiples of the basic frequency which is the Fourier series. A periodic or quasi periodic signal shows sharp spectral line in power spectrum plot, whereas for a chaotic signal it will show a broadband.

Power spectral method can be used to find the characteristic modes, and the dom-

series has to be described in a suitable phase space reconstruction. The phase space description provides a powerful tool for describing the behavior of a time series in a geometric form. According to Takens embedding theorem using a time series data X_i an embedding can be made using the vector $Y_i = X_i, X_{i+\tau} \dots X_{i+(m-1)\tau}$ which represent the original time series embedded into m dimensional phase space with τ , m being the delay and embedding dimension respectively. The time difference between two consecutive components of the delay vectors in above equation is referred to as the lag or time delay τ . If the delay time τ is too small it indicates the correlation between components whereas large τ connotes the suppression of dynamics in a lower time scale. Embedding dimension is calculated using the method of false nearest neighbourhood (FNN) [50]. The time delay is considered as the time for auto correlation to reduce to $1/e$ of the initial value.

2.3.3 Correlation dimension

Dimension of a system is defined as the power of the radius of the hypersphere (1) with which the volume of the system within the hyper sphere changes. The correlation dimension (CD) [51, 105, 71] of a time series is defined as the dimensionality of the space occupied by the points of that time series. CD is actually a measurable parameter similar to the dimension of a system; the only difference

using the following equation 2.1 where $C(l)$ is the correlation integral in a particular embedding dimension and $\|X_i - X_j\|$ is the distance between the i th and j th point in that embedding space. The scaling of the function $C(l, m)$ can be written as $C(l, m) = r^{CD}$ with the scaling index CD being called the correlation dimension given by the equation 2.2. It gives a lower bound to the fractal dimension of the underlying attractor. For a stochastic or noisy system $CD \sim m$ and for low dimensional chaotic system CD saturates to a constant value for $m > m_{sat}$. It gives a lower bound to the fractal dimension [72] of the underlying attractor.

$$C(l, m) = \lim_{N \rightarrow \infty} \frac{1}{N^2} \{\text{Number of pairs for which } \|X_i - X_j\| < l\} \quad (2.1)$$

$$CD = \frac{\log C(l, m)}{\log l} \quad (2.2)$$

2.3.4 Dimensionality analysis: Embedding dimension

Many practical methods have been developed for the determination of the minimal embedding dimension. Here in our work we propose to deploy the method called false nearest neighbourhood [50, 119] to be able to extract information about min-

neighbor S_j in a m -dimensional space followed by the calculation of the distance $\|S_i - S_j\|$. We need to iterate both points and compute the following quantity.

$$L_i = \frac{|S_{i+1} - S_{j+1}|}{\|S_i - S_j\|} \quad (2.3)$$

When L_i exceeds a given heuristic threshold L_t , the point is marked as containing the false nearest neighbour. In our experimental system we have carried out FNN method to be able to extract information about minimal embedding dimension in the presence of increasing DV. If the fraction of points for which $L_i > L_t$ is zero or at least sufficiently small then our criterion is satisfied.

2.3.5 Lyapunov exponent

Lyapunov exponents [53] describe the rate of expansion or contraction of nearby initial conditions in phase space. If we consider two points on two nearby trajectories of a chaotic attractor, in the phase space, assuming the distance between them to be $\delta x_i(0)$, and after time t , if the distance between the two trajectories becomes $\delta x_i(t)$, then the divergence (separation after time t) can be written as

$$\delta x_i(t) = \delta x_i(0)e^{\lambda_L t} \quad (2.4)$$

The nonzero positive value of λ_L identifies the chaotic nature of the fluctuations. As the exponent is the measure of how fast two points in phase space diverges for a time series so it is a direct estimate of the chaoticity of a system.

2.3.6 Renyi Entropy(Methodology)

Complexity dynamics can be well explored by means of the classical measure of disorder in a physical system, i.e the entropy [54]. Besides its initial application in the field of molecular physics, entropy has been used in statistics and information theory to develop measures of the information content of signals [Shannon, 1948]. Shannon entropy is the classical measure of information content and disorder, and for an n dimensional Probability density (PD) distribution $P(x)$, it is defined as :

$$H(P) = - \int_{-\infty}^{\infty} P(x) \log P(x) dx \quad (2.6)$$

But we restrict ourselves in making the use of the more classical Shannon information as a measure of complexity due to the presence of logarithm within the integral in equation 2.6. We rather switch to the use of Renyi entropy[54, 55] of order m as the measure of complexity. The Renyi number is by definition an entropy, i.e., a classically used measure of disorder in physical systems, and

The Shannon entropy can be recovered from the Renyi entropy as

$$\lim_{m \rightarrow 1} H_m^R(P) = H(P) \quad (2.8)$$

2.3.7 Autocorrelation

The autocorrelation time of a fluctuating signal is a measure of the temporal coherence and is obtained from the autocorrelation of the signal. For a time series of length N , $X = [X_i, i = 1, 2, \dots, n]$; the autocorrelation function $C_{auto}(\tau)$ [52] can be written as

$$C_{auto}(\tau) = \frac{\sum_{k=1}^{N-\tau} (X_{k+\tau} - \overline{X})(X_k - \overline{X})}{\sum_{k=1}^N (X_k - \overline{X})^2} \quad (2.9)$$

where \overline{X} , τ are the mean, and time lag of the time series respectively. Obviously, if a signal is periodic in time, then the autocorrelation function is periodic in the time lag τ . Autocorrelations of signals from deterministic chaotic systems typically also decay exponentially with increasing lag. Stochastic processes have decaying autocorrelations but the rate of decay depends on the properties of the process.

2.3.8 Recurrence plot

Recurrence plot (RP) analysis of nonlinear time series is a relatively new and ad-

with ones and zeroes for states X_i and X_j and find the hidden periodicity in a time series signal which is not observable by naked eye.

$$R_{ij} = H(\epsilon - ||X_i - X_j||); \quad (2.10)$$

where i, j run from 1 to the number of data points (M) in the signal. H is the Heaviside function and $||.||$ is the norm (Euclidean norm), ϵ is the choice of the threshold with 1 percent of point density in our case. A crucial parameter of RP is the threshold ϵ . Therefore, special attention has to be required for its choice. If ϵ is chosen too small, there may be almost no recurrence points and we cannot learn anything about the recurrence structure of the underlying system. On the other hand, if ϵ is chosen too large, almost every point is a neighbour of every other point, which leads to a lot of artefacts. For this case it was proposed to choose ϵ such that the recurrence point density is selected to be approximately 1 percent [56] in our case.

According to Takens embedding theorem [69] using a time series data X_i an embedding can be made using the vector $Y_i = X_i, X_{i+\tau} \dots X_{i+(d-1)\tau}$ which represents the original time series embedded into d dimensional phase space with τ being the delay. RPs are graphical, two dimensional representations showing the

in such a way that the sphere contains a predefined number of close states. The diagonal line of length l means the segment of the trajectory is rather close during l time steps to another segment of the trajectory at different time thus relating these lines to the divergence of the trajectory segments. The average diagonal line length is

$$L = \frac{\sum_{l=l_{min}}^N lP(l)}{\sum_{l=1}^N lP(l)} \quad (2.11)$$

Quantification of the characteristic measure for different structures appearing in RP form a diagnostic tool known as recurrence quantification analysis (RQA). For example, the RQA measure determinism (DET) [57] expressed in the following equation 2.12 gives the ratio of the number of recurrence points in the diagonal lines to all the recurrence points.

$$DET(t) = \frac{\sum_{l=l_{min}}^{N-t} lP_t(l)}{\sum_{l=1}^{N-t} lP_t(l)} \quad (2.12)$$

2.3.9 Bicoherency analysis based on empirical mode decomposition

- Empirical mode decomposition

and minima must have zero mean and (2) the number of extrema and the number of zero crossings differ at most by one. The first condition assures that the IMF is symmetric, and the second condition assures that no riding waves of multiple frequency exist in an IMF. These two conditions ensure that the IMF is monocomponent in frequency. Most of the experimental signals are multicomponent in nature, i.e., there exist different scales simultaneously. These signals can be considered as a superposition of fast oscillation with a slow one at the local level. Therefore, we need to decompose these signals into their inherent modes for the study of their basic structure. This EMD approach is based on the local time scales, i.e., the detection of the local maxima and minima.

- Hilbert Huang transform and bicoherency analysis

The Hilbert Huang transform (HHT) proposed by Huang et al. [58] represents the signal being analyzed in the time-frequency domain by combining the empirical mode decomposition (EMD) and the Hilbert transform. Hilbert transform of a time series $X(t)$ is written as

the basic nonlinear modes of the system and examine their mutual interactions. Since the IMF components are represented as $Z(t) = Ae^{i\phi(t)}$ the interaction among the IMF components can be studied by evaluating the IMF bicoherency factor [123, 125], represented below

$$\gamma = \frac{\langle Z_i^* Z_{i+1} Z_{i+2} \rangle}{\langle A_i A_{i+1} A_{i+2} \rangle} \quad (2.14)$$

where the angular bracket in equation 2.14 represents the time average. This definition of EMD based bicoherency is especially suitable for satisfying the phase matching or coupling. The phase matching conditions are such that the value $\langle Z_i^* Z_{i+1} Z_{i+2} \rangle$ is 0 for random $\phi_i, \phi_{i+1}, \phi_{i+2}$ and equal to $\langle A_i A_{i+1} A_{i+2} \rangle$ for $\phi_i = \phi_{i+1} + \phi_{i+2}$ indicating γ to be bounded between 0 and 1. Error in the value of bicoherency factor has been estimated by calculating the number (N) of largest wave in the triplet i.e the number of 2π . Here it is assumed that each wave period is independent implying N to represent the number of ensembles with the value of error to be $\sigma = \frac{1}{\sqrt{(N)}}$. In order to reduce the error in estimating bicoherency factor we need more number of 2π phases as the bicoherency is based on phase coupling. Having contained very few number of 2π phases, higher no of IMF's are not statisti-

$N=10000$ is the data length in our experiment. Maximum range of i will be $\log_2(N)$.

2.3.10 Surrogate data: Delay vector variance, Rank test, Zscore, Nonlinearity metrics, Structure function, Phase coherence index

Several algorithms have been proposed to generate the surrogate data [34, 45] in the literature. The most commonly used methods are: Random shuffled, Phase shuffled and Iterative Amplitude Adjusted Fourier transform methods [89, 90] (IAAFT). The method of surrogate data is introduced to test for the evidence of nonlinear dynamics. Briefly, the idea is to construct, from an experimental time series, one or more control data sets (surrogate data), which share with the original data all the linear properties (in particular, the power spectrum and autocorrelation function), but not the nonlinear properties. The method generally consists in applying the Fourier transform to the original data, followed by the randomisation of phases, and then applying an inverse Fourier transform finally. For generating phase randomised surrogate (PRS) the original data is decomposed into amplitude and phases using the Fourier transform. The phases are then randomly shuffled and from these two pieces of information in the Fourier space inverse Fourier transform

but are otherwise random. Then a certain measure, or discriminating statistics, are obtained from both the original time series and for the surrogates. If the result for the original time series deviates significantly from the distribution of the surrogates, the null hypothesis can be rejected. So the goal of generating the surrogate data only is to establish the presence of nonlinearity by excluding a reasonable alternative, called the null hypothesis. Nonlinear techniques using surrogate data have found applications in the analysis of Laser data [91], Biomedical time series (Heart rate variability, EEG, ECG, Hand Tremor [63]), Functional Magnetic resonance imaging time series (fMRI), Real world Signal like Wind data [62], Global climatic data, Financial time series data [64].

2.3.10.1 Method of analysis: structure function, phase coherence index

When we attempt to obtain phase information from data, the Fourier transformation has been the starting point for this purpose. The Fourier transformation of a time series $x(t)$ is defined as

$$X(\omega) = \int_{-\infty}^{\infty} x(t)e^{-i\omega t} dt \quad (2.15)$$

where ω is the angular frequency which provides information on amplitude and

$$\phi(\omega) = \arctan \frac{ImX(\omega)}{RealX(\omega)} \quad (2.16)$$

Hada et al., Koga [31, 30] introduced a method to evaluate the degree of phase coherence among the Fourier modes quantitatively. From a given FPF we generate two surrogate data followed by the decomposition of the original data (ORG) into the power spectrum and the phases using the Fourier transform. We then randomly scramble the phases keeping the power spectrum unchanged, and from these two pieces of information in the Fourier space, we perform the inverse Fourier transform to create the phase-randomized surrogate (PRS) whereas phase-correlated surrogates (PCS) are generated by making the phases equal without shuffling the Fourier phases. For a process or time series $X = X_t : t = 1, 2, 3 \dots n$ the m th-order structure function $S(\tau, m)$ is defined in equation 2.17 as the m th moment of the increments of $X(t)$ following D Koga and Y.H .Su et al.[87] where m is the order of the path length and τ is the measure characterising the magnification level of the curve. When the phases are correlated, the path length of the data tends to be shorter (for PCS) than the case when the phases are random.

$$S(\tau, m) = \langle |X(t + \tau) - X(t)|^m \rangle \quad (2.17)$$

$$C_{\phi}(\tau) = \frac{S_{PRS}(\tau) - S_{ORG}(\tau)}{S_{PRS}(\tau) - S_{PCS}(\tau)} \quad (2.18)$$

2.3.10.2 Delay Vector variance

Although many established methods in the field of nonlinearity already exist, there is a need for a robust method which is straightforward to interpret and visualize. The proposed delay vector variance method (DVV) [48, 88] endeavours to characterise a time series by comparing the result to those obtained for the linearised versions of the signal (surrogates). To be able to perform reasonably well on a wide variety of signals, it is desirable that the method makes use of some well established notions from nonlinear dynamics and chaos such as optimal embedding dimension, phase space geometry. It is based upon the local unpredictability of a time series, which is analysed in a standardised manner, and allows both for a straightforward visualisation, and for a quantitative measure of the nonlinearities present in a time series. Due to the standardization of the distance axis, these plots can be conveniently combined in a scatter diagram. The method employed first time in the analysis of the fluctuations of glow discharge plasma system with the novel intention of identifying nonlinearity outperforms a number of established nonlinearity measures. The approach is somewhat related to the false nearest neighbours [50]

time series data X_i an embedding $x(k)$ can be made.

- For a given embedding dimension m , a measure of unpredictability σ^2 , is computed over all sets Ω_k
- A set Ω_k is generated by grouping those delay Vectors (DV) following the time delay embedding approach [69, 88] that are within a certain Euclidean distance to $x(k)$, which is varied in a manner standardised with respect to the distribution of pairwise distances between DVs such that $\Omega_k = X(i) || |X(k) - X(i)| | < r_d$.
This way the threshold scales automatically with embedding dimension m .
- The mean, μ_d , and standard deviation σ_d , are computed over all pairwise Euclidean distance between DVs. For every set of original time series the corresponding surrogates are generated. The average over all sets normalized by the variance of the time series (σ_x) yields the measure of nonlinearity presented in the following equation 2.19.

$$\sigma^2 = \frac{(1/N) \sum_{i=1}^n \sigma_k^2}{\sigma_x^2} \quad (2.19)$$

2.3.10.3 Traditional nonlinearity metrics

To undertake the performance comparison between the proposed DVV method and other nonlinearity analysis methods, we have implemented two traditional measures of nonlinearity, which have also been used in [33], namely the third-order autocovariance, $t^{C3}(\tau)$ a higher order extension of the traditional autocovariance:

$$t^{C3}(\tau) = \langle x_k x_{k-\tau} x_{k-2\tau} \rangle \quad (2.20)$$

and a possible measure of the asymmetry due to time reversal t^{Rev} :

$$t^{Rev}(\tau) = \langle (x_k - x_{k-\tau})^3 \rangle \quad (2.21)$$

Any time series is said to be reversible if its probabilistic properties are invariant with respect to time reversal. τ is a time lag which for simplicity and convenient comparison is set to unity in all simulations.

2.3.10.4 Zscore

The surrogate data technique employed to find the presence of nonlinearity in a time series data uses a discriminating statistics M for instance predictability,

nonlinearity to estimate Z-score alternatively known as t-test, the expression of which is given below in equation 2.22. The statistics is sensitive to the nonlinear structure in the data set. It express how many standard deviation (sigmas) M of the experimental data deviates from the average M for the ensemble of surrogates.

$$Z = \frac{M_d - M_s}{\sigma_s} \quad (2.22)$$

In this formula M_d is the value of M for the experimental data, M_s is the mean of M for the surrogate data and σ_s is the standard deviation of M for the surrogate data.

2.3.10.5 Rank test

This is basically an application of the bootstrap method in statistics [14]. This involves two ingredients: a null hypothesis against which observations are tested, and a discriminating statistic. In the context of nonlinearity testing, the surrogates are a realisation of the null hypothesis of linearity. The null hypothesis is a potential explanation that we seek to show is inadequate for explaining the data; and the discriminating statistic is a number which quantifies some aspect of the time series. Many nonlinearity analysis methods compare metrics obtained for the original signal to those obtained for an ensemble of surrogates. If the metric of

2.3.11 The Continuous Wavelet Transform (CWT)

Wavelet transforms (WT) [96, 97] expand time series into time frequency space and can therefore find localized intermittent periodicity. We can have two classes of wavelet transformation such as continuous wavelet (CWT) as well as discrete wavelet transformation (DWT) but CWT is generally used for feature extraction processes. The DWT is a compact representation of the data and is particularly useful for noise reduction and data compression.

One particular wavelet, the Morlet [98], is defined as

$$\psi(s) = \pi^{\frac{1}{4}} e^{i\omega_0 s} e^{-\frac{1}{2}s^2} \quad (2.23)$$

where ω_0 is the dimensionless frequency and s is the dimensionless time. We restrict ourselves in using only Morlet wavelet due to its benefit of giving good balance of time frequency localization. The CWT of the time series $d(t)$ with respect to the wavelet $\psi(s)$ is defined as

$$W_{(d,\psi(s,t))} = d(t) * \psi(t) \quad (2.24)$$

where t is time and $\psi(s)$ is the wavelet at the scale s (which is linearly related to

to e^{-2} of the value at the edge. Here in our case CWT has been proved to be extremely beneficial in exploring the origin of finite phase coherence index.

2.3.12 Detrended fluctuation analysis

The presence of nonstationarity permits us to carry out detrended fluctuation analysis (DFA) [83] for the detection of long range correlations embedded in a nonstationary time series data. Following the approach adapted by Peng et al. [80] we first integrate the time series $y(k) = \sum_{i=1}^k [x(i) - x_{mean}]$ followed by the dividing of the time series into boxes of equal length n . A least square line representing the trend is fitted to the data. A y coordinate of the straight line segment is denoted by $y_n(k)$ in each box. Next we detrend the integrated time series $y(k)$ by subtracting the local trend, $y_n(k)$ in each box. Root mean square fluctuation of this integrated and detrended time series is calculated using the following

$$F(n) = \sqrt{\frac{1}{N} \sum_{k=1}^N [y(k) - y_n(k)]^2} \quad (2.25)$$

The process is repeated over all time scales to provide a relationship between the average fluctuation as a function of $F(n)$ and the box size n . In order to

to alternate. Power law exponent values greater than 1 indicate the existence of perfect correlated dynamics. Altogether the exponent can be viewed as the roughness of the time series, the larger the value of coefficient α the smoother will be the time series. Moreover by using the technique DFA we can detect the existence of two scaling regions over two different regimes. The change in the values of scaling exponent in different scaling region can be characterized as crossover phenomena [80, 84]. A crossover usually arises due to changes in the correlation properties of the signal at different temporal or spatial scales. The fairly robust and powerful technique DFA is used to capture the crossover phenomena for the first time in the fluctuation acquired from DC glow discharge plasma.

Chapter 3

Investigation of complexity
dynamics of inverse and normal
homoclinic bifurcation in a glow
discharge plasma

3.1 Introduction

Bifurcation analysis[6] comprises an important part of nonlinear dynamics since it can elucidate very clearly the behaviour of the system for a small change in the value of the control parameter. The qualitative changes in the dynamics of the system with the change in the control parameter values are generally classified as bifurcation and the parameter values at which they occur are called bifurcation points. Bifurcations are important scientifically as they provide models of transitions and instabilities when some control parameter is varied. Amongst the several types of bifurcations, homoclinic bifurcation[101] is one in which the system can go from a chaotic to a seemingly ordered state, wherein the time period (T) shows a scaling behaviour with control parameter [100]. Though homoclinic bifurcation with relaxation oscillations have been observed in chemical[99] and plasma[101] systems, the inverse homoclinic bifurcation[102] has not been very commonly observed.

In this chapter we report for the first time the experimental observation of inverse homoclinic bifurcation in the floating potential fluctuations with increase in discharge voltage (DV). It continues to stay in this mode for a wide range of DV's and later results in a homoclinic bifurcation. In order to comprehend the complex

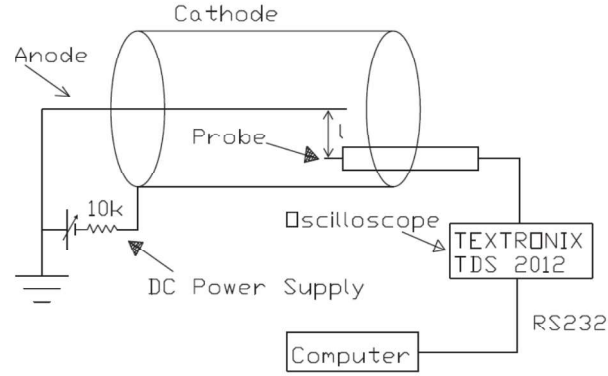


FIG. 1. Schematic diagram of the experimental setup.

Figure 3.1: Experimental setup for glow discharge plasma

A numerical modelling of the experimental observations has been attempted using a forced nonlinear dynamical equation representing the temporal dynamics of ion acoustic oscillations in presence of ionization and recombination terms. The experiments were carried out in a cylindrical hollow cathode (length=10cm, radius=5.5cm) DC glow discharge argon plasma as elaborately discussed in chapter two with a typical density and temperature of $\sim 10^7/cm^3$ and 2-6 eV respectively. In our experiment as depicted in Fig. 3.1 keeping the operating neutral pressure fixed at 0.49 mbar, DV was varied in the range from 412 to 700 volts. An unbiased Langmuir probe was used to obtain the floating potential fluctuations acquired with a sampling time of 10^{-5} sec.

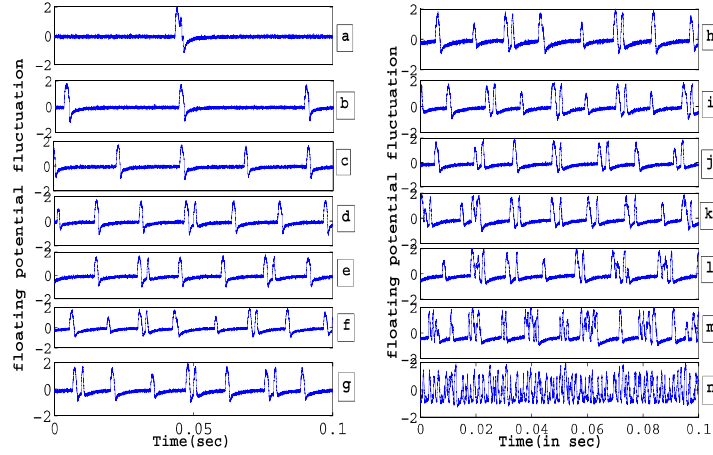


Figure 3.2: Sequential change in the raw signal at 0.490 mbar for different DV(volts): (a) 412V (b) 429 V (c) 436V (d) 440V (e) 446V (f) 451V (g) 453V (h) 455V (i) 458V (j) 462V (k) 468V (l) 469V (m) 488V (n) 495V

it is clear that at $DV \sim 412$ volts, there is only one peak and as DV was increased three peaks were observed at 429 volts. Subsequent raising in the DV increases the number of spikes until it became chaotic around 495 volts as seen in Fig 3.2n. This chaotic phase persists upto about 549 volts (Fig 3.3q) disappearing at about 565 volts (Fig 3.3r) leading to relaxation oscillations of increasing time period indicating homoclinic like bifurcation.

A comprehensive analysis of the amplitude bifurcation plotted with the peak

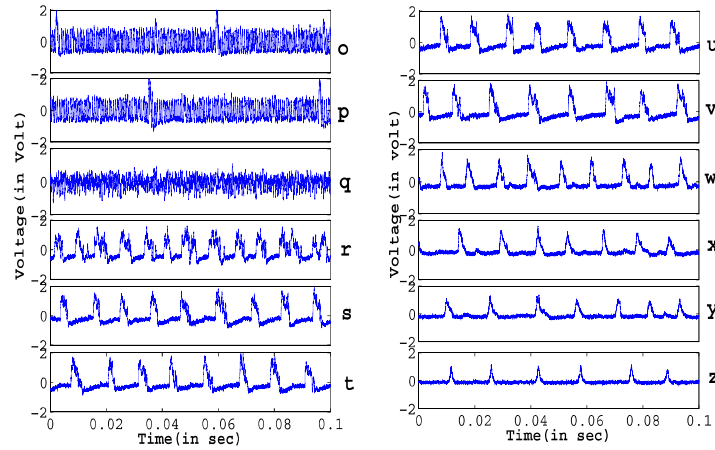
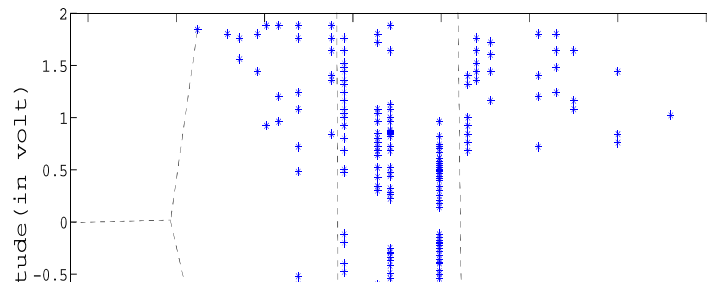


Figure 3.3: Sequential change in the raw signal at $P=0.490$ mbar for different DV(volts): (o) 514V (p) 521V (q) 549V (r) 565V (s) 570V (t) 578V (u) 605V (v) 615V (w) 625V (x) 650V (y) 680V (z) 700V



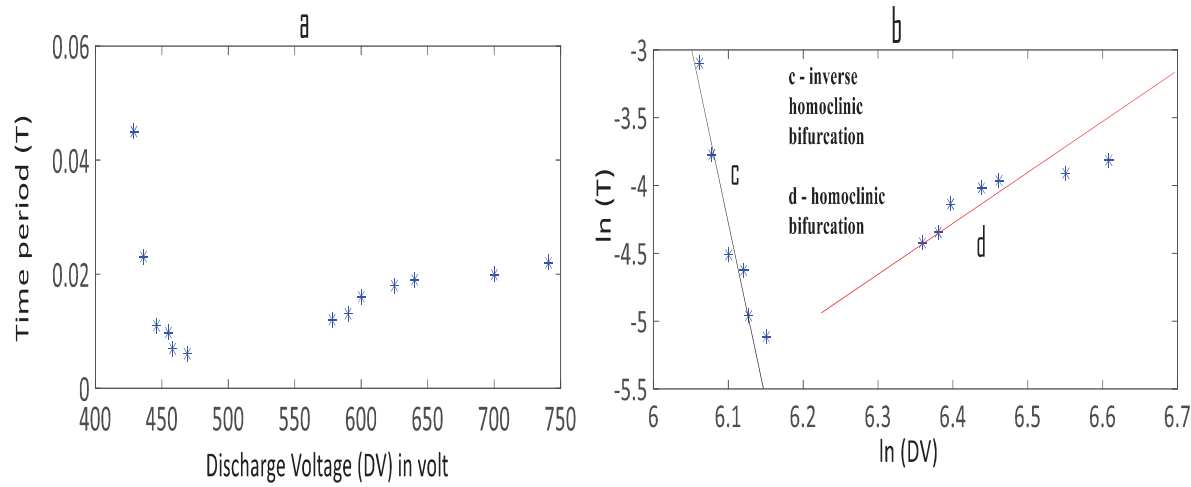


Figure 3.5: (a) Time period vs discharge voltage and (b) $\ln(T)$ vs $\ln(DV)$ showing the exponents

in region C. This diagram offers a good insight into the mechanism of system dynamics going from order-chaos-order.

Fig 3.5a initially shows a decrease, followed by an increase in the time period (T) with DV, and both of them approximately have an exponential behaviour. In Fig 3.5b we have plotted $\ln(DV)$ vs $\ln(T)$ which follows power law behaviour with exponents of ~ 2.2 and -24 respectively for the homoclinic and inverse homoclinic bifurcation. The negative scaling represents the inverse homoclinic while the pos-

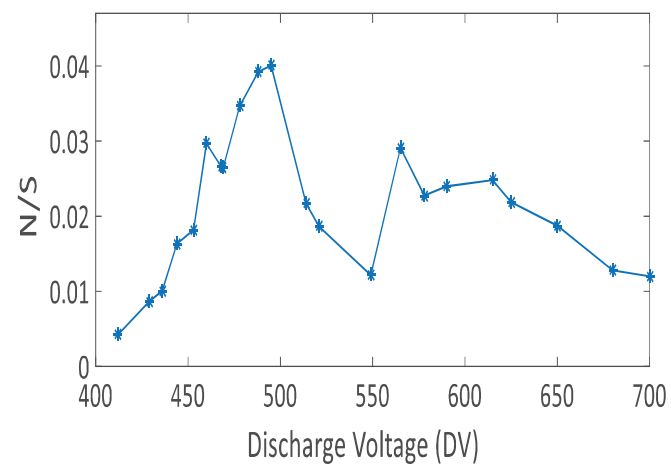
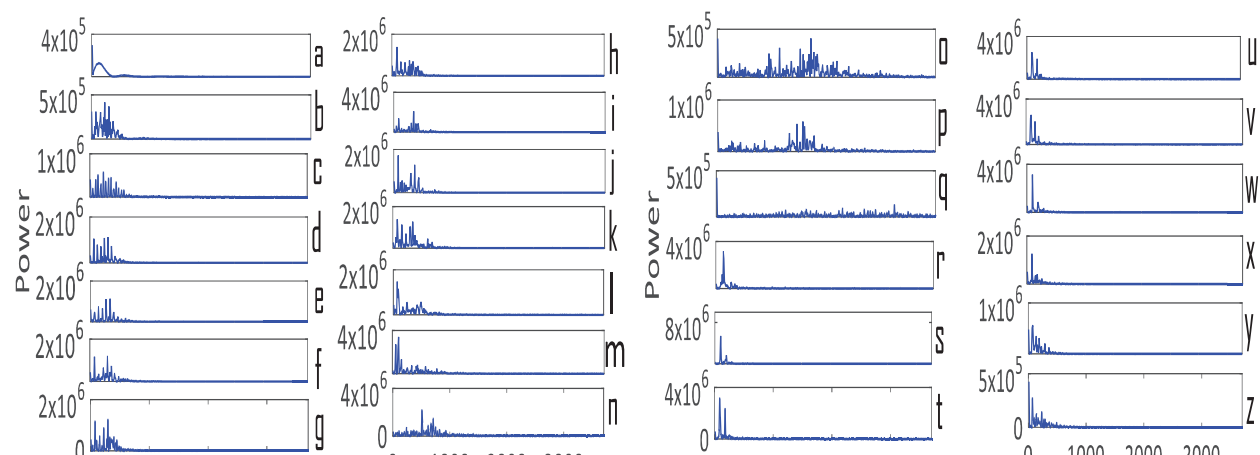


Figure 3.6: Noise to signal ratio with variation in DV



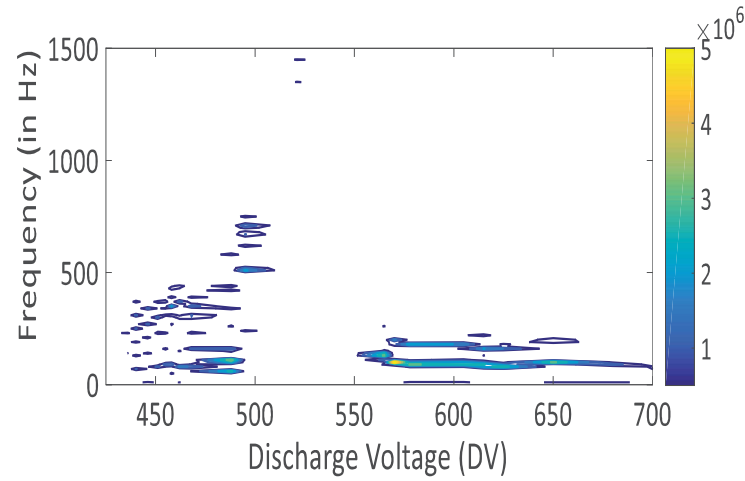


Figure 3.8: Contour Plot of Fourier spectrum with variation in discharge voltages

3.3 Power Spectral Analysis

Power spectral analysis was carried out on the raw data as shown in the Fig 3.7. Initially most of the frequencies were concentrated below 100 Hz in Fig 3.7(a-k), but around $DV \sim 514$ volt a broad band turbulence is observed with the peak frequency shifting towards 1.5 kHz. With further increase in DV it shrinks back

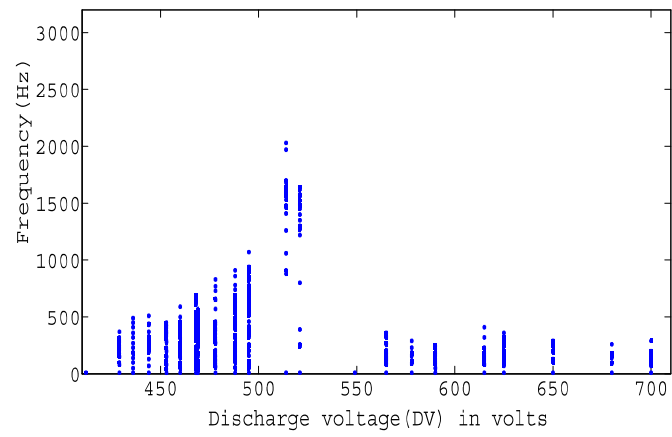
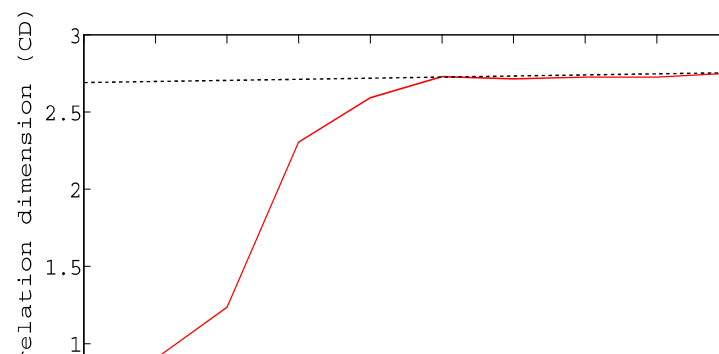


Figure 3.9: Frequency spectrum at different discharge voltages



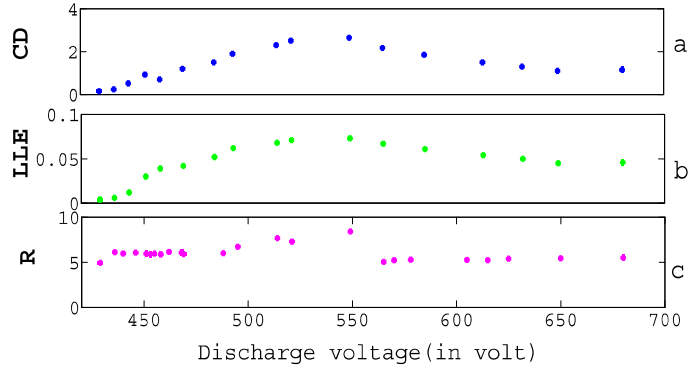


Figure 3.11: Plot of (a) Correlation dimension (d), (b) Largest Lyapunov exponent (LLE) and (c) Renyi entropy (R) with DV

3.3.1 Correlation dimension, Lyapunov exponent, Renyi Entropy

Correlation dimension which is normally estimated from the Grassberger and Procaccia technique[107] gives some idea of the complexity of the system. The method of estimating correlation dimension is explained comprehensively in chapter 2 in equation 2.2. In this paper we have estimated the same using Gaussian Kernel Algorithm(GKA)[105] developed by Diks[106]. This method has some advantages that it is computationally faster and useful in handling noisy time series data which is very common to experiments. As a test case we have shown in Fig 3.10 that a plot of the correlation dimension for $DV \sim 549$ volt saturates towards an average value of 2.6 estimated over the embedding dimension $m=7-11$, suggesting low di-

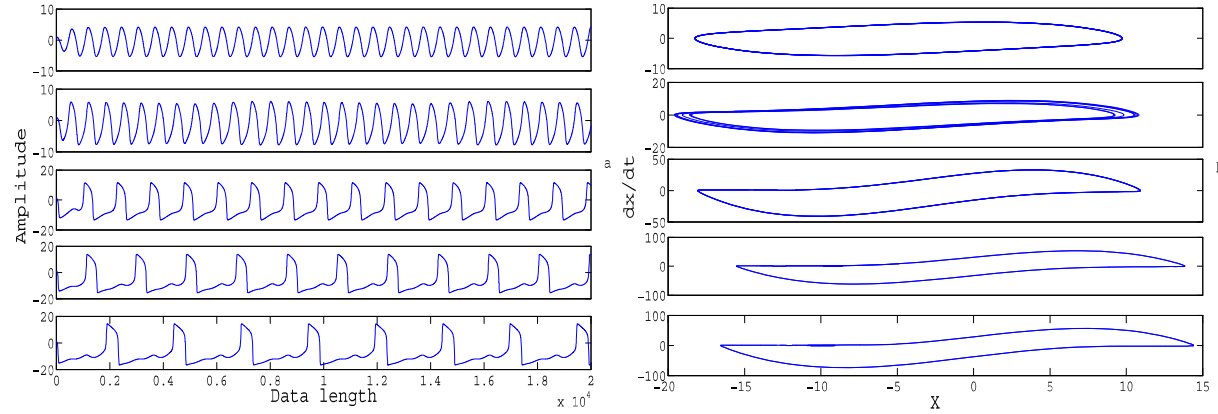


Figure 3.12: Amplitudes of the numerical solutions with the variation in A and their corresponding phase space plots

using Rosenstein's technique[53] which shows a similar behaviour to the correlation dimension.

Renyi entropy [8], an explicit measure of the complexity of the fluctuations has been discussed in detail in chapter 2 of equation 2.7 which is obtained from the Shannon entropy in equation 2.6. In Fig 3.11c we have plotted the values of the Renyi entropies (R) of order 3 with the DV. We observe that the ordered states have low entropy values whereas the chaotic states have higher entropy values. R values also follow that of CD and LLE indicating order-chaos-order.

3.4 Numerical Modelling of homoclinic bifurcations

the temporal dynamics is governed by the following second order nonlinear ordinary differential equation given by equation 3.2 where x denotes the floating potential fluctuations, and the derivatives are normalized with respect to time by ω_0 where ω_0 is equal to kc_s . k is the wave number and c_s denotes the ion acoustic speed with the form given below.

$$c_s^2 = \frac{k_B T_e}{m_i} \quad (3.1)$$

T_e and m_i represent respectively the electron temperature and ion mass. Here a , b , c and e denote the collisional, the recombination and ionization effects respectively. In the limit a , b , c and $e \rightarrow 0$, we recover the usual ion acoustic oscillations from the equation 3.2 when the forcing terms on right hand side is zero.

In order to investigate the behaviour of the nonlinear oscillations in the presence of an external discharge voltage, we include an additional term A on the right hand side of equation 3.2 that is considered to represent the DV. Although there is no explicit externally applied oscillatory voltage in the present experimental system, we consider the situation where many normal modes are generated within the plasma. Therefore, We have also included a harmonic forcing term $A \cdot f \cos \omega t$ along with the term that represents the DV. During the course of variation of discharge voltage, the plasma modes are also influenced in such a way so as to

two-body recombination, three-body recombination term. α , λ and μ are positive. ω is the frequency of the external forcing and f is the amplitude of the forcing term ($\cos \omega t$). n_0 represents the unperturbed electron density.

In this work, we have assumed $a = b = c = 0.1$, $f = 0.55$, $\omega = 1$, with the assumption that discharge voltage directly influences the ionization term, so that we consider $e(A) = A$. Fig 5.13a shows the relaxation oscillations at various values of the discharge voltage and the corresponding phase space plots are shown in Fig 5.13b . At $A = -0.6$, we observe a limit cycle oscillation, which becomes chaotic around $A = -1.2$ as clearly observed from the corresponding phase space plot. Further increase in the absolute value of A ($\sim -3.8, -5.4, -6.3$) leads to limit cycle oscillation (relaxation oscillations) whose period increases (i.e the number of peaks decreases) with increasing A . With $f = 0$, it is observed that the model exhibits oscillations whose time period increases with increase in A (absolute value). However, with non-zero values of f , homoclinic bifurcation was observed along with the occurrence of chaos for a very narrow range of values of A . This is in agreement with the second regime of experimental results where the increase in the discharge voltage shows distinct chaotic oscillations followed by the increase in the time period of relaxation oscillations. As the values of $A(-3.8, 5.4, -6.3)$

need of incorporating the forcing term which is thought to be mimicked by the self excited oscillations in the plasma. With the addition of such terms, we obtain fluctuation that display chaos and our numerical modelling exactly imitates the experimental findings.

3.5 Conclusion

We have investigated the appearance of inverse and normal homoclinic bifurcation and the associated complexity dynamics in the fluctuations of the glow discharge plasma system. The understanding of the role of nonlinearity in the plasma dynamics is quite a challenging job as it arises from many degrees of freedom as well as different sources of free energy, different types of wave-particle interaction, and growth of instabilities. The complex dynamics in the signals has been explored by estimating respectively the Lyapunov exponent, correlation dimension, Renyi entropy etc. Gaussian Kernel Algorithm is not only computationally faster algorithm but also provides a reliable estimation of the correlation dimension. The estimation of Renyi number conforms well with the observations of complexity in the fluctuating data. Though results on homoclinic bifurcation showing chaos to order have been reported before, to the best of our knowledge, this is the first

sustain the discharge current, and once sufficient current flows in the system, anode glows become smaller in size [22, 23]. The primary phenomena behind the oscillations are ionization instabilities, which happens to lie in the range of ion acoustic frequencies. Such frequencies are also observed experimentally. We have also noted that ordered to chaotic state driven by a driving force (DV) as a form a input energy to the system tends to be stabilized by homoclinic bifurcation. Another way of looking at the transition is that at higher values of DV some modes get higher energy to become dominant one resulting in the suppression of other modes so that the chaotic state disappears and the system enters into ordered state. This is same as saying that energy transfer occurs toward modes which are linearly stable. Although homoclinic bifurcation could be observed in the numerical model without the harmonic forcing term, the later was found to be responsible for driving the system through chaotic oscillations before the system began to display an increase in the time period of the relaxation oscillations. The study of this kind of bifurcation can be an useful for understanding the behaviour of bursting oscillation[24].

Chapter 4

Investigation and quantification of nonlinearity using surrogate data in a DC glow discharge plasma

In this chapter detection of nonlinearity has been carried out in periodic and aperiodic floating potential fluctuations of DC glow discharge plasma (GDP) by generating surrogate data using iterative amplitude adjusted Fourier transform (IAAFT) method. We introduce ‘delay vector variance’ analysis (DVV) for the first time which allows reliable detection of nonlinearity and provides some easy to interpret diagram conveying information about the nature of the experimental floating potential fluctuations (FPF). The method of false nearest neighbourhood (FNN) is deployed on the FPF’s to find a good embedding so as to be acquainted with the

4.1 Introduction

In our previous chapter we have explored the complexity dynamics of the floating potential fluctuation in the two regimes of our observation (normal, inverse homoclinic) by estimating some statistical parameters with increasing discharge voltage (DV). In this chapter we have carried out qualitative and quantitative aspect of nonlinearity on floating potential fluctuations (FPF's) acquired under two different values of pressures ($P=0.056, 0.085$ mbar) for increase in DV. In the context of nonlinearity, substantial amount of research work is going on to elucidate the role of nonlinearity [111], predictability [112] from various areas of science like neuroscience, physiology [113] and earth science [3] and especially in plasma physics [28]. The effect of nonlinearity is manifested as hysteresis[114], wave breaking [115], chaos and turbulence [116] and different kinds of coherent structures like solitons, shocks [117]. Hence it becomes important to verify the existence of the underlying nonlinear processes that convey information concerning the absence or presence of nonlinearity. Sudeshna et al. [118] have observed the phenomena of hysteresis in amplitude and frequency bifurcations of floating potential fluctuations in a glow discharge plasma. In the context of plasma discharges, Flanagan and Goree[27] identified the nonlinearity resulting from spatial growth of self-excited dust-density

knowledge of an appropriate embedding dimension of our glow discharge plasma system is required, which is estimated by means of a well known method called false nearest neighbour (FNN) [50]. DVV analysis has been introduced in GDP both in qualitative and quantitative ways to ensure a comprehensive characterisation of a time series by taking into account different properties namely time delay embedding, phase space geometry [106], surrogate data technique. The application of this proposed method (DVV) is concerned with detecting and analyzing nonlinear properties of a time series in order to yield a standardized characterisation of that time series that examines the local predictability over different scales. As we are already aware of the artefact of Phase randomised method (PR) for periodic data [94], we have tried to compare the results produced by IAAFT and PR method. Our IAAFT method proves to be extremely reliable in producing surrogate data for DVV analysis.

Experiments were performed under two different pressures ($P=0.056, 0.085$ mbar) by applying increasing DV. An unbiased Langmuir probe was used to obtain the floating potential fluctuations acquired with a sampling time of $2 * 10^{-7}$ sec for $P=0.085$ mbar as shown in the schematic diagram of 3.1 in the previous chapter.

4.2 Floating potential fluctuation, power spectral analysis

spectra. The range of frequencies as observed from the power spectrum are seen to lie from 4.5 kHz to 12 kHz indicating the presence of ionization instabilities. The fluctuations exhibit two periods for DV=337, 341, 350, 355 volt with the dominant frequencies being 8.5, 7.5, 1, 5.5 kHz for the above values of DV respectively. Fig 4.2 displays the variation of dominant frequencies (the frequency which has maximum power) which seem to vary in the range from 5.5 kHz to 12.5 kHz for the entire range of DV until the chaotic oscillations set in having frequencies in the range of 1.5 kHz to 7.5 kHz. Further increase in DV results in 3-period oscillations.

We present in Fig 4.3 a sequential change in FPF at $P=0.056$ mbar of gas pressure by varying DV ranging from 320 volt to 410 volt. Initially the oscillations are observed to be quasi-periodic in nature but the enhancement of DV makes the oscillations chaotic. Power spectral analysis (in Fig 4.4) carried out on the raw data shows that at the initial value of DV most of the frequencies are concentrated below 400 Hz but with the increase in DV, nonlinear interactions between different frequency components give rise to chaotic fluctuations as seen by the appearance of broad band of frequencies.

4.3 Dimensionality analysis

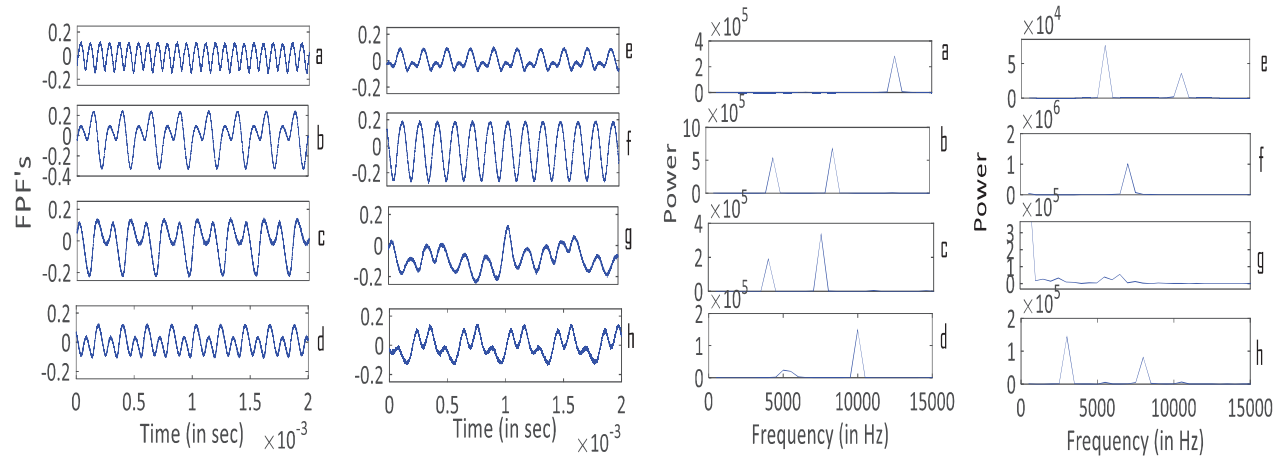
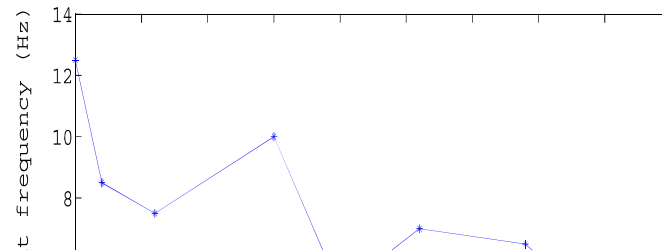


Figure 4.1: Sequential change in the FPF and frequency spectrum at 0.085 mbar for different DV(in volts) in the left and right panel respectively: (a) 335V (b) 337 V (c) 341V (d) 350V (e) 355V (f) 361V (g) 369V (h)378V



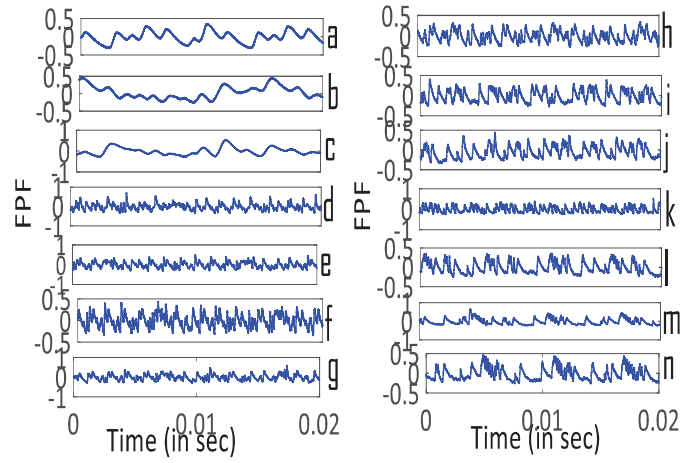
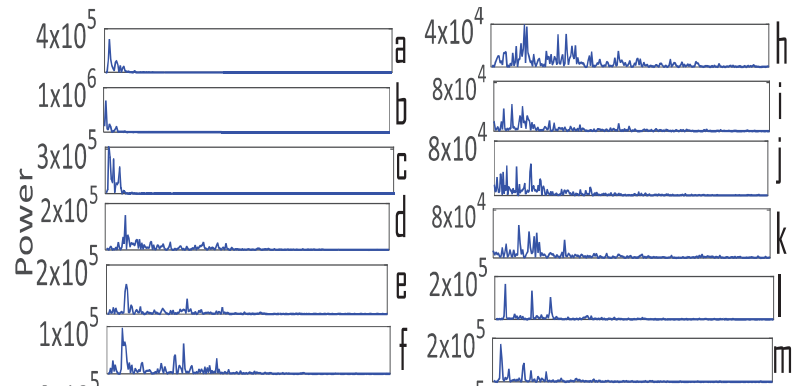


Figure 4.3: Sequential change in the raw signals at 0.056 mbar for different DV(volts): (a) 320V (b) 328 V (c) 338V (d) 344V (e) 350V (f) 357V (g) 365V (h) 372V (i) 378V (j) 384V (k) 390V (l) 395V (m) 402V (n) 410V



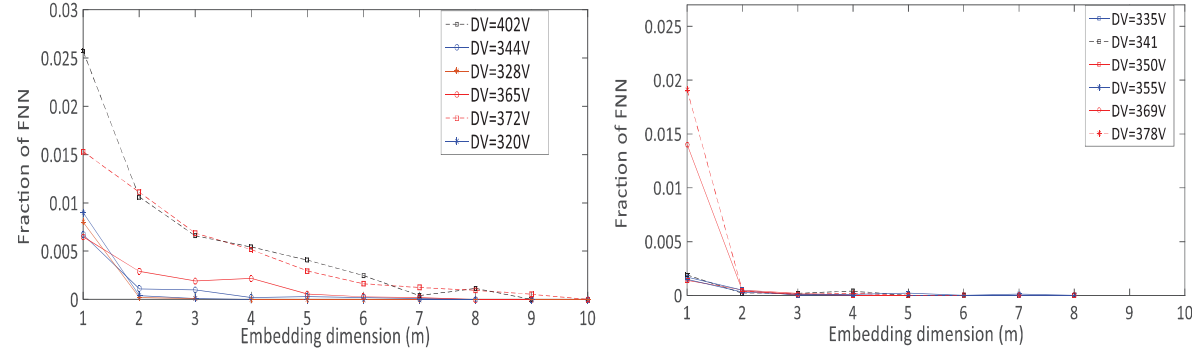


Figure 4.5: Plot of false nearest neighbourhood at $P=0.056$ mbar and $P=0.085$ mbar for different DV in the left and right panel respectively

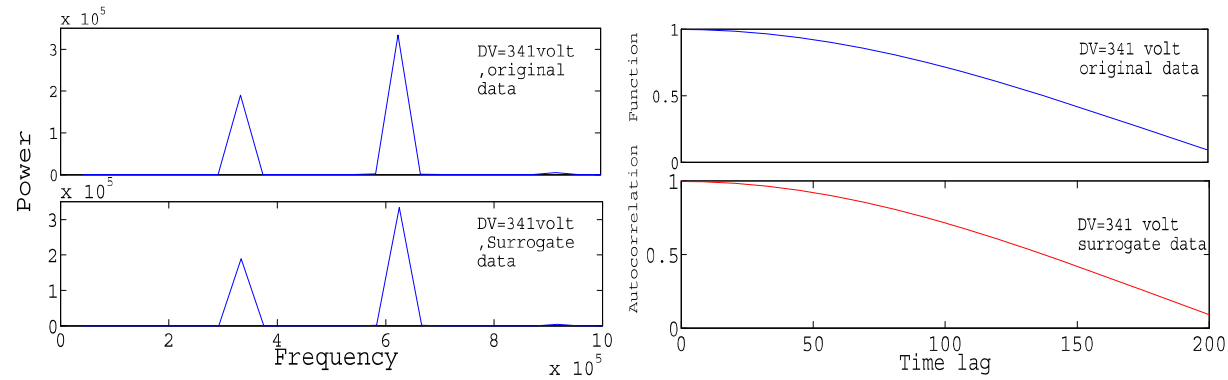


Figure 4.6: Exact Fourier spectrum and Autocorrelation function of the original and its surrogates for a particular DV=341 volt at $P=0.085$ mbar

Fig 4.5) and it almost remains at that value upto DV=328V. Further increase

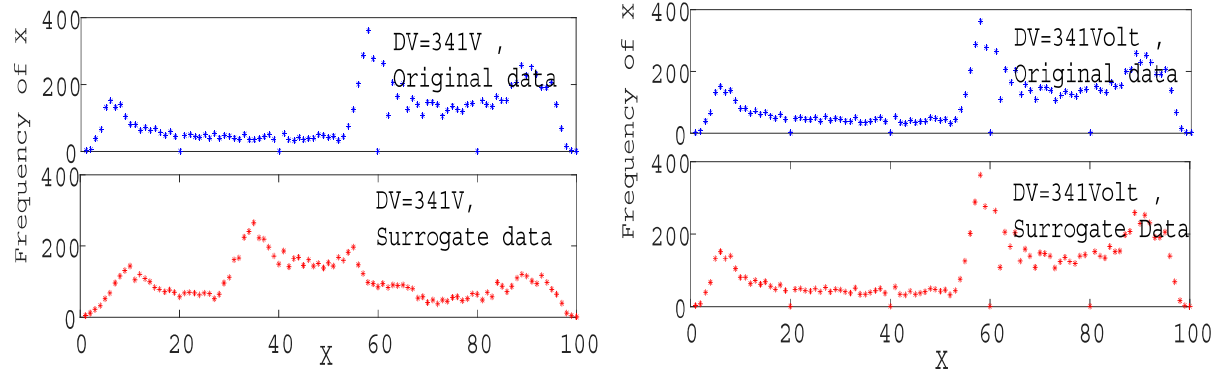


Figure 4.7: Probability distribution of original and PR surrogate data (left panel) and the same in right panel for IAAFT surrogate

4.4 Analysis with the surrogate data

Surrogate data as already discussed in chapter two are time series constructed from an experimental time series in such a way that they share all the linear properties (power spectrum and autocorrelation function) with the original data.

The goal of generating the surrogate data [71] is to establish the presence of nonlinearity by excluding a reasonable alternative, called the null hypothesis. We have shown here in the left and right panels of figure 4.6 the power spectrum and autocorrelation function given in equation 2.9 of chapter two obtained from both the original as well as surrogate time series ($P=0.085\text{mbar}$) respectively. Their identical nature leads to the conclusion that both of them bear the same linear

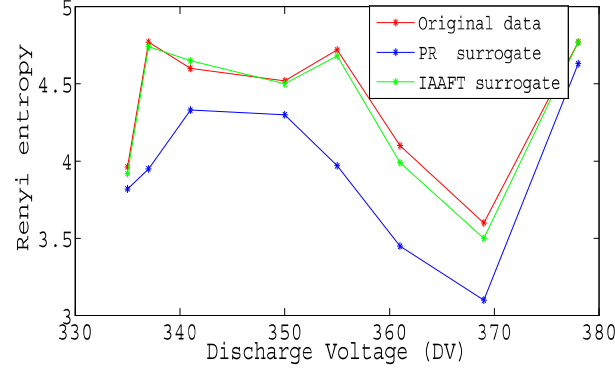


Figure 4.8: Plot of Renyi entropy of original time series along with its surrogates for $P=0.085$ mbar

Left panel of Figure 4.7 shows probability distribution of original data and the surrogate data generated by Phase randomization technique whereas right panel of the Figure 4.7 depicts the probability distribution for the original as well as IAAFT surrogate. Abscissa X in Figure 4.7 denotes the number of bins created and frequency of X in the ordinate stands for the no of points falling in the bins.

Generally a test statistics is said to be pivotal [34] if it follows the same probability distribution with that of the surrogate. The histogram obtained from the IAAFT surrogate, as shown in the right panel produces a distribution identical with that of the original. So it can be referred to as pivotal whereas the histogram generated by PR surrogate is known as non-pivotal distribution.

In figure 4.8 we have plotted the Renyi entropy(R)[120, 54] for original as well

method is more accurate and reliable as compared to PR method.

4.5 Delay vector variance analysis

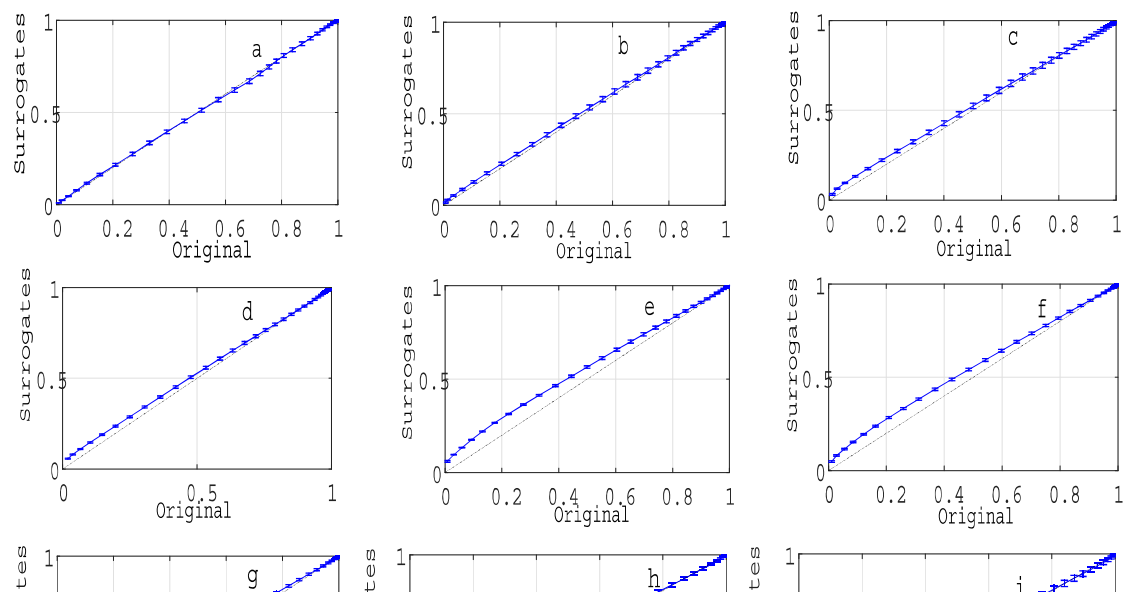
The method delay vector variance (DVV) is employed for the first time in the glow discharge plasma system with the novel intention of identifying nonlinearity. Due to the standardisation within the algorithm, the method is robust to the presence of noise. The approach for the calculation of DVV is elaborately discussed in Chapter two. The measure of nonlinearity following this approach is given in equation 4.1.

$$\sigma^2 = \frac{(1/N) \sum_{k=1}^N \sigma_k^2}{\sigma_x^2} \quad (4.1)$$

where σ^2 and σ_x^2 denote the variance of the surrogate and original time series respectively. If the DVV plots obtained from surrogate time series are similar with that of the original series or in other way if the scatter diagram coincides with the bisector line, the original time series can be supposed to be linear. The deviation from the bisector line is thus an indication of nonlinearity as already enlightened in the data analysis procedure under the section delay vector variance (DVV).

Table 4.1: Results of the rank test of nonlinearity with varying DV for P=0.056 mbar

DV	t^{Rev}	DVV
320V	36	31
328V	40	45
344V	46	45
365V	43	44
372V	50	50
384V	50	50
395V	50	50
402V	50	46
410V	48	48



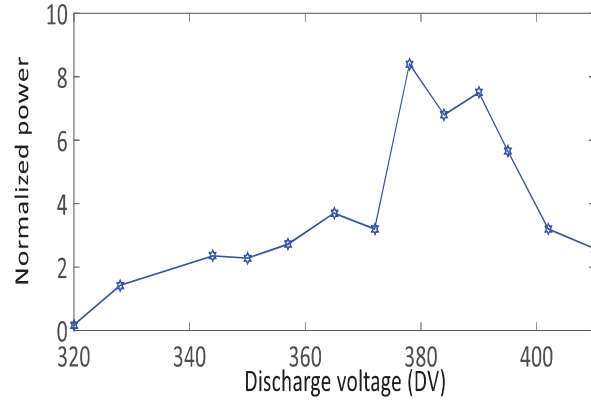


Figure 4.10: Contribution of the sum of power in different DV (in volt) for $P=0.056$ mbar

hypothesis for nonlinear quantities like time reversal t^{Rev} [88] (equation 2.21), DVV [48]. The rejection of null hypothesis for a right tailed test with 49 surrogates is satisfied when the rank of the original test statistics is computed to be 50.

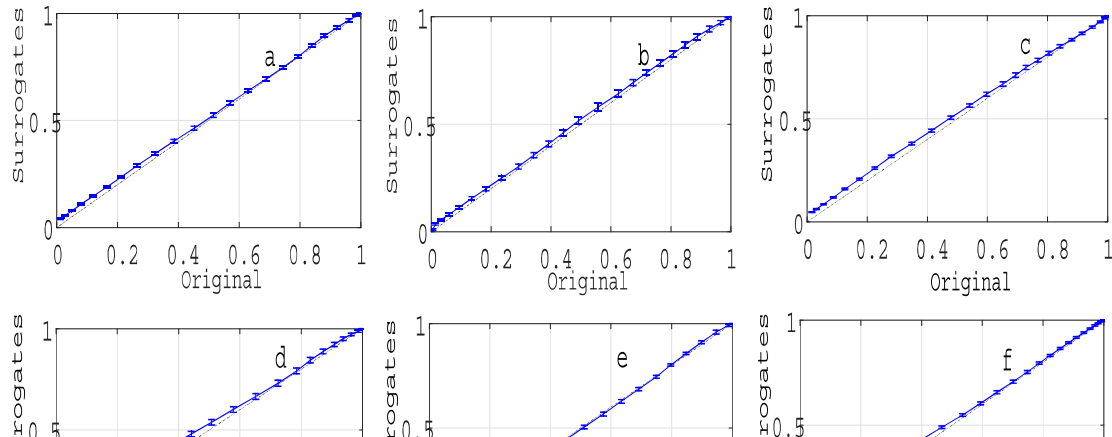
We see that an increase in the degree of nonlinearity corresponds to the deviation from bisector line. Due to the standardisation of the distance axis, these plots can be conveniently combined in a scatter diagram, where the horizontal axis corresponds to the DVV plot of the original time series, and the vertical axis corresponds to that of the surrogate time series. The error bars indicate one standard deviation from the mean of σ^2 . Initially at DV=320, 328 V scatter plots almost lie

which is also corroborated by the rank test.

In a rf dusty plasma experiment, Flanagan and Goree [27] have studied non-linearity in a naturally occurring dust density wave using neutral gas pressure as the control parameter, with the nonlinearity indicated by the presence of harmonics and quantified by total harmonic distortion. In the present work involving dc glow discharge plasma, the measure of nonlinearity is estimated by comparing the total power present in all frequencies normalized by the power in the frequency carrying maximum power. For this method we have selected power or energy that is within 10% of the maximum frequency range and eliminate the power which is below that range. The accumulation of the power or energy lying in the range of frequencies other than the power which is carried by the most dominant frequency (the frequency of maximum power) can be thought to be attributed to the presence of nonlinearity. We have plotted the normalized power against one of the control parameters DV in Fig 4.10 and the maximum power occurs at DV=372 volt where the deviation from the bisector plot becomes maximum in our DVV scatter plot (Fig 4.9). With further increase in the values of DV, normalized power goes on decreasing and finally it attains a very small value at DV=410 volt. This is also confirmed by the DVV analysis as well as by rank test as depicted in Fig 4.9.

Table 4.2: Results of the rank test of nonlinearity for P=0.085 mbar

DV	t^{Rev}	DVV
335V	24	21
337V	32	30
341V	33	35
350V	36	32
355V	29	37
361V	20	25
369V	35	42
378V	38	44



t^{Rev} and DVV is far below the expected value for satisfying the criteria for the rejection of null hypothesis. The power spectrum for this pressure as shown in Fig. 4.1 exhibits a sparse nature in contrast to the spectrum obtained at $P=0.056\text{mbar}$ making it unfavourable for the study of nonlinearity using the total power present in the different frequencies.

4.6 Conclusion

To summarize, we have been able to explore nonlinearity of two sets of experimental time series data for increasing DV, by DVV analysis, rank test, and also from the accumulation of total power or energy within the observed frequency range. The appearance of nonlinearity in the fluctuations of a glow discharge plasma has been investigated by producing a number of surrogates that reject null hypothesis. Presence of nonlinearity is seen to be prominent at low pressure in view of the decrease in collisional frequencies. Due to nonlinear interactions, different types of waves inherently present in the glow discharge system such as ionization instabilities give rise to different frequencies that are excited at $P=0.056\text{mbar}$. The DVV scatter plots for $P=0.085\text{ mbar}$ reveal no signature of nonlinearity as also indicated in the analysis using power spectrum. At this higher pressure, the dominant fre-

insight in revealing the aspect of nonlinearity. The nonlinear effects obtained from DVV plots turn out to be almost similar with the analysis based on accumulation of power and rank test confirming the robustness of the methods. Such statistical analysis techniques based on delay vector variance, rank test coordinated with conventional data analysis tools in plasma like power spectrum, wavelet analysis can be immensely beneficial for the quantification of nonlinearity inherently present in plasmas.

Chapter 5

Evidence of nonlinearity in presence of external forcing and magnetic field in a glow discharge plasma

The previous chapter was devoted to the study of nonlinearity by introducing delay vector variance method based on the surrogate data technique for increasing DV. This chapter also investigates the evidence of nonlinearity for externally applied sinusoidal forcing as well as magnetic field by implementing different statistical analysis techniques likewise delay vector variance, Zscore. An estimate of the Zscore helps in detecting the presence of nonlinearity in a somewhat quantitative

5.1 Introduction

Plasma effects are finding ever increasing applications in astrophysics, solid state physics, physics of gas discharge and research on plasma confinement and heating. Plasmas are intrinsically nonlinear whose effects manifest in the form of various exotic structures such as double layers [121], solitons, vortices, different types of waves, instabilities and turbulence [13]. Glow discharge plasma being rich in high energy, electrons and ions are capable of exhibiting many such nonlinear phenomenon [122, 118, 8]. GDPs and their counterparts like magnetrons [39] are widely used in industrial applications and hence characterizing them through nonlinear techniques can help in improving their performances.

It is for the first time in GDP system that we deploy some new well established nonlinear techniques like Zscore[94], bicoherency analysis[123], Delay vector variance (DVV) method [88] to explore nonlinearity by creating surrogate data. Delay vector variance analysis resting on the theory of time delay embedding and discussed also in the previous chapter has been implemented on both experimental and numerical results. In the context of externally excited system Koepke et al.[18] have identified a periodic nonlinear interaction between pairs of self-excited, propagating, ionization waves simultaneously present in the positive column of a neon

a magnetized thermionic plasma discharge have been investigated by Klinger et al. [26]. Investigation of nonlinearity using harmonic detection method [27, 8, 28] has been performed in RF discharge and glow discharge plasma respectively. Although a comparative study of magnetized and unmagnetized plasma oscillations has been conducted [124] in a direct current (DC) glow discharge plasma, the qualitative and quantitative measure of nonlinearity has been performed first time in our work by varying the forcing amplitude, frequency and magnetic field. Through the study of bicoherency analysis we gain information about the interaction amongst different modes obtained after performing empirical mode decomposition analysis [123, 125]. If the characteristic measure of original time series are significantly different from those for the surrogate data [126], the null hypothesis that the data can be described by linear stochastic model can be rejected.

The study of nonlinearity was carried out under two different conditions (i) application of magnetic field (ii) forcing the system by using an external oscillating electric field (Fig 2.1). An unbiased Langmuir probe was used to obtain the floating potential fluctuations acquired with a sampling time of 0.2 s, 0.5 s respectively for 1, 1.5 kHz frequency. For two values of ω (1, 1.5 kHz), forcing amplitude (A) was varied from 0.2V (min) to 8V (max) to study the effects of external forcing on the system. The magnetic field was varied from 15 to 105 Gauss (G) for these

5.1 keeping discharge voltage (DV) fixed at 343 volt and went on increasing the amplitude of forcing (A). Initially at low amplitude of forcing (A=2V) the position of the peaks in power spectrum plot shifts to 4.5 and 8.5 kHz depicted in the right panel of Fig 5.1 and in Fig 5.2. Subsequent raising in the value of A=5V, the system undergoes a transition from double period to 3 period fluctuations with the appearance of a new peak at 1.5kHz frequency. Further increase in the value of A results in generating new peaks at frequency of 5.5, 9.5kHz. The amplitudes of the peaks generated do not linearly increase with increase in the value of forcing amplitude (A).

A three dimensional analog of the Fig 5.1 is also presented in the form of contour plot in figure 5.2 with colour axis representing the power. We have carried out another set of experiment for P=0.180 mbar by pacing the plasma in the periodic regime with the 1.5 kHz frequency. The amplitudes of the power at different values of forcing amplitude (A) are plotted in the right panel of figure 5.3. For initial increase in A upto 3V only the frequencies of the dominant peak (peaks carrying maximum power) exist with the addition of 1.5 kHz frequency. Subsequent increase in A results in adding new frequencies (3, 3.7, 3.1 kHz) for A=4.6, 5.4V apart from the dominant one and the frequency by which we are pacing the

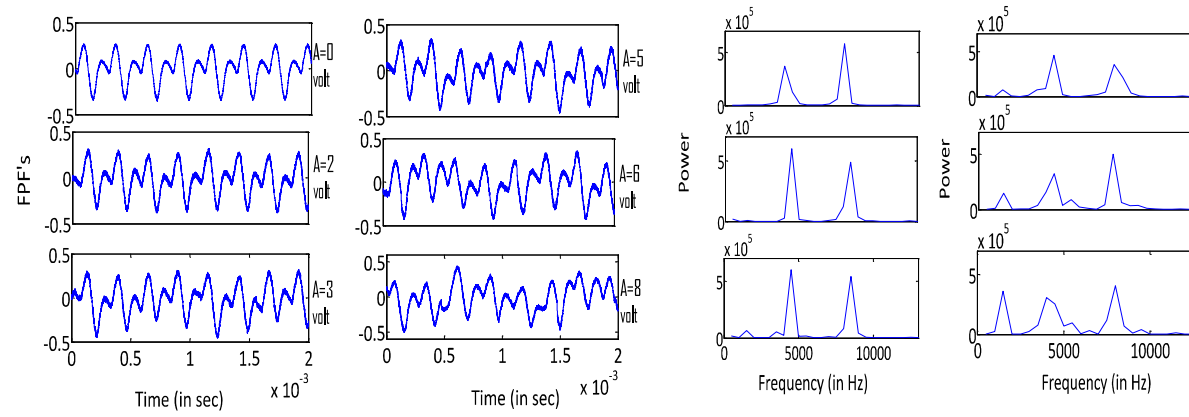


Figure 5.1: Plot of rawsignal as well as Fourier spectrum with amplitude of sinusoidal forcings (A) are 0, 2, 3, 5, 6, 8 volt for $P=0.085$ mbar

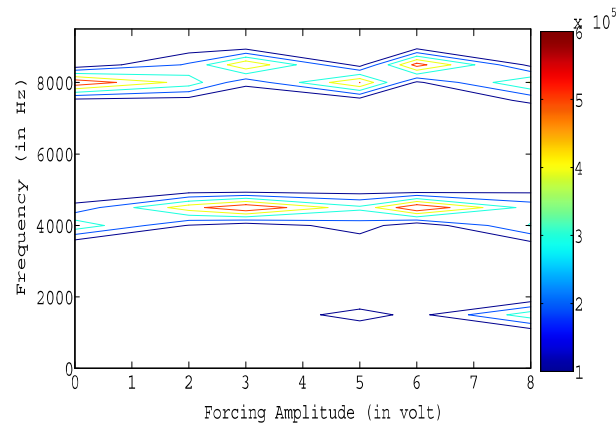
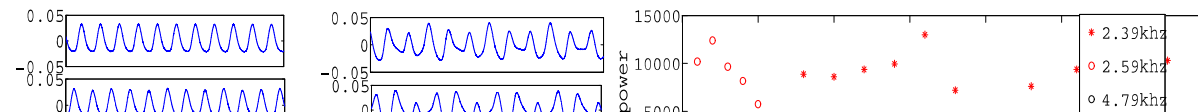


Figure 5.2: Contour Plot of Fourier spectrum with amplitude of sinusoidal forcings (A) for $P=0.085$ mbar



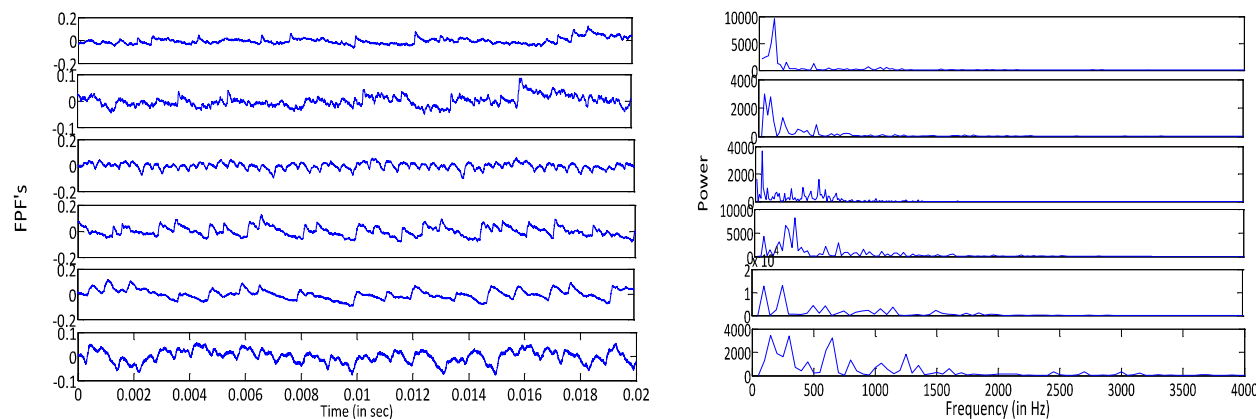


Figure 5.4: Plot of rawsignal as well as power spectrum with magnetic field strengths 0, 15, 30, 60, 90, 105 Gauss

seem to increase as indicated by the appearance of broad band which is thought to be emerged due to the nonlinear interaction between the frequencies generated . At a very high value of magnetic field of $B=105\text{G}$, we obtain the frequencies lying in the range upto 4 kHz.

As already illustrated in chapter 2 by equation 2.1 and 2.2 correlation dimension (CD) is defined as the dimensionality of the space occupied by the points of that time series. The estimation of CD requires the proper knowledge of embedding

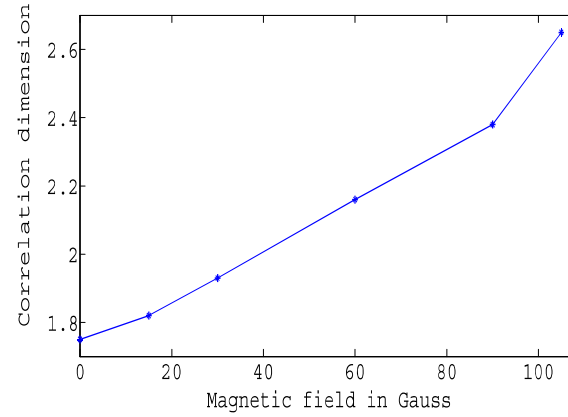


Figure 5.5: Correlation dimensions of floating potential fluctuations shown for increasing magnetic field

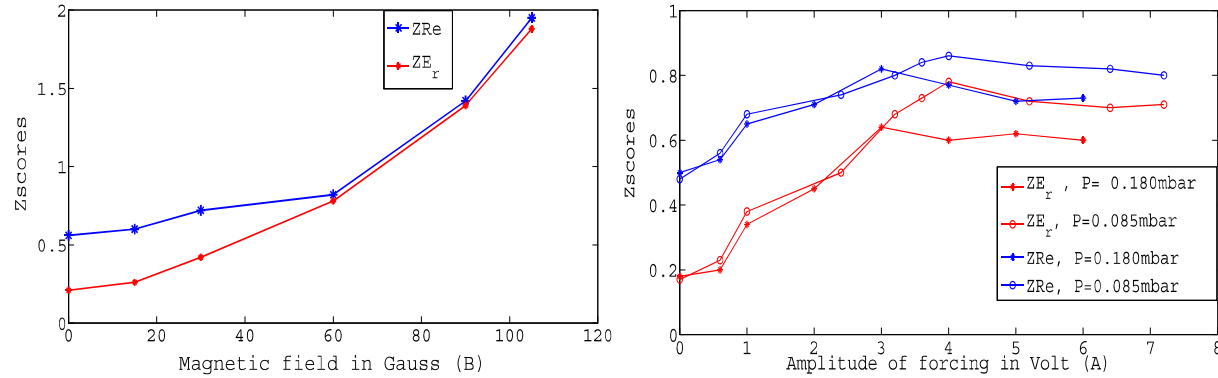


Figure 5.6: Plot of Zscores of Renyi entropy, E_r statistics for different values of B and A

5.3 Nonlinearity analysis with Zscore based on the surrogate data

mean of M for the surrogate data and σ_s is the standard deviation of M for the surrogate data. The left panel of figure 5.6 displays the Zscore values of renyi entropy, E_r statistics for increasing magnetic field whereas right panel exhibits Zscores of the same quantity for increasing A . At $B=90$ Gauss, ZE_r and ZRe surges appreciably followed by the jump to a value 1.88 and 1.16 respectively at $B=105$ Gauss. Increase in the values of B is observed to have prominent effect in increasing ZE_r and ZRe implying the rejection of null hypothesis at $B=90, 105$ Gauss.

ZE_r and ZRe values are observed to be too low initially at $A=0$ volt i.e without forcing. Increase in forcing amplitude (A) results in the increase in ZE_r and ZRe values as observed from the right panel of Fig 5.6. Further increase in the values of A does not enhance the values of ZE_r and ZRe indicating the fact that increase in A has less effect in increasing nonlinearity.

5.4 Nonlinearity analysis with delay Vector Variance analysis, rank test for increasing forcing and magnetic field

The proposed DVV method already introduced in the previous chapter nicely orchestrate the aim of exploring nonlinearity for increasing DV in glow discharge

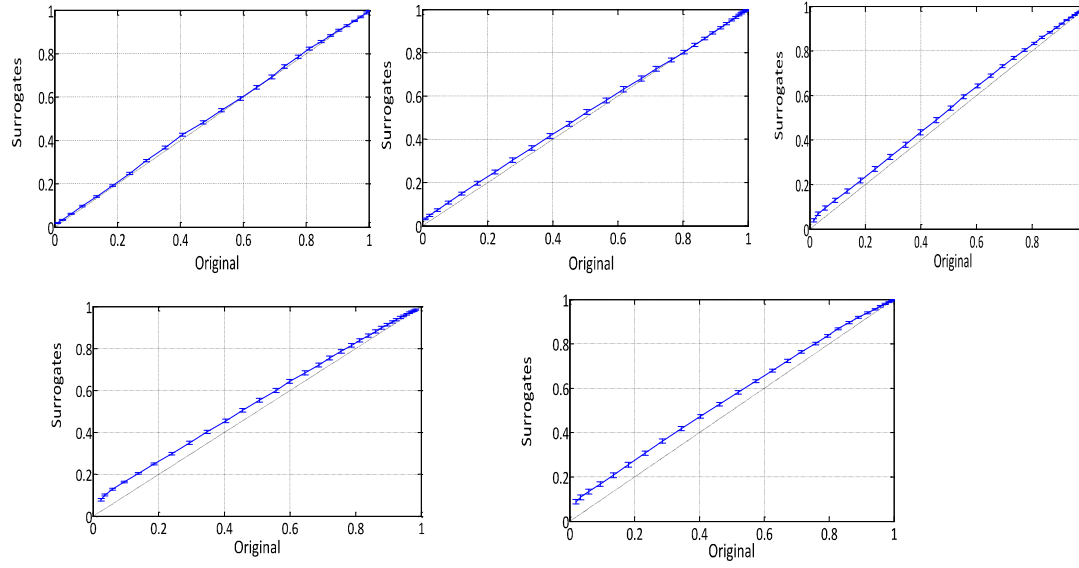
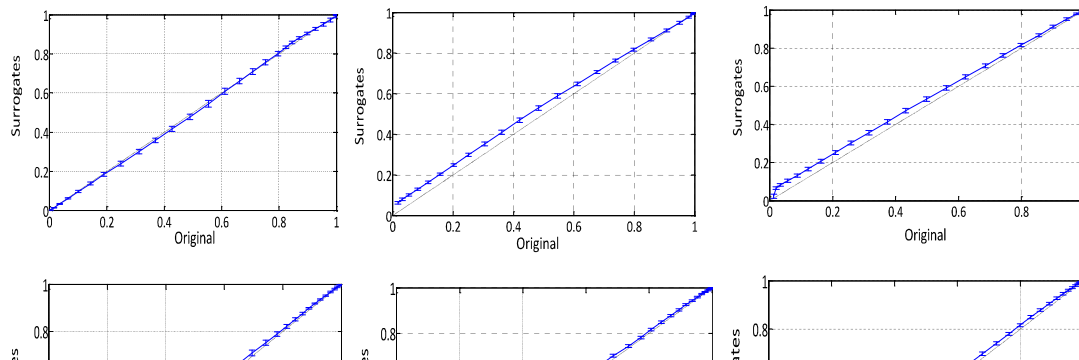


Figure 5.7: Sequential change in DVV scatter plots for $P=0.085\text{mbar}$ with magnetic field strength: $B=0, 30\text{G}, 60\text{G}, 90\text{G}, 105\text{G}$



an increase in the degree of nonlinearity corresponds to the deviation from bisector line. Horizontal axis of the DVV scatter diagrams corresponds to the DVV plot of the original time series, and the vertical axis corresponds to that of the surrogate time series with the error bars indicating one standard deviation from the mean of σ^2 . For portraying the DVV scatter plots we put the embedding dimension computed from the FNN method[49].

DVV scatter diagrams obtained from the figure 5.7 for magnetic field indicates that initial increase in magnetic field (B) have less effect in increasing nonlinearity whereas at higher value of B=90 Gauss nonlinearity increases appreciably and at B=105 Gauss we observe prominent deviation from bisector line. So increase in magnetic field appears to have significant effect on nonlinearity as ensured from the quantitative estimation of Zscores in Figure 5.6.

At A=0 i.e without forcing the first DVV scatter plot does not display any nonlinearity but the application of forcing at $A = 2V$ causes the DVV scatter plot to deviate from the bisector line. Further increase in the value of A does not produce more deviation from the bisector line with the deviations remaining almost same at $A = 3, 5, 6V$. The interesting fact is that the maximum value of

Table 5.1: Results of the rank test of nonlinearity with varying magnetic field (B) for P=0.085 mbar

B	Zscore	DVV
0G	32	29
30G	38	42
60G	46	48
90G	50	50
105G	50	50

rank test in order to be enlightened with both the qualitative and quantitative aspect respectively. Table 5.1 represents the rank test for detecting the rejection of null hypothesis for Zscore, DVV. The rejection of null hypothesis for a right tailed test with 49 surrogates is satisfied when the rank of the original test statistics is computed to be 50 and the null hypothesis is rejected to satisfy the presence of nonlinearity at higher value of magnetic field. In a rf dusty plasma experiment, Flanagan and Goree[27] have studied nonlinearity in a naturally occurring dust density wave using neutral gas pressure as the control parameter, with the nonlinearity indicated by the presence of harmonics and quantified by total harmonic distortion. In the present work involving externally excited DC glow discharge plasma, the measure of nonlinearity is estimated by comparing the total power present in all frequencies normalized by the power in the frequency carrying max-

power is seen to increase with B with the maximum power occurring at maximum value of B where the deviation from the scatter plots also becomes maxima along with Zscore.

The effect of the external sinusoidal forcing on the plasma lying in the periodic regime is viewed in terms of the generation of the frequencies and interactions amongst them. As already discussed above that we have paced the system with sinusoidal signal (by function generator) of frequency (f)=1 kHz without applying any magnetic field keeping the plasma in a period 2 regime ($P=0.085\text{mbar}$) with frequencies of 4, 8 kHz termed as (f_{01}, f_{02}) . The frequency spectrum shows peak at frequencies of 4.5 and 8.5 kHz $(f_{01} + f/2, f_{02} + f/2)$ for $A=2\text{V}$. When the perturbation amplitude (A) is changed to 5V, in addition to the frequencies of $(f_{01} + f/2, f_{02} + f/2)$ a new frequency of $3f/2$ is generated which is only due to the external frequency applied by function generator. Subsequent increase in A generates frequencies of $(f_{01} + 3f/2, f_{02} + 3f/2)$ and the nonlinear interaction between the frequencies are thought to have attributed to various statistical features obtained from DVV plots, Zscore and bicoherency analysis. The amplitude of the peaks with frequencies does not linearly increase if we keep increasing the value of our forcing amplitude (A). The plot of the total power divided by power

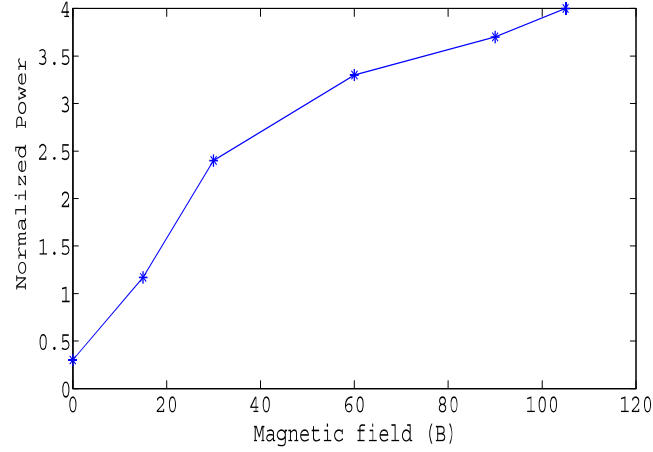


Figure 5.9: Contribution of the sum of power with different B (in Gauss)

are perturbing the plasma.

5.5 Results with bicoherency analysis

After performing the empirical mode decomposition a nonlinear technique (described in chapter two), introduced by N.E. Huang et al. for the analysis of non stationary and nonlinear signals on the FPF's we are left with intrinsic mode functions (IMF's) represented in the form of $Z_i(t) = A_i e^{(j\phi(t)t)}$ where $A = \sqrt{(X^2 + Y^2)}$, $\phi = \arctan(Y/X)$ are the amplitude and instantaneous phase angle respectively and Y is obtained by taking the Hilbert transformation on the signal X. We then continue to investigate the interaction between the different modes by estimating

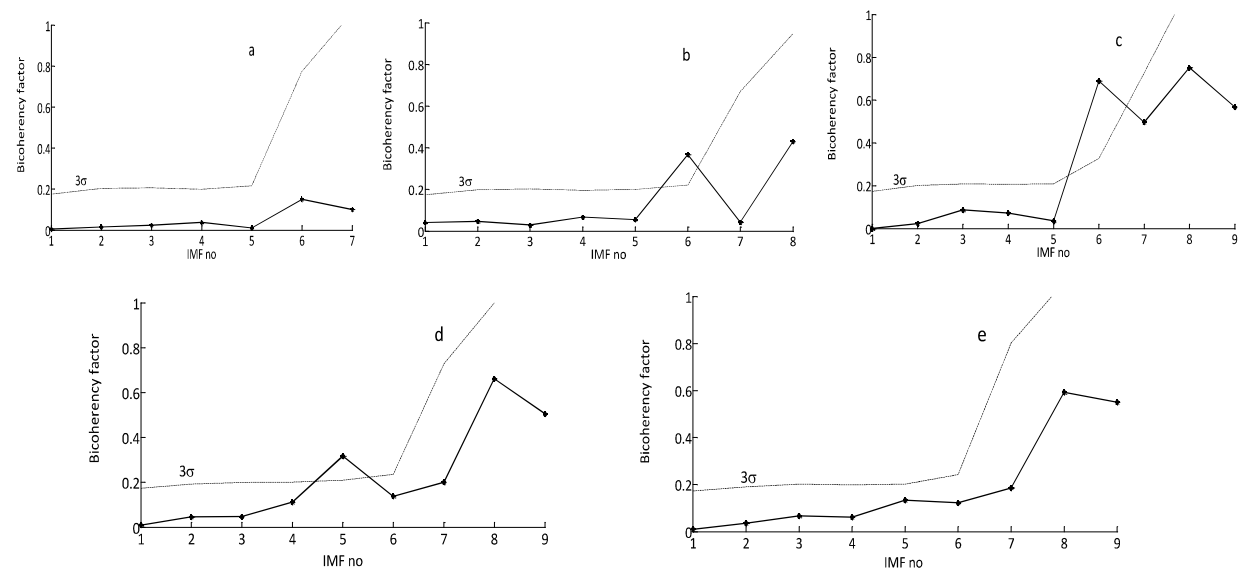
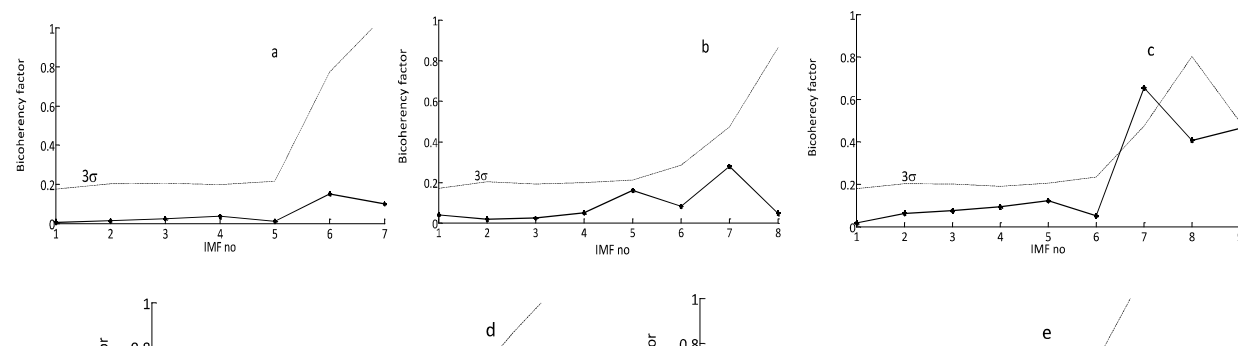


Figure 5.10: Bicoherency factor for A a) 0V b) 2V c) 3V d) 5V e) 6V



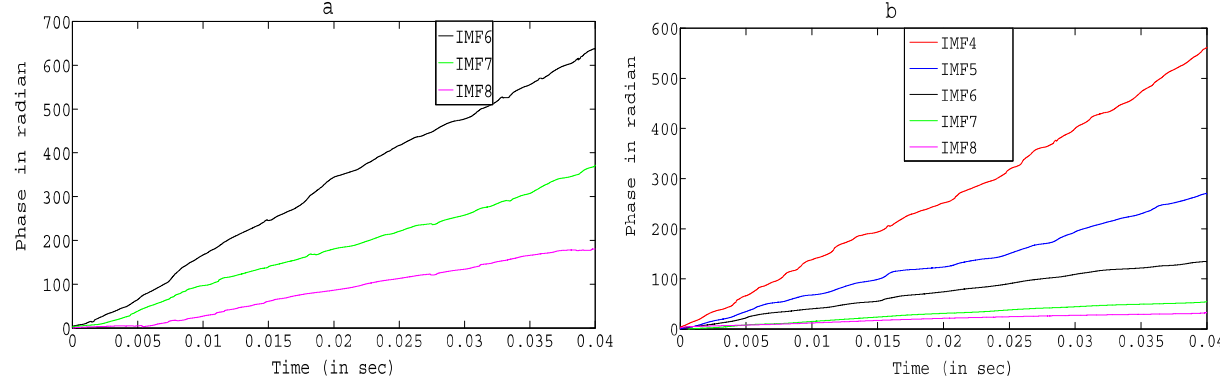


Figure 5.12: Unwrapped phases of IMFs a) Forcing b) Magnetic Field

to $A=2, 3$ Volt whereas we have interactions amongst 5-7 IMFs corresponding to $A=4$ volt. The triplet interaction between the modes are explored in terms of the interaction between the frequencies 15, 8.4, 5.09 kHz in figure 5.12a obtained from the slope of curve as $\omega = \frac{d\phi}{dt}$. The interaction between the modes again disappears at higher value of $A=6$ volt shown in Figure 5.10e which consolidate our DVV analysis.

Portrayed in Figures 5.11 a-e are the effect of increasing magnetic field on the interaction between the modes. The triplet interaction between the modes goes on increasing as we increase B upto 105G. At the intermediate value of $B=60$ G Fig 5.11c reveals the interaction amongst 7-9 IMFs. Finally at $B=105$ G 4th-6th IMFs in Fig. 5.11 d are seen to remain above the error value, so we take into

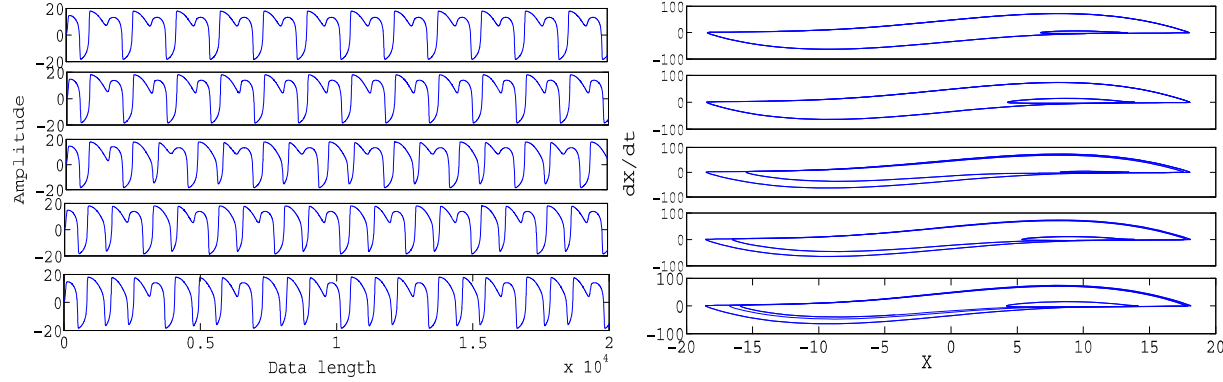


Figure 5.13: Amplitudes of the numerical solutions with the variation in F and their corresponding phase space plots

5.6 Numerical Modelling

In order to understand the experimental observations, i.e the system dynamics in presence of forcing, we have used the analytical model developed by Kadji et al [108, 128] based on two fluid equations in the presence of source term representing the effects of ionization and recombination. In this chapter we include a term representing the applied external sinusoidal forcing in the right hand side of equation 5.1 along with the term A which is considered to serve the role of DV .

$$\ddot{x} + (a + e + bx + cx^2)\dot{x} + x + a(ex + \frac{b}{2}x^2 + \frac{c}{3}x^3) = A + F \cos \omega t \quad (5.1)$$

where $x = n_1/n_0$; $a = \nu/\omega_0$; $e = \alpha/\omega_0$; $b = 2\lambda n_0/\omega_0$; $c = 3\mu n_0^2/\omega_0$; and $\nu, \alpha,$

at $t=0$. The parameters a, b, c, e are assumed to take the following values $a=0.10$, $b=0.08$, $c=0.06$, $e=-4.5$.

Fig 5.13a shows the time series obtained by solving equation 5.1 at different values of $F=12.4, 13.2, 13.4, 14.2, 14.6$ keeping A, e fixed at the values of 6 and -4.5 respectively and the corresponding phase space plots are shown in Fig 5.13b. At $F=12.4$ time series exhibits two period relaxation oscillation with one of the period being less dominant than the other. At $F=13.2$ we can observe prominent two period oscillation followed by the emergence of three period oscillation at $F=13.4, 14.2$. Further increase in F leads to the oscillation having more than 3 periods. This is in agreement with our experimental result where we have obtained our result by increasing the amplitude of forcing keeping DV fixed. Increase in the value of F keeping c fixed in our simulation is analogous to the increase in A with the DV being fixed in our experiment.

5.6.1 DVV analysis for simulated data

Now we proceed to apply our DVV method on numerically simulated data depicted in Figure 5.13 and compare it with our experimentally obtained DVV plots portrayed in Figure 5.8. DVV scatter plots of the Figure 5.14 are generated by

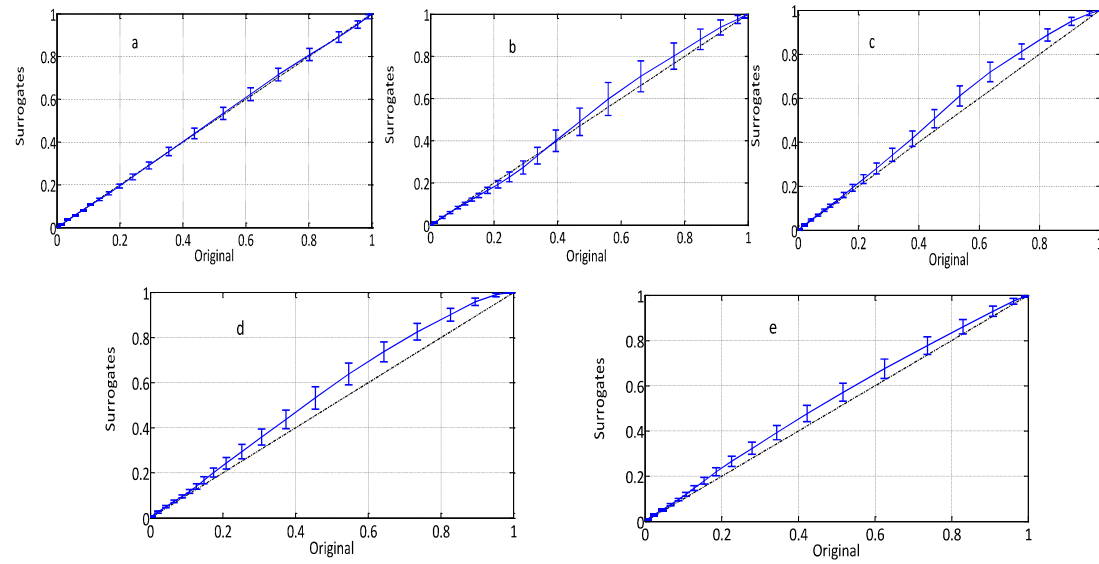
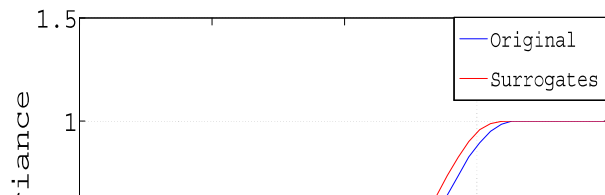


Figure 5.14: DVV scatter plot of the numerical solution for a) $F=12.4$ b) $F=13.2$ c) $F=13.4$ d) $F=14.2$ e) $F=14.6$



that DVV plots at the extreme right will converge to unity since for the maximum span all DVV's belong to the same set and σ^2 of the surrogate will become equal to that of original time series which is reflected in Fig 5.15 where we have plotted variance σ^2 against the standardized distance for $F = 13.4$ and the plot is observed to converge at unity. The convergence of the DVV plots at the extreme right is ensured by keeping the span parameter in our simulation at appropriate value.

5.7 Conclusion

We have explored the feature of nonlinearity in an experimental time series data obtained in the FPF's of GDP for various values of external forcing as well as magnetic field (B) by DVV, Zscores, bicoherency analysis. The experimental DVV plots have been compared with those obtained from the numerical model depicting ion acoustic fluctuation in presence of ionization and recombination effect. Pacing the plasma kept in the periodic regime with a sinusoidal frequency chosen below the dominant frequency, we are able to get additional frequencies apart from the dominant one and the one by which plasma is driven. However, the sparse nature of power spectrum is thought to contribute less to the emergence of nonlinearity which is also ensured by the DVV scatter plot applied on experimental as well as

to interaction and the accumulation of power lying in this frequencies are believed to contribute to the deviation in DVV scatter plots. Between every collision in strong magnetic field the plasma particles traverse a distance on the order of Larmor radius. The increase in magnetic field have effect in confining the charged particles by hindering the random motion with the wall. The diffusion coefficient can be estimated in terms of the mean free path length and collision frequency. An increase in the magnetic field strength reduces the collision frequency leading to an increase in the ionization in the plasma. These effects are thought to contribute to the emergence of nonlinearity in plasma which are missing in the absence of the magnetic field. The reason motivates us to explore the feature of nonlinearity by DVV, Zscore as well as by bicoherency analysis. The complexity of the system is observed to increase while increasing the magnetic field as verified from the increase in correlation dimension. The nonlinear effects obtained from DVV plots corroborate with the analysis based on accumulation of power and rank test, bicoherency, and quantitative estimation of Zscore confirming the robustness of all the methods. The results acquired with the bicoherency analysis featuring the interaction between the modes with the application of magnetic field are consistent with the DVV scatter plots and the values of the instantaneous frequencies which eventually fall in the range of some known frequencies of the system like ion

beyond 1. Here we have considered the limit of 3σ as error estimation, hence the maximum theoretical limit of error can be 3. Thus when the error crosses the value 1 for n th IMF, any IMF beyond the n th IMF is not statistically suitable for performing bicoherency analysis. We have at last carried out numerical modelling for which resembles the experimentally obtained system dynamics. Nonlinearity of the numerically obtained solutions have been investigated with the DVV method and we compare it with our experimental DVV scatter plots ensuring the robustness of the method. The results obtained using numerical modelling show a qualitative agreement with the experimental observation which is taken in the spirit of motivation only.

Chapter 7

Quantification of scaling exponent with crossover type phenomena for different types of forcing in DC glow discharge plasma

This chapter covers a detailed study of the scaling region using detrended fluctuation analysis test by applying different forcing such as noise, sinusoidal and square signals on the floating potential fluctuations (FPF) acquired under two different pressures in a DC glow discharge plasma. The transition in the dynamics is observed through recurrence plot techniques which is an efficient method to observe the critical regime transitions in dynamics. The complexity of the nonlinear

at $P=0.12\text{mbar}$ only one dominant scaling region is observed whereas the forcing applied on fluctuation ($P=0.04\text{mbar}$) two prominent scaling regions have been obtained using different forcing amplitudes indicating the signature of crossover phenomena. Furthermore a persistence long range behaviour has been observed in one of these scaling regions. A comprehensive study of the quantification of scaling exponents has been carried out with the increase in amplitude and frequency of sinusoidal, square type of forcings. The scalings exponent is envisaged to be the roughness of the time series. The method provides a single quantitative idea of the scaling exponent to quantify the correlation properties of a signal.

7.1 Introduction

In recent years there has been a growing evidence that many physical and biological system have no characteristic length scale and exhibit a power law correlation. Traditional approaches such as power spectrum, correlation analysis are suited to quantify correlations in a stationary signal [77, 78]. However many signals that are the output of complex physical [79] and biological system are said to contain nonstationarity. Almost all methods of time series analysis, traditional linear or nonlinear, must assume some kind of stationarity [61]. In many applications of linear (frequency based) time series analysis [49], stationarity has to be valid only up to the second moments (weak stationarity). Then the obvious approach is to test for changes in second or higher order quantities, like the mean, the variance, skewness, kurtosis. A number of statistical tests for stationarity [80, 82] in a time series have been proposed in the literature. Most of the tests we are aware of are based on ideas similar to the following: Estimate a certain parameter using different parts of the sequence. If the observed variations are found to be significant, that is, outside the expected statistical fluctuations, the time series is regarded as nonstationary. In case of traces of nonstationarity being detected, we are allowed to carry out modified root mean square analysis termed as detrended fluctuation

to have different correlation properties. In the last one decade DFA has emerged as an important technique to study scaling and long range temporal correlation in a nonstationary time series [134] which has been extensively studied in literature. It has been successfully applied to the diverse areas of research such as DNA [135, 136], neuron spiking [137], heart rate dynamics [138, 139], economical time series, long time weather report [140] etc. DFA is based on the idea that if the time series contains nonstationarities then the variance of the fluctuations can be studied by successively detrending using linear quadratic, cubic higher order polynomial in a piecewise manner. Most real time series exhibit persistence i.e subsequent element of the time series are correlated [86]. The study of the self similarity and scaling in physics, socio economic sciences in the last several years has brought in new insights and new ideas for modeling them. For instance one of the important empirical results of the market dynamics is that the probability distribution of price returns r in a typical market displays a power law [141] i.e $P(r) \sim r^\alpha$ where $\alpha = 3$. Similar power laws appear for the cumulative frequency distribution of earthquake magnitudes [142]. While the spectral analysis (Fourier method), wavelet transform modulus maxima (WTMM) analyze the time series directly the DFA is based on the random walk theory, similar to the Hurst rescale range analysis. Presence of strong trends associated with nonstationarity can lead

the scaling exponent by applying different forcing amplitude along with the reliable detection of the change in the value of scaling exponent in different scaling region characterised as crossover phenomena. In addition to this we have qualitatively and quantitatively revealed the underlying physics of the complexity dynamics when the system goes through a transition with the help of recurrence plot (RP) along with recurrence quantification analysis (RQA) [47] as changes in the dynamics during the measurement period usually constitute an undesired complication of the analysis and the knowledge of transition between chaotic, laminar or regular behaviour is essential to understand underlying mechanism behind a complex system [149]. Such techniques have been extensively used in diverse fields such as earth science, plasma, earth science, economy to gain understanding about the nonlinear dynamics of complex system. It has also been utilized as an emerging tool to analyze simulation data of ion temperature gradient turbulence [150] and dissipative trapped electron mode turbulence [151] and to characterize transport dynamics. The experimental setup made use for studies, observations reported in the previous chapter has been in this chapter also.

7.2 Floating potential fluctuation, Recurrence plot, Recurrence quantification analysis

recurrence quantification measures determinism (DET), and entropy (ENT) are computed for our experimental results and plotted with respect to the forcing amplitudes of noise, sinusoidal, square forcing respectively in Fig. 7.1a - 7.1d. In this work, we are studying the dynamics as well as the statistical property of the plasma fluctuations obtained while applying different types of forcing. Starting with the noise forcing, increase in amplitude of this forcing lead to the constantly decreasing trend in the values of DET, entropy. DET expressed by the equation 2.12 in chapter two determines whether a signal is periodic or not whereas Entropy illustrates the complexity of the system through the statistics of the diagonal lines lengths in the RP.

DET is very close to 1 for a purely periodic signal. It has been observed that with increase in the sinusoidal forcing amplitude (Fig. 7.1b) measures of DET almost shows an increasing trend as the recurrence plots displayed in Fig. 6.4 shows prominent arrangement of uninterrupted diagonal lines indicating the increase in DET values. In case of square forcing (Fig. 7.1c) the DET, entropy values both exhibit same trend showing minima at $A=2V$ corresponding to the RP plot in Fig. 6.3d where the RP plot displays some prominent uninterrupted bold diagonal lines with some scattered points. Here increase in A beyond $2V$ lead

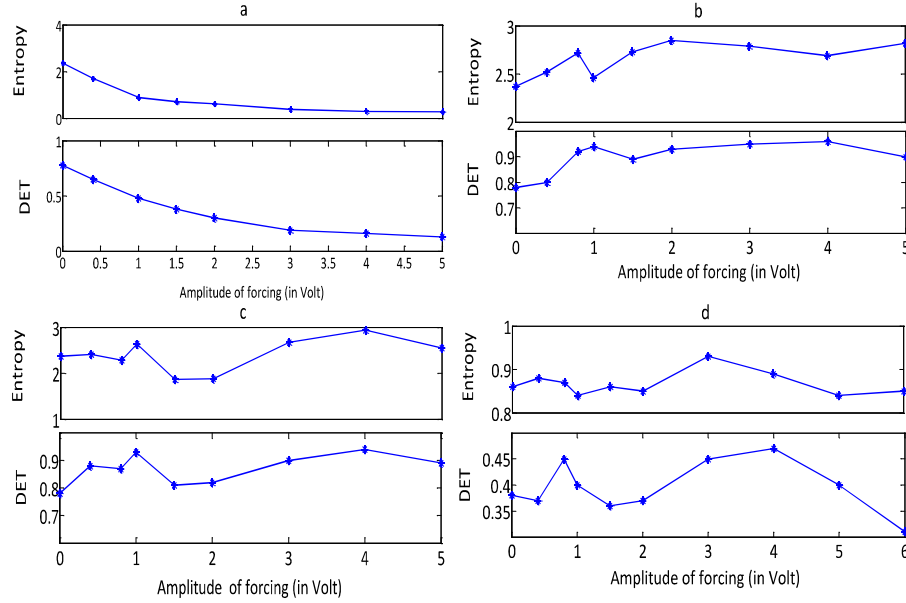


Figure 7.1: Variations of recurrence quantification variables DET, Entropy for increase in a) noise forcing b) sinusoidal forcing c) square forcing d) sinusoidal forcing applied on chaotic fluctuations ($P=0.04\text{mbar}$)

the underlying physics of the system dynamics.

7.3 Nonstationary, Detrended fluctuation analysis

Almost all methods of time series analysis, traditional linear or nonlinear, must assume some kind of stationarity. Therefore, changes in the dynamics during the measurement period usually constitute an undesired complication of the analysis.

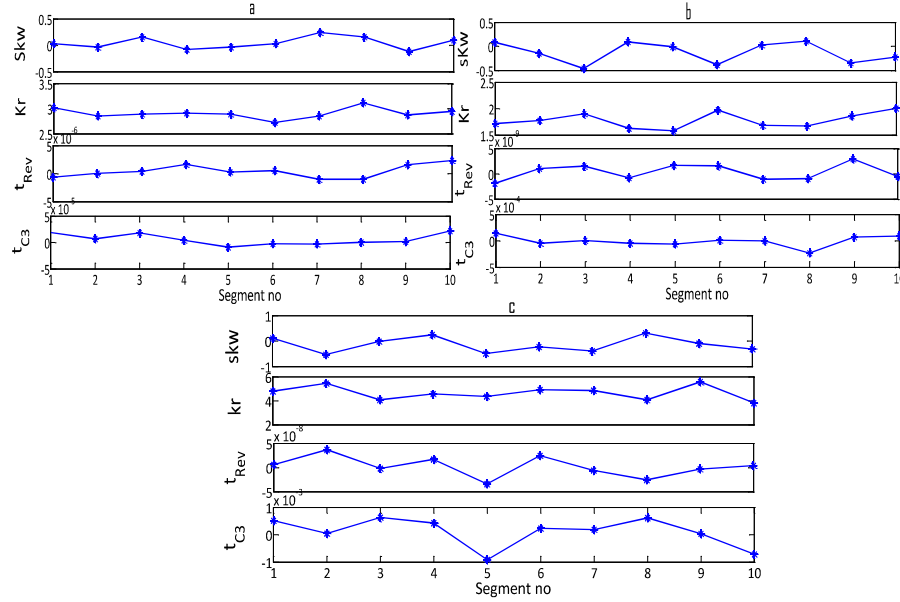


Figure 7.2: plot of kurtosis, skewness, time reversal t_{rev} , and third autocovariance t_{C3} at different segments of the time series for a) noise b) sinusoidal c) square forcing with $A=2V$

[48] in different parts of the segments of a time series. If the value of the parameters of nonlinearity measured reveal significantly different values in different segments then the time series can be classified as a non-stationary one. In performing this operation window length of the data containing 1000 points has been chosen to be 10. Shown in Fig. 7.2 are the estimate of skewness and kurtosis, time reversal t_{rev} , and third autocovariance t^{C3} in different segments of a time series with the

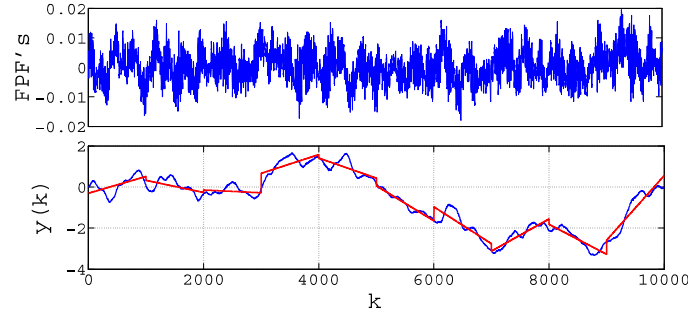


Figure 7.3: Integrated time series superposed on least square fitted trend

$$F(n) = \sqrt{\frac{1}{N} \sum_{k=1}^N [y(k) - y_n(k)]^2} \quad (7.1)$$

The process is repeated over all time scales to provide a relationship between the average fluctuation as a function of $F(n)$ and the box size n . In order to produce more accurate result, the largest box size we use is $N/10$ where N is the total no of points in the FPF's. A linear relationship on a log log graph indicates the presence of scaling with scaling exponent being α implying that $F(n) \sim n^\alpha$. Value of α greater than 0.5 and less than or equal to 1.0 indicates persistent long range correlation and that lying with 0.5 to 1 represent different type of power law

7.4 Results of DFA analysis with crossover phenomena

We illustrate the results in Fig. 7.4a and 7.4b using the above mentioned technique on the fluctuations acquired with increasing sinusoidal and square forcing amplitudes respectively for $P=0.12\text{mbar}$. We can clearly observe only a main scaling region upto $n \sim 403$ and beyond that there is a saturation region indicating very small slope. The values of the scaling exponent estimated from the increasing trend of Fig. 7.4a, 7.4b are clearly portrayed in Fig 7.5. Irrespective of the nature of forcing, the increase in amplitude of the external forcing leads to the increase in scaling exponent α initially from the value of ~ 1.12 . Values of α for sinusoidal as well as square forcing amplitudes are seen to increase from $A=0$ to $A=1\text{V}$ followed by the slight increase upto $A=3\text{V}$ in Fig. 7.5. Further increase in A lead to a saturation in the values of α . Shown in the Fig. 7.4c is the DFA analysis for increasing sinusoidal forcing amplitude applied on some chaotic FPF's having maximum lyapunov exponent (LE) of ~ 0.2 acquired at low pressure of 0.04mbar . The slope of the curve allows us to check the scaling exponents for the values of the external forcing with increasing amplitude. Unlike the Fig. 7.4a, 7.4b here the appearance of two scaling regions are prominently referred to as the

Meticulous inspection of figure 7.6 reveals a clearly abrupt transition from one linear regime to another. For forcing amplitude of $A=1V$, two slopes are very close to each other. However with increase in voltage this transition becomes more prominent and abrupt transition is noted with the crossover appearing around $n \sim 488$ as seen from figure 7.6. To clarify this point we have inserted the zoom view of scaling at higher amplitude of $A=4V$. In the 2nd scaling region we find the values of α to remain very close to 1 or greater than 0.5 indicating persistence long range behaviour.

Fig. 7.7 represents the DFA analysis for four different time series namely the original data and the rest three generated by applying three different types of forcing i.e noise, sinusoidal, square forcing. The scaling exponent obtained from the slope of $F(n)$ vs n in a double log graph depends paramountly on choosing the value of the box size n . It can be noticed that Fig. 7.7 exhibits mainly one scaling region or slope for the four curves over the range of n ($33 < n < 403$) for a fixed $A=2V$. The values of the slope α estimated for the main scaling region are 1.68 (sinusoidal), 1.09 (noise), 1.39 (square) 1.12(no forcing) indicating the correlated dynamics. The smaller values of the scaling exponent for increasing square forcing amplitude than the sinusoidal one are also observed from Fig. 7.5 implying the

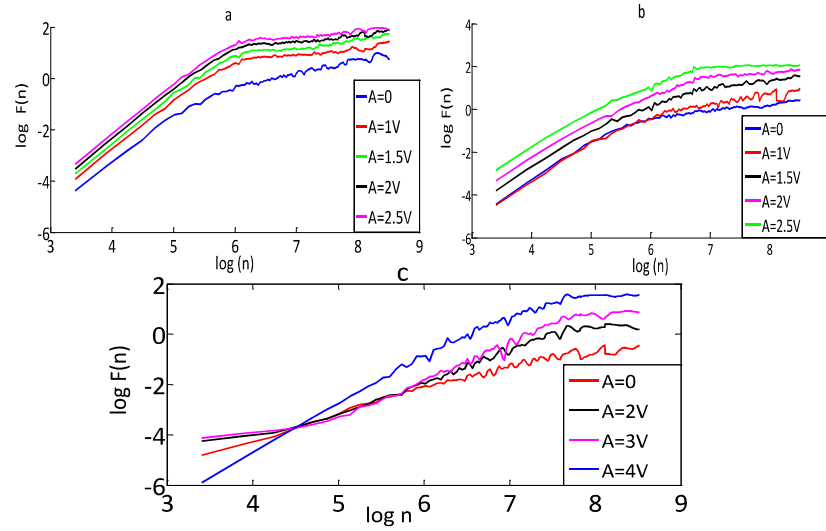


Figure 7.4: Plot of $\log F(n)$ vs $\log(n)$ for increase in a) sinusoidal forcing b) square forcing c) sinusoidal forcing on FPF for $P=0.04\text{mbar}$

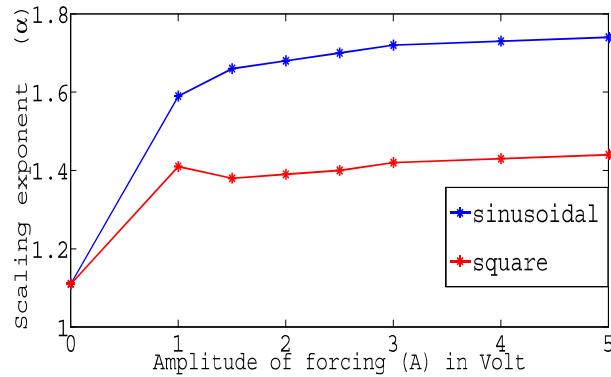


Figure 7.5: Variation of scaling exponent with increase in amplitudes of the sinusoidal as well as square forcing for $P=0.12\text{mbar}$

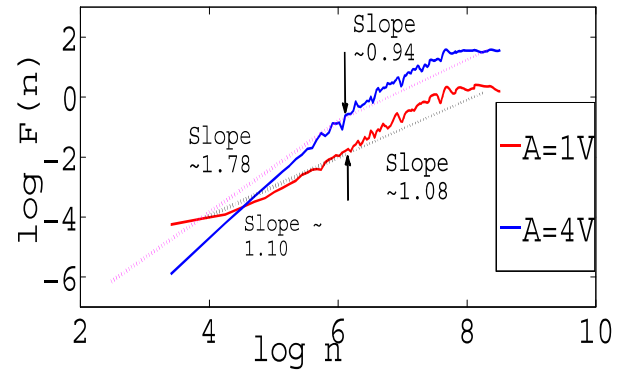


Figure 7.6: Shift in the values of α from low n to high n for sinusoidal forcing applied on fluctuation acquired for $P=0.04\text{mbar}$

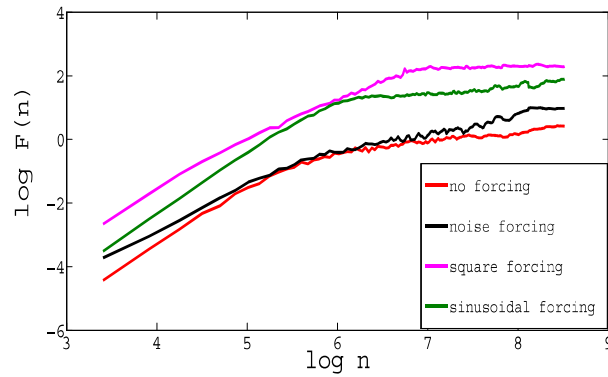


Figure 7.7: Plot of $\log F(n)$ vs $\log(n)$ for no forcing and different types of forcing i.e noise, sinusoidal, square applied with $A=2\text{V}$ for $P=0.12\text{mbar}$

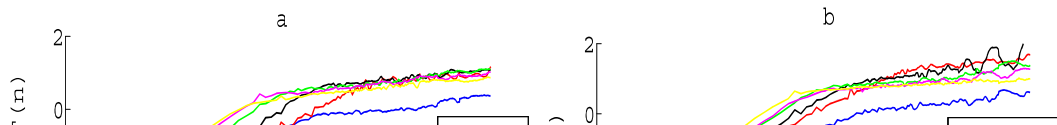


Table 7.1: Results of the quantitative values of the scaling exponent for forcing applied on FPF's obtained at low $P=0.04$ mbar

A (in V)	slope(region1)	slope(region2)
0	1.05	0.95
1	1.10	1.08
2	1.39	0.98
3	1.49	0.96
4	1.78	0.94
5	1.81	0.92

Table 7.2: Scaling exponent values for increasing frequencies of square and sinusoidal forcing for $P=0.12$ mbar

f (in kHz)	slope(sinusoidal)	slope(square)
0	1.11	1.11

7.5 Conclusion

To summarize we carried out DFA analysis to quantify scaling exponent for different amplitudes of sinusoidal, square forcings. The shift in the values of scaling exponent from one scaling region to the other indicated as crossover phenomena is observed when external forcing is added on fluctuation having Lyapunov exponent ($LE \sim 0.2$) greater than that acquired at $P=0.12\text{mbar}$ ($LE \sim 0.03$). A crossover usually arises due to changes in the correlation properties of the signal at different temporal or spatial scale. The external sinusoidal forcing on the particular type of floating potential fluctuation is observed to have an impact on changing the correlation properties of the signal as the fluctuations respond to the driving force. Generally the findings of crossover also suggest the possibility of multiple scaling exponents characteristics of multi-fractal signals. The evidence of crossover phenomena is associated with the presence of long range scaling exponent with increase in A which is also ensured in our work as the values of the scaling exponent in one of the scaling regions are found to lie greater than 0.5 and very close to 1. Different nonlinear parameters are estimated in different segments of the time series to detect nonstationarity behaviour. Hence we tried to estimate the scaling exponent with the help of DFA analysis in a non-stationary time series. The emergence of

transition. The considered recurrence measures exhibit an instantaneous change which was noticed in both RPs and RQA measures through variables like DET, Entropy. The estimated scaling exponents is higher in case of sinusoidal forcings than the square forcing at any value of the amplitude or frequency of applied forcing implying the decreasing roughness of the FPF for sinusoidal forcing than the square forcing which is reflected also in the entropy values obtained from RQA analysis. The most striking feature of our observation is how crossovers in the correlation behavior can be detected reliably and determined quantitatively. A crossover is due to the change in the correlation properties of a signal at different time or space scales though it can result from nonstationarity in the signal. It is the advantage of DFA that it can systematically remove trends embedded in a nonstationary time series and in this way we can gain insight into the scaling behaviour. Correlations in the fluctuations physically imply that they do not decay fast enough and the system possesses long memory. This work highlights the potential of RQA along with the DFA analysis which can be used to explore and develop the dynamical system theory of plasma oscillation of different plasma system like glow discharge, double plasma, dusty plasma. Quantification of scaling exponents has potential application in case of stock market, econophysics, foreign exchange rates, neuron spiking, that is in diverse areas of research field. The scal-

Chapter 8

Interplay of transitions between oscillations with emergence of fireballs and quantification of phase coherence, scaling index in a magnetized glow discharge plasma in a toroidal assembly

Interplay of transition of floating potential fluctuations in a glow discharge plasma in the toroidal vacuum vessel of SINP tokamak has been observed in our last chapter. We have studied the evolution of associated anode fireball dynamics under the action of increasing vertical, toroidal as well as increasing vertical field at a fixed toroidal field (mixed field) of different strength. Estimation of phase coherence in-

scaling exponent has been carried out for increasing values of the parameters. A persistence long range behaviour associated with the nature of the anode glow has been investigated in case of higher values of toroidal and mixed field whereas increasing the discharge voltage, vertical magnetic field leads to a perfectly correlated dynamics with values of scaling exponents greater than unity.

8.1 Introduction

Fireballs [152] are studied in a glow discharge device consisting of cathode biased negatively with respect to grounded chamber wall. When the positively biased electrode is immersed in a plasma a glow around the electrode is observed. Anode fireballs are discharge phenomena near the positively biased electrode. These are highly nonlinear phenomena involving the physics of sheaths, double layer [121], ionization beam and possibly external circuit interaction. Fundamental questions remain with respect to the peculiar shape of the fireballs, the physics of relaxation oscillation [153] including waves and instabilities created by the non-Maxwellian distributions both in magnetized and unmagnetized plasma. A steady state double layer requires a momentum balance [152] or flux ratio $\frac{J_e}{J_i} = \sqrt{\frac{m_i}{m_e}}$. The lack of the pressure or momentum balance would not lead to a stationary configuration. In many situations fireball grows but does not reach equilibrium due to unequal ion production and losses resulting in a repetitively pulsating fireball [154]. Generally the fireball phenomena occurs when electrons accelerated in the sheath of the positively biased electrode excite or ionize the neutrals leading to the expansion of the sheath into a double layer of potential just above the ionization potential. The common assumption that a fireball can collect as many electrons emitted from

chaos theory [157]. In this final chapter we have investigated of the dynamics of the fireball [158], followed by the quantification measure of phase coherence index [30] and scaling index within the context of surrogate data and using detrended fluctuation analysis (DFA) [80] respectively in a magnetized glow discharge plasma in a toroidal assembly [159]. The values are found to be related physically with the evolution of the glow. Much effort has been endeavoured to study the intricacies involving the topics like finite nonlinear interactions and its associated phase coherence index [32, 31] in magnetohydrodynamic turbulence in solar wind. Here in our study we address for the first time the evidence of finite nonlinear interaction by trying to find the correlations among phases for increasing discharge voltage (DV), vertical, toroidal magnetic field (B_V, B_T) and the mixed field (B_{V+T}) in the toroidal vacuum vessel of SINP tokamak [160]. At last we have carried out the DFA analysis [82, 141] to estimate the scaling exponent (α) associated with the fireball dynamics for exploring the presence or absence of persistence long range behaviour [86, 145].

8.2 Floating potential fluctuation, power spectral analysis, phase space plot

8.2.1 Increasing DV, vertical and toroidal magnetic field (B_V, B_T)

With increase in DV the nature of the transitions (Fig. 8.1) is observed to be of homoclinic type upto 0.42 kV. Beyond this value, the FPF's again become relaxation type which is seen to change to regular periodic behaviour at 0.46 kV. This nature persisted upto 0.50 kV after which some irregularities appear in the regular sinusoidal behaviour. So the transitions undergo a homoclinic behaviour and subsequently get modified to regular periodic oscillation followed by the irregular type at high values of DV. The corresponding phase space plot for homoclinic one occupies a larger lateral volume as shown in Fig. 8.5A c-d. The transitions from homoclinic type to relaxation oscillation is prominent in Fig. 8.5A d-e whereas at the higher DV values irregular oscillations are observed in phase space plot of Fig. 8.5A k-l.

Now keeping the DV at a value of 0.44 kV we apply vertical magnetic field upto $B_V=11.78$ Gauss (G). The plasma floating potential fluctuations were found to show oscillatory features of different type depending on the intensity of the applied

the shape of almost spherical for $B_V=11.79\text{G}$. During the change of B_V from 7.29G to 10.11G the phase space volume almost remains same as depicted in Fig 8.5B f-j.

The transitions with the application of toroidal magnetic field (B_T) exhibit a drastic change. Similar to the observations in presence of B_V here also the emergence of relaxation oscillation with slow and fast time scale takes place upto $B_T=5.63\text{G}$ and there is gradual increase in the phase space volume (Fig.8.5C a-e). After that the system undergoes a chaotic behaviour with a sudden emergence of broadband characteristics which is prominent if we apply vertical field in presence of a toroidal field that is kept fixed portrayed in Fig. 8.4 h-j. The chaotic nature of the FPF for increasing B_T has been depicted in Fig. 8.3 f-p and is reflected also in the corresponding phase space plots. At low values of B_T the amplitudes of the chaotic oscillation are seen to be very low which get increased with the increase in B_T (Fig 8.3). When B_T reaches 11.2G , we can observe the emergence of some sort of relaxation oscillation having the chaotic nature persisting upto 11.84G as seen in the right panel of Fig. 8.3. Further change in the nature of the relaxation oscillations takes place at a high value of $B_T \sim 12.8\text{G}$. The chaotic attractor volume is seen to occupy largest region at $B_T \sim 14.4\text{G}$ (Fig 8.5C p). Finally we try to

increasing B_V , B_T and 2-19 percent for variation in B_{V+T} . So increasing magnetic field is observed to play an important role in enhancing the noise values in our experiment.

The frequency carrying maximum power (dominant frequencies) with the variation in DV, B_V , B_T have been plotted in Fig. 8.6. The dominant frequencies with DV are seen to lie from $150 \sim 900$ Hz. A minimum frequency of 250 Hz has been obtained at $DV \sim 450V$ followed by the increase in dominant frequencies upto 500V where maximum dominant frequency of 850 Hz have been achieved. The application of vertical field gradually enhances the frequencies after 6G and a sharp increase in the value of main frequency is noted at $B_V \sim 11.79$ Gauss. Toroidal magnetic field has impact in changing the frequency values to a large extent in a quite random way. A range of dominant frequencies(850, 1750, 2200, 2550, 1150) Hz have been noted with a prominent maxima at 2550 Hz at $B_T=9.6G$ along with the presence of a local maxima of 2200 Hz at 11.84G. The values of the main frequencies with the application of increasing vertical field on a fixed $B_T(8.56G)$ remain from minimum of 450Hz to maximum of 2950 Hz with the maximum frequency being achieved at around $B_V = 7.01$ Gauss. Further increase in the values of (B_{V+T}) the frequency with maximum power shows a gradual decreasing trend.

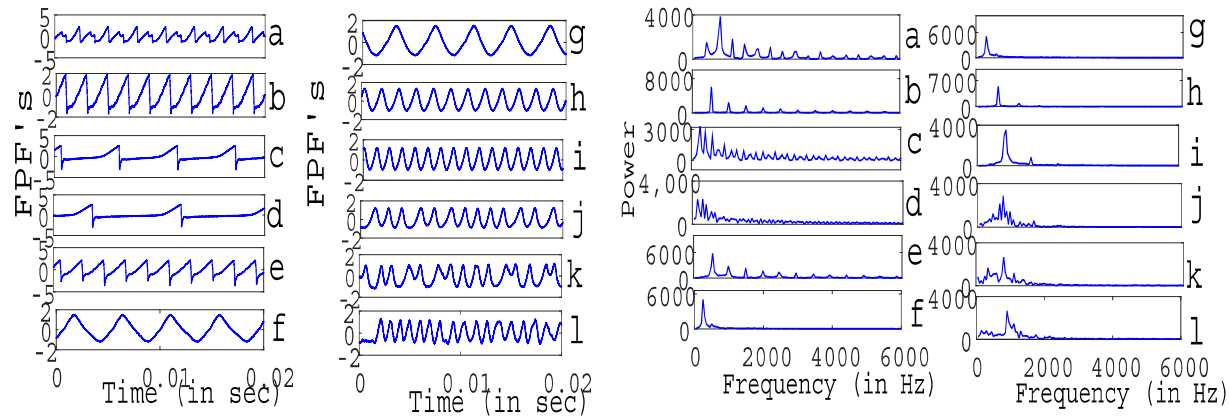
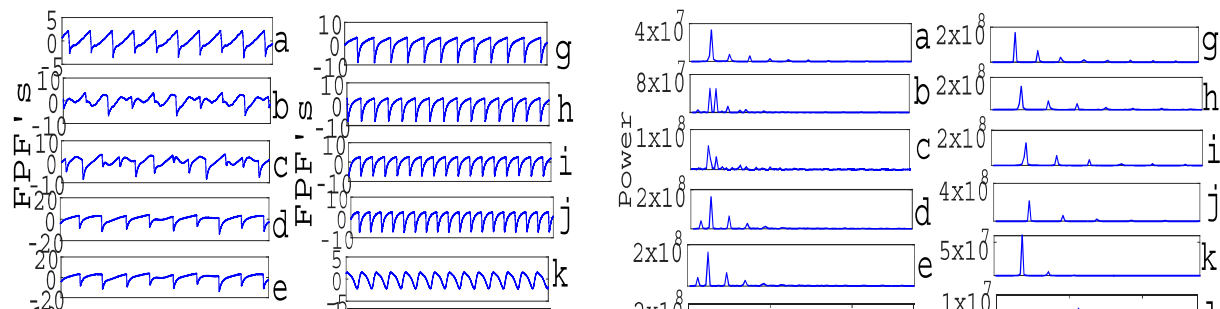


Figure 8.1: Sequential change in the raw signals and frequency spectrum for different DV (in Volts) in the left and right panel respectively: a) 390V b) 400V c) 410V d) 420V e) 430V f) 450V g) 460V h) 480V i) 500V j) 520V k) 550V l) 600V



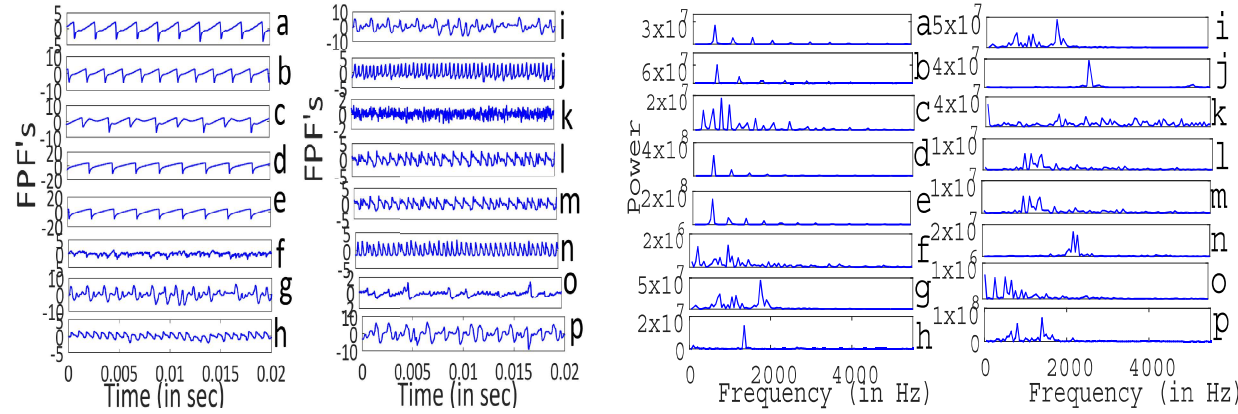
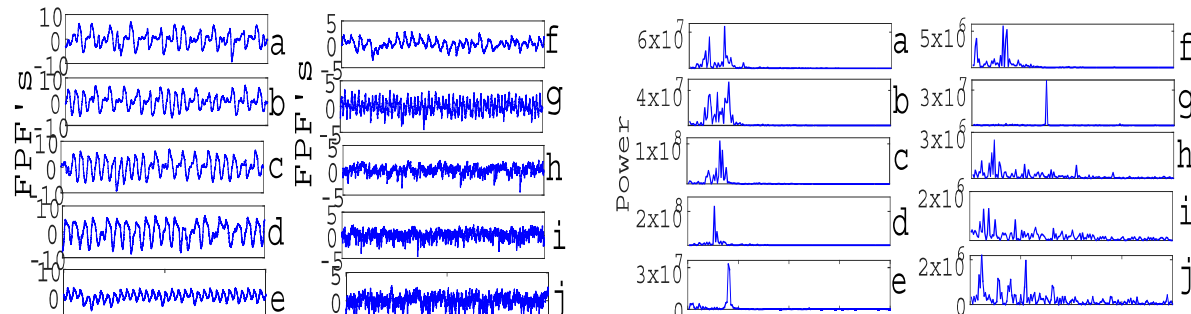


Figure 8.3: Plot of FPF and power spectrum with the variation in B_T in the left and right panel respectively: a) 0G b) 1.28G c) 2.30G d) 3.07G e) 5.63G f) 7.098G g) 8.06G h) 8.76G i) 8.98G j) 9.6G k) 10.24G l) 11.2G m) 11.52G n) 11.84G o) 12.8G p) 14.4G for $DV=0.44\text{kV}$



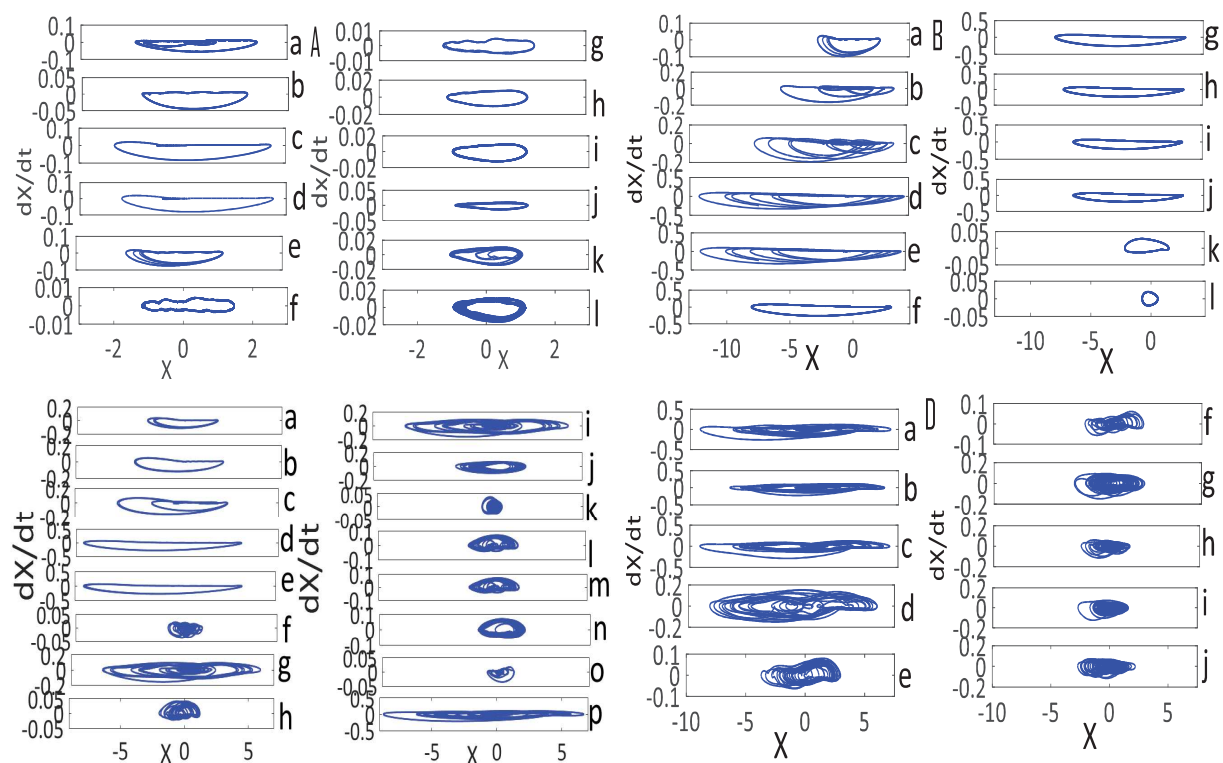


Figure 8.5: Sequential change in phase space plot for same values of DV , B_V , B_T , B_{V+T} mentioned in raw signal and power spectral plot for A) Discharge voltage B) Vertical magnetic field C) Toroidal magnetic field D) Increasing vertical field

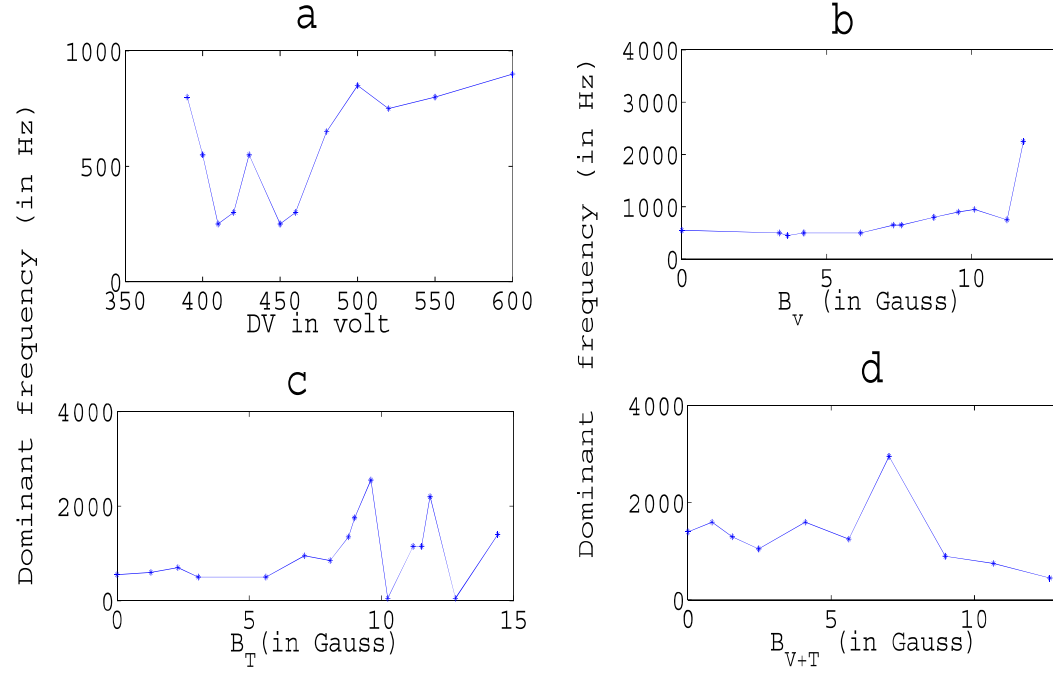


Figure 8.6: Dominant frequency with the variation in a) Discharge voltage(DV) b) Vertical magnetic field (B_v) c) Toroidal magnetic field (B_T) d) Vertical field at fixed B_T of 8.45G (B_{V+T})

anode is encapsulated, partially or fully, by ions and quasi-neutrality of plasma leads to the formation of double layers. To start with, when the plasma was formed a small fireball was found to be attached to the anode at a particular position (here left side) as depicted in Fig 8.7. With the emergence of relaxation oscillation the position of the glow was found to rotate along clockwise direction aligning itself to the back side of the electrode for DV=0.40kV and then shift to

little elongated corresponding to the time series at $B_V=4.21\text{G}$ showing relaxation oscillation with increasing rise time in comparison to that observed for $B_V=0$, 3.65G at the beginning. When the rise time scale of the relaxation oscillation get steeper, fireball aligns itself only to the right side of the electrode (Fig 8.8 d). The anticlockwise rotation of the position of the fireball (Fig. 8.8 e,f,g) is observed when the slope of the rise time is again slightly changed. Most interestingly, on complete reversal of the nature of the time scale of the relaxation oscillation ($B_V=11.23\text{G}$) (Fig. 8.2k) a comparatively broader shaped fireball near the electrode was observed in Fig 8.8h which is seen to persist in shape but with slight increase in intensity when regular periodic oscillation at $B_V=11.79\text{G}$ appears as shown in Fig. 8.8 i.

An elliptical shaped nature of the fireballs was persistent for the relaxation oscillation generated in presence of low toroidal field upto 5.63G . The size of glow in Fig 8.9b is observed to occupy larger space than that observed in Fig 8.9a. With the emergence of chaotic oscillations at intermediate values of toroidal field (upto $B_T=8.96\text{G}$), a self rotation of the glow takes place and finally the fireball is seen to take position on the back side of the electrode as seen in Fig 8.9d. The appearance of relaxation oscillation bearing the chaotic nature lead to the generation of a completely different shaped glow compared to the previous ones(

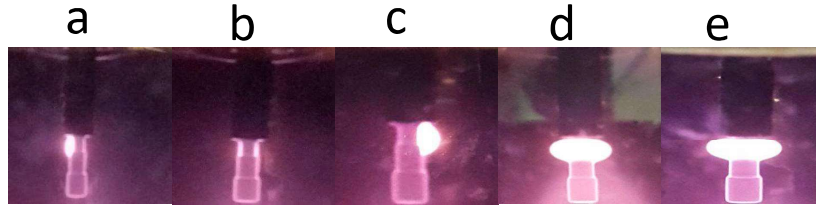


Figure 8.7: Photograph of the anode glow with variation in DV a) 390V b) 400V c) 420-440V d) 460V e) 520V

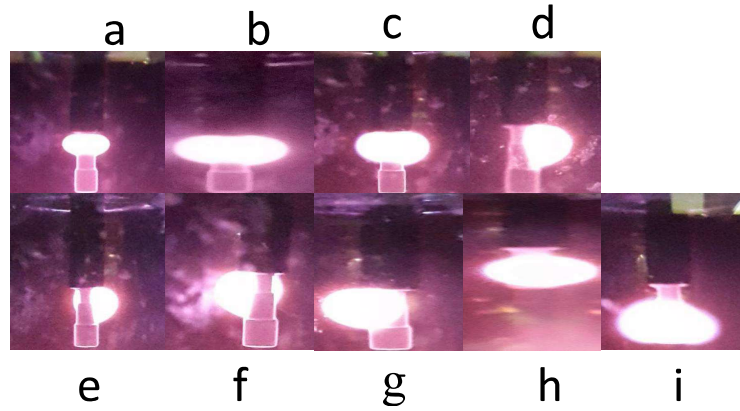


Figure 8.8: Sequential change in the anode glow for increasing vertical magnetic field B_V a) 3.65G b) 4.21G c) 6.18G d) 7.29G e) 8.70G f) 9.54G g) 10.10G h) 11.23G i) 11.79G for DV=0.44kV

Gradual increase in B_{V+T} leads to the slight increase in plasma density along with the fireball size as checked by visual inspection from Fig. 8.9 c-d.

8.4 Method of analysis: path length, phase coherence index

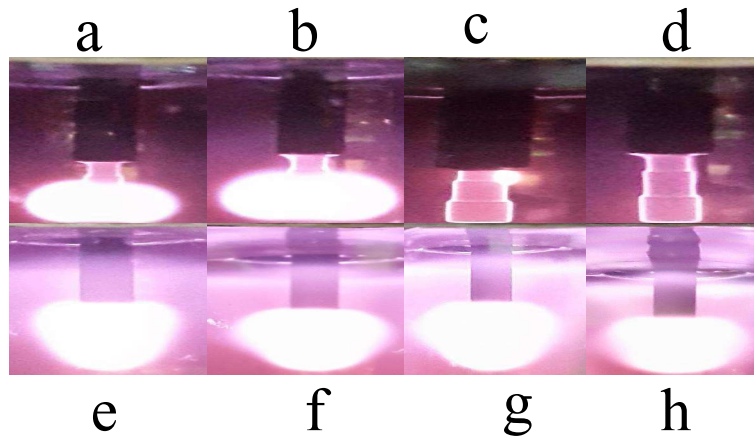


Figure 8.9: Sequential change in the glow for increasing toroidal magnetic field B_T a) 1.28-2.30G b) 3.07-5.63G c) 7.09G d) 8.06-8.98G e) 9.6G f) 10.24G g) 11.2-11.84G h) 11.84-14.4G for $DV=0.44\text{kV}$



phase randomised surrogate data while that is seen to remain constant for phase constant surrogate. If the original data has random phase then $C_\phi(\tau)$ would be 0 whereas $C_\phi(\tau)=1$ if the phases are completely correlated. The profile of phase coherence index with variation in τ for the FPF's with B_T , B_{V+T} is shown in Fig 8.11. We find that C_ϕ varies over the range from 0.01 to maximum 0.5 for a wide range of the values of τ for $B_{V+T}=12.63\text{G}$ whereas C_ϕ takes the value from a minimum of 0.01 to 0.24 for B_T of 9.6G.

The plot of phase coherence index with the variation in discharge voltage, vertical, toroidal, mixed magnetic fields has been portrayed in Fig. 8.12. The value $C_\phi(\tau)$ takes it maximum when the phenomena of homoclinic transition occurs for increasing DV. For initial increase in vertical magnetic field the values of phase coherence index are shown to lie in a constant range but the higher values of B_V has led to the increase in $C_\phi(\tau)$ as marked in the figure where the shape of the glow starts taking some sort of distorted elliptical shape from the original spherical shape. In the marked portion, the maximum value corresponds to the case where the toggling of the time scale in relaxation oscillations takes place i.e the rise, decay time of the relaxation oscillation completely get changed as observed from Fig 8.2 j-k. Gradual increase in the value of $C_\phi(\tau)$ within the region from $B_V=6\text{G}$

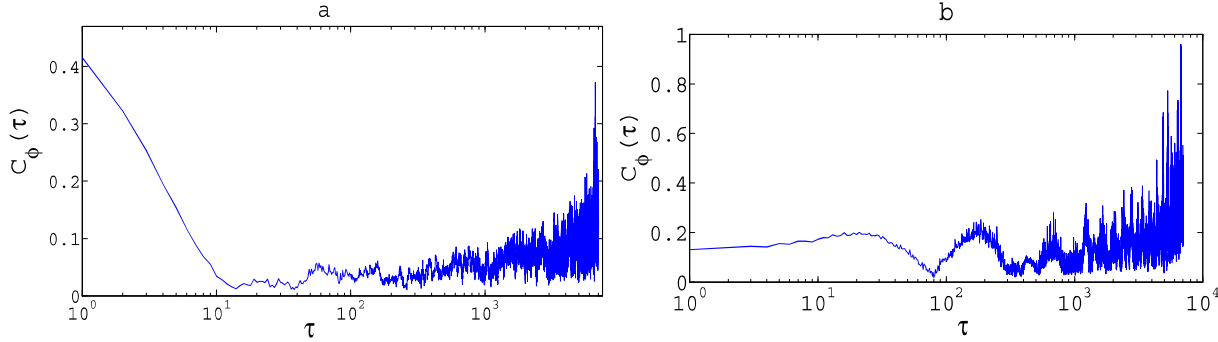


Figure 8.11: Profile of phase coherence index with τ for a) $B_T = 9.6G$ b) $B_{V+T} = 12.63G$

shaped glow different from the previous ones correspond to the maximum values of C_ϕ . At a value of $B_T=9.6G$ a sudden appearance of very low amplitude FPF resulted in minimum correlation between the wave phase (lowest values of $C_\phi(\tau)$) followed by the constant values of C_ϕ in high toroidal magnetic field region where the glow shapes are seen to remain same (Fig. 8.9 f-h). Here also we can observe that the maximum phase coherence index is associated with the power/energy occupying in a larger region of frequency band. Finally the application of B_V at fixed toroidal field i.e (B_{V+T}) leads to the smooth increase in the values of phase coherence index in a region marked by red rectangle implying the enhancement in

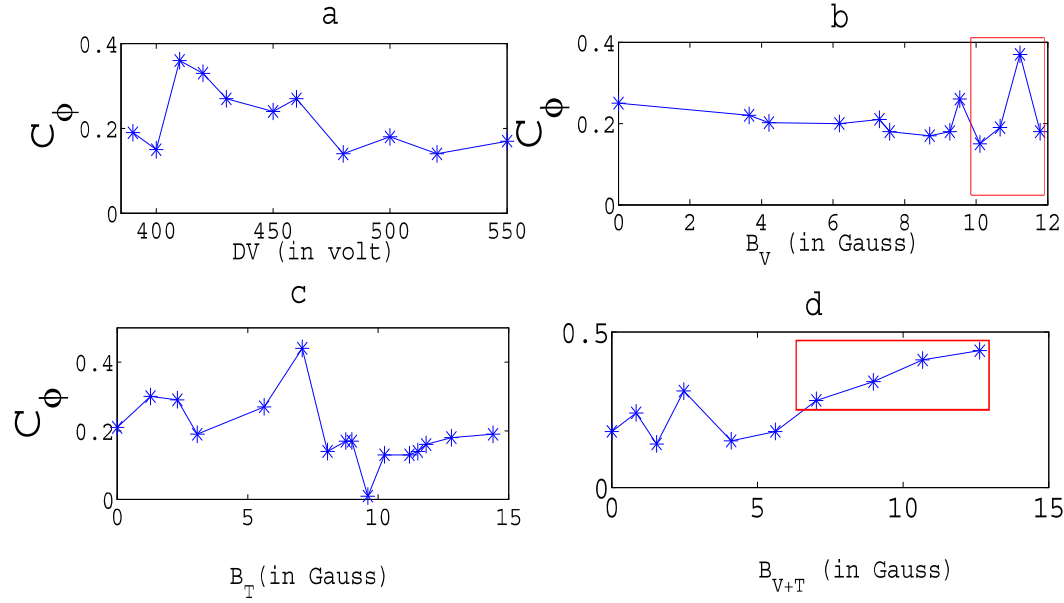


Figure 8.12: Plot of phase coherence index with variation in a) Discharge voltage(DV) b) Vertical magnetic field (B_V) c) Toroidal magnetic field (B_T) d) Vertical field at fixed B_T (B_{V+T})

8.5 Results of detrended fluctuation analysis (DFA)

To illustrate the DFA algorithm we use the time series shown in Fig 7.3 (in chapter seven) as an example along with the integrated time series with the solid red lines(lower panel of Fig 7.3) indicating the trend estimated in each box by a least square fit. Chapter seven presents an elaborate description to provide a relationship between the root mean square fluctuation as a function of $F(n)$ expressed in

acquired with increasing B_T , B_V , B_{V+T} respectively in Fig. 8.13, Fig. 8.14. The slope of the curves allows us to check for the scaling exponent after carrying out DFA analysis. DFA performed on the fluctuations in the left panel of fig 8.13 with toroidal field upto 8.98G yield the values of α to be 1.28, 1.31, 0.99, 1.24, 1.27, 1.25. Power law exponent values greater than 1 indicate the existence of perfect correlated dynamics. Altogether the exponent is viewed as the roughness of the time series, the larger the value of the coefficient α the smoother will be the time series. The hint of long range correlated dynamics ($0.5 < \alpha < 1$) is found for $B_T=5.63\text{G}$ where the corresponding FPF abruptly change its nature of relaxation oscillation. The prominent signature of the existence of long range behaviour has been observed from the slope of the curves in right panel of Fig 8.13. The values of the estimated scaling exponent are found to lie within $0.5 < \alpha < 1$ for DFA executed on FPF's acquired under high value of B_T from 9.34G to 14.4G. The application of B_{V+T} yield the values of scaling exponents of 1.36, 1.23, 0.91;(1.09,0.54); 0.72,0.78, 0.75 indicating a toggle from perfect correlated dynamics to a long range persistence. A phenomena worth observing is the prominent region of double scaling ($\alpha=1.09$, 0.54) which is observed for $B_V=11.2\text{G}$ followed by the long range behaviour. So the appearance of long range behaviour is noted only under the application of high B_T or the mixed field B_{V+T} . The values of the scaling exponent can also be

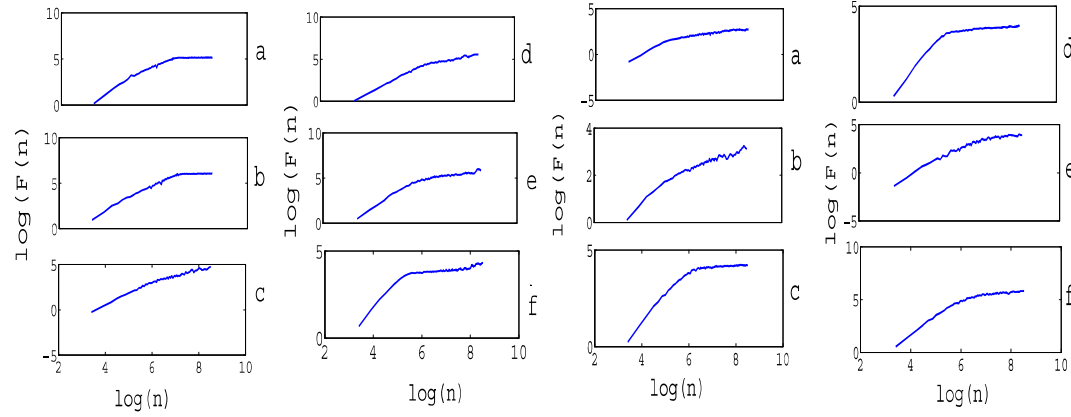


Figure 8.13: Plot of $\log F(n)$ vs $\log(n)$ for increasing toroidal voltage a) 0G b) 1.28G c) 5.63G d) 7.09G e) 8.06G f) 8.98G in the left panel and a) 9.34G b) 10.24G c) 11.52G d) 11.84G e) 12.8G f) 14.4G

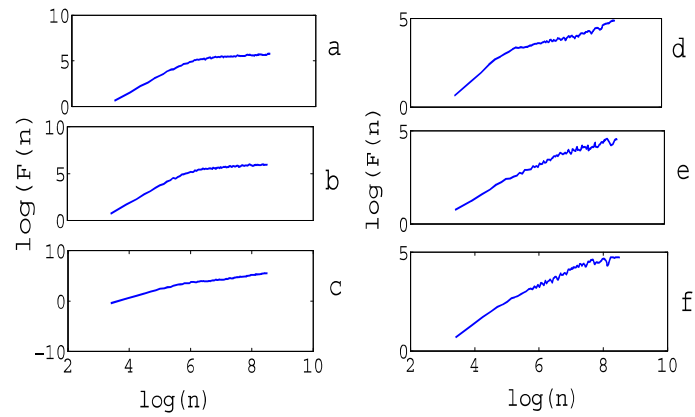


Figure 8.14: Plot of $\log F(n)$ vs $\log(n)$ increasing B_V at fixed B_T (B_{V+T}) a) 0.84G b) 2.47G c) 5.61G d) 7.01G e) 10.66G f) 12.63G

Table 8.1: Results of the quantitative values of the scaling exponent for increasing discharge voltage (DV) and vertical magnetic field (B_V)

DV (in V)	slope(α)	B_V (in G)	slope(α)
390	1.22	3.64	1.37
410	1.14	6.17	1.39
430	1.40	8.70	1.36
450	1.78	9.54	1.70
460	1.79	10.66	1.53
480	1.81	11.78	1.54

8.6 Conclusion

To summarize, the study of the interplay of oscillations with parameters like DV, B_V , B_T , B_{V+T} has been carried out with the simultaneous observation of the dynamics of the fireball. Estimation of the phase coherence index to characterise the correlation between the modes has been accomplished. The change in the dynamics of the fireball along with the corresponding phase coherence index values has been studied in detail. The results of finite C_ϕ demonstrate the existence of finite phase correlation indicating the nonlinear wave interaction in process. For the case of increasing DV we found the maximum correlation at the instant of the occurrence of homoclinic transition. Display of dominant frequencies with the variation in B_V , B_T , B_{V+T} has been carried out (Fig. 8.6) to understand about

experiment, emergence of inverted pear shaped glow upon the application of B_T correspond to the maximum correlation between phases quantified by maximum C_ϕ and long term persistence. The smooth increase in C_ϕ for higher B_V occurs during the spreading of glow on both sides of the electrode. When the plasma production and losses get out of the balance the fireballs can undergo relaxation oscillation. Growth and collapse of the fireball can be considered runaway processes whose time scales are governed by the ion transit time through the fireball. The recovery process depends on the density replenishment from the background plasma which may take longer due to the lower density and larger scale. In the context of the shape of the fireball we know that the fireball structure must be in a force balance $m_e n_e v_e = m_i n_i v_i$ otherwise it would not be a stationary structure. In a uniform unmagnetized plasma with all radial forces cancelling each other fireballs of spherical or cylindrical geometries can be obtained.

Talking about scaling exponents, the evidence of long range correlated dynamics is noted for higher values of B_T whereas the toggling from perfect correlated dynamics to long range persistence via double scaling region has been observed for B_{V+T} . The persistence long range behaviour in presence of higher B_T corresponds to the pear shaped glow depicted in Fig. 8.9e-h. The shape of this particular nature of fireballs also indicates the presence of long range correlated dynamics in

Chapter 9

Overall Conclusion

In this chapter, a quick recapitulation has been made on the works discussed in this

9.1 A quick recapitulation

Our thesis presents the experimental observation of different nonlinear phenomena appearing in a glow discharge plasma with the implementation of various nonlinear and statistical analysis techniques. The results acquired with the help of various techniques nicely orchestrate the aim of our thesis work. Such statistical analysis techniques based on delay vector variance, rank test, Zscore coordinated with conventional data analysis tools in plasma like power spectrum, wavelet bicoherency analysis, can be immensely beneficial for the quantification of nonlinearity inherently present in plasma devices. The measurement of different dimensions, statistical quantities, scaling exponents enable us to distinguish different degrees of complexity of rich phase space structures exhibited by self and externally excited glow discharge plasma. The observed complexity dynamics presented in our thesis work is mainly due to nonlinear interaction between the components of complex system, and arises due to different instabilities in the plasma system. The origin of these oscillations are due to: 1) Interplay of internal complex system parameters, called self excited oscillation, 2) External forcing, called forced oscillation. Plasma is a common example of complex system consisting of electrons, ions and neutral particles and it contains numerous sources of free energy like energetic electrons

resulting from the space charge configurations, density and temperature gradients, velocity shear and the various dynamical processes that are prevalent in a plasma such as ionization and recombination mechanisms. These form the driving engine for many nonlinear dynamical processes that are observed in the bulk of the plasma. In our work, a number of parameters e.g., discharge voltage, pressure, magnetic field, external perturbation (sinusoidal, square, noise forcings), etc. are identified to control the plasma dynamics of the system. A brief summary of our obtained results is enumerated below:

- After the introductory part in chapter one, and experimental, data analysis techniques in chapter two, chapter three presents an experimental observation of order-chaos-order transitions in the relaxation oscillations of a glow discharge plasma with variation in the discharge voltage. We report for the first time the experimental observations of inverse homoclinic bifurcation in the floating potential fluctuations with increase in DV. It continues to stay in this mode for a wide range of DVs and later results in a homoclinic bifurcation. In order to comprehend the complex dynamics of the observations, we have carried out a detailed analysis using standard nonlinear techniques

frequencies. Such frequencies are also observed experimentally. At last a numerical modelling of the experimental observations has been attempted using a forced nonlinear dynamical equation representing the temporal dynamics of ion acoustic oscillations in presence of ionization and recombination terms. Although there is no explicit externally applied oscillatory voltage in the present experimental system, we consider the situation where many normal modes are generated within the plasma which are attributed to the origin of various self excited relaxation oscillations. Since the plasma can contain a wide spectrum of frequencies, we feel that they can nonlinearly interact and give rise to several harmonic terms depending on the plasma conditions. This leads to the need of incorporating the forcing term in the right hand side of equation 3.2 which is thought to be mimicked by the self excited oscillations in the plasma. The harmonic forcing term in the numerical modelling is found to be responsible for driving the system through chaotic oscillations before the system began to display an increase in the time period of the relaxation oscillations.

- Chapter four deals with aspect of nonlinearity for increasing DV in the floating potential fluctuations of DC glow discharge plasma by generating surro-

in a plasma systems arises from the most fundamental processes, namely, the wave-wave and wave particle interactions. In view of the concept of plasma physics the measure of nonlinearity is estimated by comparing the total power present in all frequencies normalized by the power in the frequency (dominant frequency) carrying maximum power. Presence of nonlinearity is seen to be prominent at low pressure in view of the decrease in collisional frequency leading to the increase in ionization. Due to nonlinear interactions, different types of waves inherently present in the glow discharge system such as ionization instabilities give rise to different frequencies that are excited at $P=0.056$ mbar. The results obtained from DVV plots turn out to be almost similar with the analysis based on accumulation of power and rank test confirming the robustness of the all methods.

- In chapter five we study the evidence of nonlinearity in presence of external forcing and magnetic field using the DVV method in conjunction with Zscore, bicoherency by providing some easy to interpret diagrams. The analysis involving DVV has also been implemented to study numerically simulated results by a second order nonlinear ordinary differential equation derived from the fluid equations of plasma for the first time. The results show qualitative

momentum with each other. In our experiment when we paced the system with sinusoidal signal of frequency $f=1$ kHz, keeping the plasma in a period 2 regime ($P=0.085$ mbar) with frequencies of 4, 8 kHz (f_{01}, f_{02}), the frequency spectrum shows peak at frequencies of 4.5 and 8.5 kHz ($f_{01} + f/2, f_{02} + f/2$) for $A=2V$. When the perturbation amplitude (A) is increased to 5V, in addition to the frequencies ($f_{01} + f/2, f_{02} + f/2$) a new frequency of $3f/2$ is generated which is only due to the external perturbation frequency. Subsequent increase in A generates frequencies of ($f_{01} + 3f/2, f_{02} + 3f/2$) and the nonlinear coupling/interaction amongst the frequencies are thought to have attributed to various statistical features obtained from DVV plots, Zscore and bicoherency analysis. The plot of the total power divided by power in the harmonics is seen to increase with B with the maximum power occurring at maximum value of B where the deviation from the DVV scatter plots also becomes maximum.

- Next chapter contains the study on the existence of finite phase coherence index i.e finite correlation by estimating phase coherence index for different types external forcing techniques likewise noise, sinusoidal, square etc. Finite nonlinear interaction obtained from phase coherence index values is observed

revealed by estimating phase coherence index and performing DVV analysis. The estimate of phase coherence index corroborates our nonlinearity analysis using DVV. Origin of this type of correlation is illustrated using continuous wavelet transform. Existence of power/energy concentration in a large region of frequency band is thought to be attributed to the increase in phase coherence index values in case of square, sinusoidal forcings which can also be regarded as one of the physical reasoning for the variation in C_ϕ . The transition in the dynamics is observed through recurrence plot techniques.

- Chapter VII covers a detailed study of scaling region using detrended fractal analysis test in the externally excited GDP by applying different forcing amplitudes. In case of sinusoidal, noise, square forcing applied on fluctuation acquired at $P=0.12$ mbar only one dominant scaling region is observed whereas the forcing applied on fluctuation ($P=0.04$ mbar) two prominent scaling regions have been explored reliably using different forcing amplitudes indicating the signature of crossover phenomena. A persistence long range behaviour is revealed in one of these scaling regions with α lying in the range from $0.5 < \alpha < 1$. Different nonlinear parameters are estimated in different segments of the time series to detect nonstationarities. The complexity of the

fireball under the action of increasing DV, vertical, toroidal as well as increasing vertical field at a fixed toroidal field (mixed field) of different strength. The dynamics of the fireballs and the associated FPF are considered to be driven by $E \times B$ in the direction of the cylindrical symmetry of the electrode. Existence of power/energy concentration in a large region of frequency band is attributed to the gradual increase in phase coherence index values for increasing B_T, B_{V+T} . A comprehensive study of the dynamics of the fireball has been corroborated with the values of phase coherence, scaling index. The anode glow or fireball appears when the discharge current is too low to sustain the discharge. This glow supplies energy, in the form of positive potential gradient, to the electrons so that additional ionization takes place and hence discharge current increases. At the initial stages of discharges the electrons do not have sufficient energy near the anode to reach it, and hence the anode glow occurs.

In our experiment, emergence of inverted pear shaped glow upon the application of B_T correspond to the maximum correlation between phases quantified by maximum C_ϕ and long term persistence. This work is aimed to gain insight about effect of magnetic field in the form of $E \times B$ force in glow discharge

So the behavior of the nonlinear dynamical phenomena dealing with the self and externally excited oscillations and its origin are mainly explored in the framework of basic plasma physics. We have tried to give possible physical as well as dynamical explanations of the observation of such complex nonlinear features associated with the plasma dynamics. We believe that all the analysis presented in our work nicely cooperate with each other and corroborate with the analysis and concept of basic plasma physics phenomenon executing perfectly the aim of this thesis work.

9.2 Future prospects and conclusive remarks

The impetus behind the works contained in this thesis is to provide a clear understanding of the aspect of nonlinearity, complexity dynamics. The thesis also provides an extensive discussion to reveal the complexity dynamics, nonlinearity in the self and externally excited glow discharge plasma using different nonlinear, statistical techniques and associate it with the basic plasma physics.

- In our thesis work we have used the analytical model developed by Kadji et al.[108] based on two-fluid equations for understanding the observation in presence of external forcing, DV. We have added a constant term (A) and

magnetic field to investigate the interaction between the different modes has been carried out using the EMD based bicoherency method. As mentioned earlier this method is commonly used for the processing of non-stationary and nonlinear signals and does not require any predefined basic functions as in Fourier or Wavelet transform. Fourier based bicoherency method is more familiar and well known to all where the sinusoidal functions act as a basis. So in addition to the EMD based bicoherency, the use of Fourier bicoherency would be a good choice to substantiate our analysis of nonlinearity.

- We have studied the nonlinear interactions introducing different types of external forcing by estimating the phase coherence index to characterise the correlation of phases among Fourier modes in a given time series by employing surrogate data technique. Existence of phase coherence index has been demonstrated introducing continuous wavelet transform (CWT). This type of study is known to bear important implications in various charged particle transport processes. We also plan to extend our study on phase coherence by using a combination of wavelet transform and Hilbert Huang transform in the future.
- Estimation of phase coherence, long range scaling index (using DFA) have

interactions that is responsible for the emergence of nonlinearity.

- Evolution of associated anode fireball dynamics under the action of vertical, toroidal magnetic fields as well as the combination of the both the field of different strength has been observed in the above device. The study reveals that fireball dynamics is associated with the correlation between phases. So understanding the dynamics of the oscillation along with the dynamics of fireballs through the techniques is a crucial step for the characterisation of the device for application purposes.
- In addition to the aforementioned, the idea of chaos control, synchronization and the investigation of non-chaotic attractors by applying two non-commensurate periodic signals would be a very interesting in challenging areas of study.
- Finally to validate our experimental observation in the magnetized glow discharge plasma in toroidal assembly, we are planning to develop a numerical model which is already consummated for the experimental results obtained from glow discharge plasma on cylindrical geometry. .

Glow discharge plasma (GDP) being rich in high energy electrons and ions

manufacturing the very large scale integrated circuits (ICs) used by the electronics industry which are also critical for the aerospace, automotive, steel, biomedical, and toxic waste management industries. Nonlinear phenomena including nonlinear structures are observed in laboratory plasmas, fusion devices, radio-frequency plasmas, microwave devices, and in naturally occurring plasmas such as in magnetosphere, inter stellar plasma. Devices that have no end with geometries such that the magnetic field lines close on themselves (toroidal geometry) offer many advantages for plasma confinement. Generally for the purpose of the confinement of plasma, poloidal magnetic field is normally superposed on the toroidal field resulting in helical field lines (as in Tokamak) as the most important application of the man made plasmas is in the control of thermonuclear fusion reactions which hold a vast potential for the generation of power. Generally the presence of density gradient in plasma causes the particle to diffuse from dense regions to regions of lower density. In device like GDP presence of externally applied magnetic field helps in reducing the diffusion of charged particle across the field lines indicating that strong magnetic fields are helpful in plasma confinement. In the presence of a magnetic field, the plasma supports a larger variety of natural modes. So the application of magnetic field provides an excellent platform to study and understand various rich nonlinear phenomenon. Within the realm of physics, nonlinearity is

different parametric regimes. The investigation on the method of phase coherence presented in this dissertation is known to have implication in various transport processes of charged particle. We sincerely hope that the works elaborated in this thesis can help us to enrich the understanding of the concept of nonlinearity not only in glow discharge plasma but also in other plasma devices and enlighten our way to proceed furthermore in this direction.

Appendix

(Related to Chapter-3,5)

We consider plasma composed of electrons described by Boltzmann distribution and the cold ions described by continuity and momentum equations. The electron density distribution, the ion continuity and momentum equations are

$$n_e = n_0 \exp(e\phi/k_B T_e) \quad (\text{A.1})$$

$$\frac{\partial n_i}{\partial t} + \nabla \cdot (n_i v_i) = S \quad (\text{A.2})$$

$$n_i m_i \frac{dv_i}{dt} = n_i e E - m_i n_i \nu_i v_i \quad (\text{A.3})$$

Since electrostatic modes are considered, $E = -\nabla\phi$. All the variables are linearized by considering $n_{e,i} = n_0 + n_1$, $v_i = 0 + v_1$, $\phi = 0 + \phi_1$.

From thermodynamic arguments [109, 110] the local macroscopic electric field E , can be written as

$$\begin{aligned}
S &= \frac{\partial S}{\partial E}(pn_1 + qn_1^2 + rn_1^3 + \dots) \\
&= -\alpha n_1 - \lambda n_1^2 - \mu n_1^3
\end{aligned} \tag{A.5}$$

Carrying out Fourier decomposition in space and assume that the nonlinearities arises in time variables only i.e. only temporal variations of the 2nd and 3rd order terms of n_1 are taken into consideration and linearizing equations A.1-A.3 we obtain

$$\frac{d^2 n_1}{dt^2} - \frac{k_B T_e}{m_i} \nabla^2 n_1 - \nu_i \left(S - \frac{dn_1}{dt} \right) - \frac{dS}{dt} = 0 \tag{A.6}$$

The spatial variation of the perturbed quantity n_1 is taken of the form e^{ikz} where k is the wave vector in the z direction, and utilizing $c_s^2 = \frac{k_B T_e}{m_i}$, we obtain from equation (A.6) by utilizing equation (A.5) for S ,

$$\frac{d^2 n_1}{dt^2} + (\alpha + 2\lambda n_1 + \nu_i + 3\mu n_1^2) \frac{dn_1}{dt} + \omega_0^2 n_1 + \nu_i (\alpha n_1 + \lambda n_1^2 + \mu n_1^3) = 0 \tag{A.7}$$

where $\omega_0 = kc_s$.

The following normalization of variables is carried out by considering $\tilde{t} = \omega_0 t$; $x = n_1/n_0$; $a = \nu_i/\omega_0$; $b = 2\lambda n_0/\omega_0$; $c = 3\mu n_0^2/\omega_0$, $e = \alpha/\omega_0$. On the right hand

Bibliography

- [1] L. Tonks, and I. Langmuir, Physical Review, **33**, 195 (1929).
- [2] E.N Lorenz, J. Atmos. Sci. **20**, 130 (1963)
- [3] B.M. Battista, C. Knapp, T. McGee and V. Goebel, Geophysics, **72**, H29 (2007).
- [4] S. Lovejoy, F. Agterberg, A. Carsteanu, Q. Cheng, J. Davidsen, H. Gaonach, V. Gupta, I. L'Heureux, W. Liu, S.W. Morris, S. Sharma, R. Shcherbakov, A. Tarquis, D. Turcotte, V. Uritsky, Earth and space science news, **90**, 455-456, (2009)
- [5] R.M Anderson and R.M May, Nature, **280**, 361 (1979)
- [6] S.H. Strogatz, Nonlinear dynamics and chaos (Perseus Books, Reading, Massachusetts, (1994), 44-60

- [10] B. Shokri and S. M. Khorashadizadeh, Phys. Plasmas, **13**, 052116 (2006).
- [11] T. Klinger, F. Greiner, A. Rohde, A. Piel, and M. E. Koepke, Phys. Rev. E **52**, 4316 (1995).
- [12] Md. Nurujjaman, R. Narayanan and A.N Sekar Iyengar, Phys .Plasmas, **16**, 102307(2009)
- [13] M.A. Lieberman, A.J. Lichtenberg, (2005), Principles of Plasma Discharges and Materials Processing, (John Wiley and Sons).
- [14] J. Theiler , S. Eubank, A. Longtin, B. Galdrikian, and J. Doyne Farmer, Physica D, **58**, 77-94, (1992)
- [15] A.L. Goldberger, The Lancet, **347**, 1312-1314 (1996)
- [16] A.L. Goldberger, DR Rigney, West BJ. Chaos and fractals in human physiology. Sci Am **262**, 42-49 (1990)
- [17] M. Feigenbaum, J. Stat. Phys. **19**, 25, (1978).
- [18] M. E. Koepke, T. Klinger, F. Seddighi, and A. Piel Phys. Plasma **3**, 4421, (1996).

- [23] Md. Nurujjaman, Ramesh Narayanan, and A. N. Sekar Iyengar, *Chaos*, **17**, 043121 (2007)
- [24] Teresa Ree Chay and John Rinzel, *Biophysics Journal* **47**, 357-366 (1985)
- [25] Catalin M. Ticos, Epaminondas Rosa, Jr., William B. Pardo, Jonathan A. Walkenstein, and Marco Monti, *Physical Review Letter*, **85**, 14, (2000)
- [26] Klinger T, Greiner F, Rohde A and Piel A **2**, *Phys. Plasma*, (1995)
- [27] T. M. Flanagan and J. Goree, *Phys. Plasmas* **18**, 013705 (2011)
- [28] T. M. Flanagan and J. Goree, *Phys. Plasmas*, **17**, 123702 (2010)
- [29] M. Ciszak, O. Calvo, C. Masoller, Claudio R. Mirasso, and R. Toral, **90**, 204102, (2003)
- [30] Daiki Koga, A.C.-L Chian, Tohru Hada and E.L Rempel, *Phil. Trans. R. Soc. A*, **366** 447-457, 2008
- [31] Tohru Hada, Daiki Koga, Eiko. Yamamoto, *Space Science Reviews*, **107**, 463-466, (2003)
- [32] Daiki Koga, A.C.-L Chian, Tohru Hada, Phase coherence of foreshock MHD waves: Wavelet analysis *Space Science Reviews*, **107**, 495-498, (2003)

- [36] S. Ghosh, Pankaj Kumar Shaw, A. N. Sekar Iyengar, M. S. Janaki, Debajyoti Saha, Alpha Michael Wharton, and Vramori Mitra, Physics of Plasmas, **11**, 032303 (2014)
- [37] F. F. Chen, Introduction to plasma physics and controlled fusion, Plenum Press, New York, (1984).
- [38] V.P Budaev, S Savin, N Ohno, S. Takamura, Intermittency and extended self- similarity in space and fusion plasma: boundary effects. Plasma Phys Control fusion, **50**, 7 (2008)
- [39] B. B. Sahu, Jeon G. Han, Masaru Hori, and Keigo Takeda, Journal of applied Physics, **117**, 023301 (2015)
- [40] B. Bora, H. Bhuyan, M. Favre, E. Wyndham, and H. Chuaqui, International Journal of Applied Physics and Mathematics, **1**, (2011)
- [41] Subir Biswas, A. N. S. Iyengar and Rabindranath Pal, **19**, 032310, (2012)
- [42] Cristina Masoller, Chaos, **7**, 455, (1997)
- [43] M.L Goldstein and D.A Roberts, Phys. Plasmas, **6**, 4154-4160, (1999);
- [44] A C.-L. Chian, F. A. Borotto, and W. D. Gonzalez, The Astrophysical Jour-

- [47] Eckman J.-P, Kamphorst S. Recurrence plots of dynamical systems. Europhys. Lett , **4**, 973-977, (1987)
- [48] T. Gautamaa, D. P. Mandic, and M. M. Van Hulle, Phys. Rev. E **67**, 046204 (2003).
- [49] Henri, D.I. Abarbanel, Reviews of modern Physics, **65**, 4, (1993)
- [50] Liangyue Cao, Physica D **110**, 43-50 (1997)
- [51] K.P. Harikrishnana, R. Misra, G. Ambika, A.K. Kembhavi, Physica D, **215**, 137-145, (2006)
- [52] Davide Barbieri and Alessandro Vivoli, Physica A, **355**, 190 (2005)
- [53] M. T. Rosenstein, J. J. Collins, and C. J. De Luca, Physica D **65**, 117 (1993)
- [54] S.L. Gonzalez Andino, R. Grave de Peralta Menendez, G. Thut, L. Spinelli, O. Blanke, C.M. Michel, M. Seeck, and T. Landis, Human Brain Mapping **11**, 46-57 (2000)
- [55] Willians WJ, Brown ML, Hero AO, Proc SPIE Int Soc Opt Eng, **1566**, 144-156 (1991)
- [56] J.P. Zbilut, J.-M. Zaldvar-Comenges, F. Strozzi, Phys. Lett. A , **297**, 173181

- [59] John P. Higgins, Yale Journal of Biology and Medicine, **75**, 247-260 (2002)
- [60] Osvaldo A. Rosso and Cristina Masoller, Phys. Rev. E, **79**, 040406(R), (2009)
- [61] M. De Domenico and V. Latora., Europhysics Letters, **91**, 3 (2010);
- [62] Jian-Guo Wu, Henrik Lundstedt, Geophysical Research Letters, **23**, 319322, (1996)
- [63] S.Leistedt, M.Dumont, J.-P.Lanquart, F.Jurysta,P.Linkowski, Clinical Neurophysiology, **118**, 940-950, (2007);
- [64] Thomas Lux, Michele Marchesi, Nature, **397**, 498-500, (1999)
- [65] Nils C. Stenseth, Atle Mysterud, Geir Ottersen, James W. Hurrell, Kung-Sik Chan, Mauricio Lima, Science, **297**, 1292-1296, (2002)
- [66] Dimitri Komatitsch, Jeroen Tromp, Geophysical Journal International, **139**, 806-822, (1999)
- [67] Karen M. Leighly, The Astrophysical Journal, **125**, 297-316, (1999)
- [68] Milan Palu, Physics Letters A, **213**, 138-147, (1996)
- [69] Lyle Noakes, International Journal of Bifurcation and Chaos, **1**, 867, (1991)

- [74] U. Rajendra Acharya, Oliver Faust, Vinitha Sree, G. Swapna, Roshan Joy Martis, Nahrizul Adib Kadri, Jasjit S. Surif, Computer Methods and Programs in Biomedicine, **113**, 55-68, (2014)
- [75] K. P. Harikrishnan, R. Misra, G. Ambika, and R. E. Amritkar, Chaos, **19**, 043129, (2009)
- [76] A. Hyvriinen, E. Oja, Neural Networks, **13**, 411-430, (2000)
- [77] A. Witt, B.D. Malamud, Surveys in Geophysics, **34**:541-65 (2013)
- [78] R. L. Stratonovich, Topics in the Theory of Random Noise, Gordon and Breach, New York, (1981), Vol. 1.
- [79] J.M. Hausdorff, C.K. Peng, Z. Ladin, J.Y. Wei and A.L. Goldberger, J. Appl. Physiol. **78**, 349-358 (1995)
- [80] C.K. Peng, Shlomo Havlin, H. Eugene Stanley, Ary L. Goldberger, Chaos, **5**, 1 (1995)
- [81] Yanfei Kang, Danijel Belui and Kate Smith-Miles, Chaos, **24**, 023114 (2014)
- [82] C.K. Peng, J. Mietus, J.M. Hausdorff, Shlomo Havlin, H. Eugene Stanley,

- [85] H. Chaudhuri, C. Barman, A. N. S. Iyengar, D. Ghose, P. Sen, B. Sinha,
The European Physical Journal, **222**, 827-838, (2013)
- [86] U Deka, A Rao, M Nurujjaman, Physica Scripta, **90**, 125602 (2015)
- [87] Xu Y. H., Jachmich S. and Weynants R. Phys. Plasma, **11**, 5413 (2004)
- [88] Temujin Gautamaa, Danilo P. Mandic b, Marc M. Van Hulle , Physica D
190, 167176 (2004)
- [89] D. Kugiumtzis, Physical Review E **60**, 2808-2816 (1999)
- [90] V. Venema, F. Ament, C. Simmer Nonlin. Processes Geophys, **60**, 321328,
2006
- [91] R. Roy, K. Thornburg, and J. Scoot, Phys. Rev. Lett. **72**, 2009 (1994).
- [92] K.P. Harikrishnan, R. Misra, G. Ambika, Commun Nonlinear Sci Numer
Simulat, **14**, 36083614, 2009
- [93] Chiranjib Barman, Hirok Chaudhuri, Debasis Ghose, Argha Deb, Bikash
Sinha, Journal of Earthquake Science, **1**, 1-21, (2014)
- [94] C.J. Stam, J.R.M. Pijn, W.S. Pritchard, Physica D **112**, 361-380 (1998)

- [98] C. Torrence and G. P Compo, Bulletin of the American Meteorological Society, **79**, 61-78 (1998)
- [99] Gerardo J. Escalera Santos, M. Rivera, M. Eiswirth, and P. Parmananda, Physical Review E **70**, 021103 (2004)
- [100] Md. Nurujjaman, P. S. Bhattacharya, A. N. Sekar Iyengar, Physical Review E **80**, 015201 (2009)
- [101] Md. Nurujjaman, A. N. Sekar Iyengar, P. Parmananda, Physical Review E **78**, 026406 (2008)
- [102] Pinaki Pal, Krishna Kumar, Priyanka Maity, and Syamal Kumar Dana, Physical Review E, **87**, 023001 (2013)
- [103] Erzilia Lozneanu, Mircea Sanduloviciu, Chaos Solitons and Fractals, **18**, 335-343 (2003)
- [104] Erzilia Lozneanu, Mircea Sanduloviciu Chaos, Solitons and Fractals, **30**, 125-132 (2006)
- [105] Dejin Yu, Michael Small, Robert G. Harrison, and C. Diks, Physical Review E, **81**, 4 (2000)

- [109] Hsuan H. C. S., Ajmera, R. C. and Lonngren, K. E., Appl. Phys. Lett., **11**, 9-277 (1967).
- [110] B. E. Keen and W. H. W. Fletcher, J. Phys. D: Appl. Phys., **3**, 1868-1885, (1970).
- [111] Michael Small, Dejin Yu, Robert G. Harrison, Colin Robertson, Gareth Clegg, Michael Holzer, and Fritz Sterz, Chaos **10**, 268 (2000)
- [112] Martin Casdagli, Physica D **35**, 335-356 (1989)
- [113] R. Andrzejak, K. Lehnertz, F. Mormann, C. Rieke, P. David and C. Elger, Phys. Rev. E **64**, 061907 (2001)
- [114] A. M. Daltrini, S. A. Moshkalev, T. J. Morgan, R. B. Piejak, and W. G. Graham, Applied Physics Letters **92**, 061504 (2008)
- [115] Jin-Gen Wang, G. L. Payne and D. R. Nicholson, Phys. Fluids B, **4**, 1432 (1992).
- [116] Hirdesh K. Pharasi, Krishna Kumar, and Jayanta K. Bhattacharjee, Physical Review E **90**, 041004R (2014)

- [120] Debajyoti Saha, Pankaj Kumar Shaw, M. S. Janaki, A. N. Sekar Iyengar, Sabuj Ghosh, Vramori Mitra and Alpha Michael Wharton Physics of Plasmas **21**, 032301 (2014)
- [121] S. K. Saha, S. Raychaudhuri, S. Chowdhury, M. S. Janaki, and A. K. Hui, Phys. Plasmas, **19**, 092502, 2012.
- [122] Md. Nurujjaman, A.N. Sekar Iyengar, Physics Letters A, **360**, 717-721, (2007).
- [123] R. Jha, D. Raju and A. Sen, Phys. Plasma **13**, 082507 (2006)
- [124] Bornali Sarma, Sourabh S Chauhan, A M Wharton and A N Sekar Iyengar, Phys. Scripta, **88**, 065005, (2013)
- [125] Pankaj Kumar Shaw, Debajyoti Saha, Sabuj Ghosh, M.S. Janaki, A.N. Sekar Iyengar, Chaos Solitons and Fractals, **78**, 285-296, (2015)
- [126] F.H. Lopes da Silva, J.P. Pijnb, D. Velisb, P.C.G. Nijssenc, International Journal of Psychophysiology, **26**, 237-249, (1997)
- [127] T. Yamada, S.-I. Itoh, S. Inagaki, Y. Nagashima, S. Shinohara, N. Kasuya,

- [130] V. Carbone, L. Sorriso-Valvo, E. Martines, V. Antoni, and P. Veltri Physical Review E **62**, R49 (2000)
- [131] Wootton A J et al Phys. Fluids B **2**, 2879 (1990)
- [132] White R, Chen L and Lin Z Phys. Plasmas **9**, 1890 (2002)
- [133] Debajyoti Saha, Ramesh Narayanan, R.D Tarey , M.S Janaki, A.N. Sekar Iyengar, Proceedings International work conference on time series analysis (ITISE) 2016 ISBN: 978-84-16478-93-4
- [134] James D. Hamilton, Econometrica, **57**, 357-384 (1989)
- [135] S. V. Buldyrev, N. V. Dokholyan, A. L. Goldberger, S. Havlin, C.K. Peng, H. E. Stanley, and G. M. Viswanathan, Physica A, **249**, 430 (1998)
- [136] H. E. Stanley, S. V. Buldyrev, A. L. Goldberger, S. Havlin, C.-K. Peng, and M. Simons, Physica A, **273**, 1 (1999)
- [137] S. Blesic, S. Milosevic, D. Stratimirovic, M. Ljubisavljevic, Physica A, **268**, 275 (1999)
- [138] Y. Ashkenazy, M. Lewkowicz, J. Levitan, S. Havlin, K. Saermark, H. Moel-

- [141] Xavier Gabaix, Parameswaran Gopikrishnan, Vasiliki Plerou, H. Eugene Stanley, *Nature*, **423**, 267-270 (2003);
- [142] MEJ Newman, *Contemporary Physics*, **46**, 323-351, (2005)
- [143] Z Chen, PC Ivanov, K Hu, HE Stanley, *Physical Review E*, Effect of non-stationarities on detrended fluctuation analysis, **65**, 041107 (2002)
- [144] Jan W. Kantelhardt, Eva Koscielny-Bundea, Henio H.A. Regoa, Shlomo Havlinb, Armin Bundea, *Physica A*, **295**, 441-454 (2001)
- [145] Pankaj Kumar Shaw, Debajyoti Saha, Sabuj Ghosh, M.S. Janaki, A.N. Sekar Iyengar, *Physica A*, **469**, 363371, (2017)
- [146] Y.H. Liu, P. Cizeau, M. Meyer, C.K. Peng, H.E. Stanley, *Physica A*, **245**, 437 (1997)
- [147] M. Ausloos, N. Vandewalle, P. Boveroux, A. Minguet, K. Ivanova, *Physica A*, **274**, 229 (1999)
- [148] M. Ausloos, K. Ivanova, *Physica A*, **286**, 353, (2000)
- [149] James Ladyman, James Lambert, Karoline Wiesner, *European Journal for*

- [152] R L Stenzel, C Ionita, R Schrittwieser, Plasma Sources Sci. Technol. **17**, 035006 (2008)
- [153] R L Stenzel, J Gruenwald, C Ionita, R Schrittwieser, Phys. Plasmas, **18**, 062113 (2011)
- [154] R L Stenzel, J Gruenwald, C Ionita, R Schrittwieser, Plasma Sources Sci. Technol, **21**, 015012 (2012)
- [155] Manash Kumar Paul, P. K. Sharma, A. Thakur, S. V. Kulkarni, and D. Bora, Physics of Plasmas, **21**, 062112 (2014)
- [156] Dimitriu D.G, Afiori M, Ivan L M Ionita C, Schrittwieser R, Plasma Phys. Control. Fusion, **49**, 237-248 (2007)
- [157] Ionita C, Dimitriu D.G and Schrittwieser R, Int J. Mass spectrum, **233**, 343-354 (2004)
- [158] R L Stenzel, R Schrittwieser, IEEE Transaction on Plasma Science, **17**, 4, (2008)
- [159] Sabuj Ghosh, Pankaj Kumar Shaw, Debajyoti Saha, M.S. Janaki, and A.N. Sekar Iyengar, Phys. Plasmas, **23**, 093511, (2016)